Ultrasonic Guided Wave and Acoustic Emission Techniques for monitoring corrosion in Reinforced Concrete Structures

A Thesis

submitted in fulfillment of the requirement for the award of degree

of

DOCTOR OF PHILOSOPHY

in

CIVIL ENGINEERING

Submitted by

Ashutosh Sharma

Reg. No.: 951302003

Supervisor(s)

Dr. Shruti Sharma
Associate Professor
Civil Engineering Department

Dr. Sandeep Kumar Sharma
Associate Professor
Mechanical Engineering Department

DEPARTMENT OF CIVIL ENGINEERING

THAPAR INSTITUTE
OF ENGINEERING & TECHNOLOGY
(Deemed to be University)

Patiala-147004

July, 2018

CERTIFICATE

I, **Ashutosh Sharma,** hereby declare that the thesis entitled, **"Ultrasonic Guided Wave and Acoustic Emission Techniques for monitoring corrosion in Reinforced Concrete Structures,"** submitted to Thapar Institute of Engineering and Technology, Patiala, in partial fulfillment of the requirement for the award of Degree of **Doctor of Philosophy** in **Civil Engineering** is a record of original and independent research work done by me during 2013-2018. This thesis has been conducted under the supervision and guidance of **Dr. Shruti Sharma**, Associate Professor, Civil Engineering Department, Thapar Institute of Engineering and Technology, and **Dr. Sandeep Kumar Sharma**, Associate Professor, Mechanical Engineering Department, Thapar Institute of Engineering and Technology. It has not formed the basis for the award of any Degree to any candidate of any university.

25/07/2018

Ashutosh Sharma

Date: 25/7/18

This is to certify that above statement made by the candidate is correct to the best of my knowledge.

25/7/2018

Dr. Shruti Sharma

Supervisor
Associate Professor
Civil Engineering Department

25/7/2018

Dr. Sandeep Kumar Sharma

Supervisor
Associate Professor
Mechanical Engineering Department

ABSTRACT

Corrosion of reinforcement is one of the principal causes of premature failure of Reinforced Concrete (RC) structures. In India, the annual loss due to corrosion has been estimated about 4% of the country's gross domestic product (GDP) i.e., about USD 40 billion in a year in both infrastructure and industry segments. Exposure to extreme environments and the continuous ingress of chlorides in concrete from various sources neutralises the protective passive layer of concrete which is alkaline with a pH ranging from 12 to 13. The presence of moisture and oxygen leads to the formation of oxides and the initiation of reinforcement corrosion takes place. Corrosion of reinforcement in concrete affects the durability of the RC structures in two ways: the formation of rust products with larger volume than steel leads to spalling and the cracking of the concrete cover; and the area of cross-section of the steel bars reduces drastically due to dissolution of the steel leading to pit formation and hence, loss in the tensile strength and load carrying capacity of the structure. Therefore, an early prognosis and diagnosis of corrosion-induced damage in RC structures could facilitate the engineers to adopt correct repair measures.

A large variety of non-destructive techniques have been reported by researchers worldwide for detecting corrosion-induced damage in RC structures like visual inspection, electrochemical, Optical methods, PZT and piezo ceramic patches etc. but they suffer from practical applications owing to large civil infrastructure. Recently, the advent of wave propagation technologies for damage detection in RC structures have given a new dimension to damage monitoring capabilities. In this work, an integrated approach using active Ultrasonic Guided Wave (UGW) and passive Acoustic Emission (AE) technique for corrosion monitoring in RC structures has been attempted. Active UGW monitors the deterioration of reinforcing bar while corrosion takes place in RC structure whereas the AE technique listens to the cracks and records the damage in the surrounding concrete.

Initiation of corrosion in RC structures before it can be observed visually is done using the two techniques. For this, AE sensors were mounted on the concrete

surface and typical guided wave modes were propagated through the embedded rebar. The NDT results were co-related with the already established electrochemical techniques. Active monitoring using UGW was found to have limited significance for tracking the initiation of corrosion when only the outer surface of the reinforcing bar is affected. Surface modifications on the embedded rebar during the initial stages of corrosion is clearly indicated by the L(0,1) mode. On the other hand, passive monitoring using AE clearly identified the onset and the initiation of corrosion during the early stages. The origin and the location of micro-cracks were well identified with the help of AE event maps.

Further, the techniques were used to investigate the progression of corrosion-induced damage in RC structures. It was found that UGW clearly differentiated the surface corrosion from the pitting corrosion with the help of specific guided wave modes. On the other hand, AE parameters like AE hits and cumulative signal strength (CSS) successfully picked up the regions of initiation of steel depassivation and progression of corrosion in the form of micro- and macro-cracking in the surrounding concrete. From the AE event maps, the entire damage progression from initiation of corrosion damage to damage progression in the later stages could be clearly observed.

Further, the effect of varying rates and different corrosion environments were investigated using the two wave propagation techniques. It was confirmed that corrosion mechanism is unaltered by varying rates of accelerated corrosion though the damage progression is delayed and picked up by both UGW and AE. In case of RC beams subjected to accelerated corrosion in the absence of chlorides simulating slow corrosion, UGW confirmed that pitting is insignificant due to slow steel-concrete bond deterioration, by picking up only delamination. On the other hand, AE clearly indicated the corrosion initiation as well as progression stages by cumulative AE hits.

The efficacy of UGW and AE techniques was also investigated to monitor the corrosion impediment offered using Fiber Reinforced Polymer (FRP) wraps on corroding RC cylinders. UGW monitoring with surface-seeking and core-seeking modes established that pulse-echo method is suitable to assess corrosion delay in FRP wrapped samples. The recorded AE hits exhibited significant decrease after

the wrapping was done indicating success in corrosion impediment. This was confirmed by drop in the values of amplitude of AE hits from 100 dB to 65 dB after wrapping. No peak/knee was observed in the CSS curve, indicating that FRP wraps effectively delayed the corrosion progression.

It is observed that corrosion-induced damage in RC structures can effectively be tracked right from initiation to progression to concrete cracking using an integrated health monitoring approach involving wave propagation technologies of active ultrasonic guided wave and passive acoustic emission techniques along with benchmark electrochemical measurements. This would go a long way in non-destructive evaluation of residual capacities of reinforcements, which would help a great deal in devising a post-corrosion maintenance strategy of RC structures.

ACKNOWLEDGEMENT

First and foremost, I am beholden to the Almighty and I bow before Him for his umpteen blessings and bestowing in me the grit and confidence to carry out the research work.

I extend my thanks to **Dr. Prakash Gopalan**, Hon'ble Director, Thapar Institute of Engineering and Technology, for giving me the opportunity to undertake Ph.D.

I convey heartfelt and sincere gratitude to my research supervisor **Dr. Shruti Sharma**, Associate Professor, Civil Engineering Department and **Dr. Sandeep Kumar Sharma**, Associate Professor, Mechanical Engineering Department. Their valuable support, advice, and encouragement inspired me to complete the research work on time.

I am honour bound and profoundly thankful to the doctoral committee members- **Dr. Naveen Kwatra**, Professor and Head of Department, Civil Engineering Department, **Dr. Maneek Kumar**, Professor, Civil Engineering Department, **Dr. Shweta Goyal**, Associate Professor, Civil Engineering Department, and **Dr. Kulvir Singh,** Professor, School of Physics, Thapar Institute of Engineering and Technology, for their support and invaluable comments. I am also thankful to **Dr. Abhijit Mukherjee,** Professor, Civil Engineering Department, Curtin University, Bentley for his invaluable guidance throughout my work.

Further, I wish to thank those persons who helped me in structural lab and concrete lab: Ram Sumiran, Virendran Sharma, Amarjeet Singh, Munish Kapila, Roop Kumar and many others.

I am grateful to my wife, Sakshi who stood like a rock in my difficult times and worked relentlessly to provide me full support. I would also like to thank my family: my father, Sh. S.L. Sharma, my mother, Smt. Rekha Sharma, Maruti Sharma (elder brother), Shilpa Gupta (sister-in-law), Anutra Sharma (niece), Sh. Harish Aneja (father-in-law), Smt. Renu Aneja (mother-in-law), and Abhilash Aneja (brother-in-law) for their endless support. Their love, patience, persistent

encouragement, and good virtuous understanding enabled me to complete the research work successfully.

Ashutosh Sharma

TABLE OF CONTENTS

LIST OF FIGURES

LIST OF TABLES

ACRONYMS AND ABBREVIATIONS

AE	Acoustic Emission
BE	Bar End Echo
CC	Chloride Corrosion
CFRP	Carbon Fiber Reinforced Polymer
CFST	Concrete Filled Steel Tubes
CSS	Cumulative Signal Strength
DT	Destructive Testing
EPMA	Electron Probe Microscope Analyse
FRP	Fiber Reinforced Polymer
GFRP	Glass Fiber Reinforced Polymer
GWT	Guided Wave Testing
HCP	Half-Cell Potential
HI	Historic Index
IE	Interface Echo
MARSE	Measured Area under Rectified Signal Envelope
MS	Mild Steel
NDT	Non-destructive testing
OC	Oxide corrosion
PAC	Physical Acoustic Corporation
PE	Pulse Echo

PT	Pulse Transmission
RC	Reinforced Concrete
SAFEM	Semi-Analytical Finite Element Method
SEM	Scanning Electron Microscope
SI	Severity Index
SiGMA	Simplified Green’s functions for moment tensor analysis
STFT	Short-time fourier transform
TOA	Time Of Arrival
TOF	Time-Of-Flight
UGW	Ultrasonic Guided Wave
WT	Wavelet Transform

CHAPTER 1

INTRODUCTION

1.1 BACKGROUND

Reinforced concrete (RC) is used to build durable structures worldwide due to its high tensile strength, compressive strength, stiffness, and cost-effectiveness. RC structures are expected to have excellent service lives with minimal maintenance [1, 2]. Numerous factors such as chlorides and carbon dioxide present in the environment, acid rain, aggressive chemicals released by industries, water-cement ratio of concrete, availability of oxygen at cathodic region, etc. greatly reduce the serviceability and life of RC structures. Amongst various types of deterioration, corrosion of reinforcement is most serious and one of the principal causes of premature failure of RC structures [3, 4]. Exposure to extreme environments and continuous ingress of chlorides in concrete from various sources neutralise the protective passive layer of concrete which is alkaline with a pH ranging from 12 to 13 [5–10]. The presence of moisture and oxygen leads to the formation of oxides resulting in the initiation of corrosion. Corrosion of reinforcement in concrete affects the durability of RC structures in two ways: formation of rust products with larger volume than steel leads to spalling and cracking of concrete cover; and reduction in cross-sectional area of steel bars due to dissolution of steel leads to pit formation and eventually lowers the tensile strength and load carrying capacity of RC structure [11–14].

Corrosion of reinforcement is an unavoidable problem being faced by the cement and concrete industry worldwide. The most affected areas are offshore structures, such as marine airports, platforms, bridges, harbours, tunnels and vessels exposed to harsh marine environment such as tides, storms etc. Typically, restoration work is needed within 15 years of constructing a building in the coastal region. The overall repair and maintenance of RC structures due to reinforcement corrosion cost 1-2 % of yearly rate of new construction. In India, deterioration due to corrosion is alarming since the structures are exposed to adverse environmental attack due to acid rains, severe monsoon and long coast line. The annual loss due to corrosion has been estimated about 4 % of the country's domestic product i.e., about USD 40 billion in a year in both infrastructure and industry segments. Hence, in order to reduce the heavy maintenance costs and ensure safe use of RC structures, it is imperative to monitor the health of structures which could predict the corrosion induced-damage in RC structures much before it reaches to catastrophic levels [8, 15, 16].

In the pursuit of suitable technique for monitoring corrosion-induced damage in RC structures, the research community has proposed a number of techniques that keep a track on the onset and propagation of corrosion in new or pre-existing RC structures [8, 12, 17, 18]. The corrosion monitoring techniques in RC structures have been broadly classified as destructive and non-destructive testing techniques. Destructive testing (DT) involves removal or, uncovering of a piece of RC structure in order to determine the extent of damage or contamination caused by the penetration of chlorides or carbon dioxides. Commonly, pull-out and mass loss methods are used for destructive testing [16, 19, 20]. The pull-out strength test determines the bond strength between steel and concrete. After conducting the pull out test, the reinforcing bars are weighed to determine the mass loss of corroded steel bar in comparison to actual non-corroded steel bar. The extent of deterioration of reinforcing bar can thus be assessed from the mass loss. Therefore, pull-out and mass loss test can be effectively used to quantify the damage induced due to corrosion in RC structures. However, destructive testing techniques are rarely applied to building structures or, large non-building structures (e.g. bridges and dams) due to the prohibitive cost of re-constructing a building, or a portion of building. Therefore, Non-Destructive Testing (NDT) techniques are largely preferred over the conventional destructive testing.

NDT techniques can detect corrosion without causing any damage to RC structure. These techniques are reliable and cost-effective. A number of NDT techniques have been proposed by research community that can be used either independently or, in combination to provide an estimate of the overall condition of RC structure for corrosion induced damages. Broadly, they can be classified under following distinct categories:

- Visual Inspection [12, 21, 22],
- Electrochemical methods (like open circuit potential measurement [16, 23], surface potential measurement [8], concrete resistivity measurement [12, 15], linear polarization resistance measurement [24], galvanostatic pulse transient method [25], electrochemical impedance spectroscopy [24], electrochemical noise [26] methods
- Radiographic methods like X-ray and Gamma radiography, acoustic tomography etc. [27], infrared thermography [28]
- Optical sensing methods involving Fiber optic sensors [29], use of piezoelectric patches [30, 31]
- Elastic Wave based methods like impact echo [32], ultrasonic guided wave [20, 33–51], acoustic emission [18, 52–92].

Although a host of NDT techniques are attempted by researchers, visual inspection has remained the most popular technique for monitoring corrosion [18]. However, by the time visual inspection detects the corrosion of concrete, the overall strength of RC might be compromised. The electrochemical methods for corrosion monitoring are qualitative in nature [18, 93, 94]. They provide information about the likelihood of corrosion but are unable to estimate the rate and extent of corrosion and the loss of capacity thereof. Some advanced methods like electro-magnetic methods suffer from the limitation of attenuation of travelling waves due to accumulation of rust. The infrared tomography technique offers a qualitative analysis of damage due to corrosion but fails to quantify it. Strain sensing methods such as fibre optic sensors are able to monitor localised states of strain only [18]. Also, these methods suffer from practical limitations of restrained access and large dimensions of civil engineering structures.

Recently, wave based techniques have been explored, which are able to monitor RC structures by simply observing the variation in wave characteristics due to corrosion. Depending on the method of application and monitoring, wave propagation techniques can be classified as active or passive monitoring techniques. Monitoring techniques such as ultrasonic guided wave or impact echo, involves the external excitation of a wave into the structure in order to monitor and study the variation in its propagation characteristics with damage. The transmitted or reflected wave changes due to corrosion. Hence, they can be related to discontinuities or damages in the structure. Passive monitoring techniques such as acoustic emission, involves the use of sensors on the structure without external excitation and listening to the changes inside the structure with damage progression.

In this work, it is proposed to use active ultrasonic guided waves (UGW) in combination with passive acoustic emission (AE) to study corrosion in RC structures to evaluate their efficacy for corrosion monitoring. Following section provides a brief insight into the mechanism of corrosion in RC structures to understand the process.

1.2 CORROSION IN REINFORCED CONCRETE STRUCTURES

Corrosion in RC structures affects the RC structure in two ways. Firstly, it results in cracking and spalling of concrete, secondly, it is accompanied by the loss of cross-section of the rebar. This increases the possibility of structural failure greatly. Hence, it is important to understand the mechanism of corrosion in terms of its onset, progression and finally the failure of the structure. The highly alkaline nature of concrete (pH ranges between 12 and 13), due to the presence of hydroxides of calcium, sodium and potassium, provides a dense pseudo passive

layer which prevents the steel bar from corrosion. This pseudo passive layer is essentially made of an iron oxide film (Fe_2O_3). However, in cases of extreme environmental conditions i.e., in the presence of excess oxygen, water and aggressive ions such as chlorides, the passive layer depletes. And the process of corrosion is initiated. The presence of chloride ions is primary for the corrosion of steel reinforcing bars in concrete. The pre-existing cracks in concrete give way to the ingress of chloride ions. The possible source of chlorides include: aggregates, mix water, admixtures (accelerators), de-icing chemicals, sea water etc. As per the oxide film theory, the ingress of chloride ions depletes the passive oxide film thereby exposing the reinforcing bar to the corrosive agents and initiates corrosion [8].

Carbonation is another form of corrosion that takes place when carbon dioxide (CO_2) penetrates concrete and dissolves in the pore solution. This results in the formation of carbonic acid which further reacts with the alkalis in the cement and the reduction in the overall pH value takes place. In case of a very low pH value and excess amount of water and oxygen, the passive layer depletes and the corrosion is initiated. However, the process of carbonation is very slow in sound concrete and is not considered an important factor in initiation of corrosion.

Reinforcement corrosion is an electrochemical process that involves the transfer of electrons from anode to cathode. The two cases of corrosion advancement in RC structures are considered- 1) in the presence of oxygen and in the absence of chlorides 2) in the presence of chlorides and in the absence of oxygen. The first case can be termed as oxide corrosion and the second case can be termed as chloride corrosion.

In case of oxide corrosion, two half-cell reactions occur at both anodic and cathodic portion of reinforcing steel, in the absence of an electric supply [95].

At anode, oxidation of iron (Fe) takes place with generation of electrons.

$$\boldsymbol{Fe \rightarrow Fe^{2+} + 2e^{-}} \quad (1.1)$$

At cathode, these electrons are consumed by cathode for the reduction of oxygen to form hydroxyl ions (OH^-).

$$\boldsymbol{H_2O + \frac{1}{2}O_2 + 2e^{-} \rightarrow 2OH^{-}} \quad (1.2)$$

These hydroxyl ions combine with ferrous ions (Fe^{2+}) to form ferrous hydroxide.

$$\boldsymbol{Fe^{2+} + 2OH^{-} \rightarrow Fe(OH)_2} \quad (1.3)$$

In presence of oxygen and water, the ferrous hydroxide is further oxidized and takes the shape of rust i.e., Fe_2O_3.

$$\boldsymbol{4Fe(OH)_2 + O_2 + H_2O \rightarrow 4Fe(OH)_3} \quad (1.4)$$

$$\boldsymbol{2Fe(OH)_3 \rightarrow Fe_2O_3.H_2O} \quad (1.5)$$

When these reactions occur close together, or at the same location, it is termed as microcell, and when they occur at widely spread locations, it is termed as macrocell [96]. The anodic reactions release intermediate corrosion product, Fe^{2+} into solution continuously. With the passage of time, corrosion propagation of reinforced steel results in an increase in the volume of corrosion products and a decrease in the cross-sectional area of steel bar [97]. These corrosion products exert tensile stresses in concrete and degrades the bond between steel and concrete. This leads to cracking and spalling of concrete cover which exposes the reinforcement to outside environment [98]. As a result, the load carrying capacity and service life of RC structures gets reduced [99]. **Fig. 1.1** depicts the mechanism of reinforcement corrosion in structures.

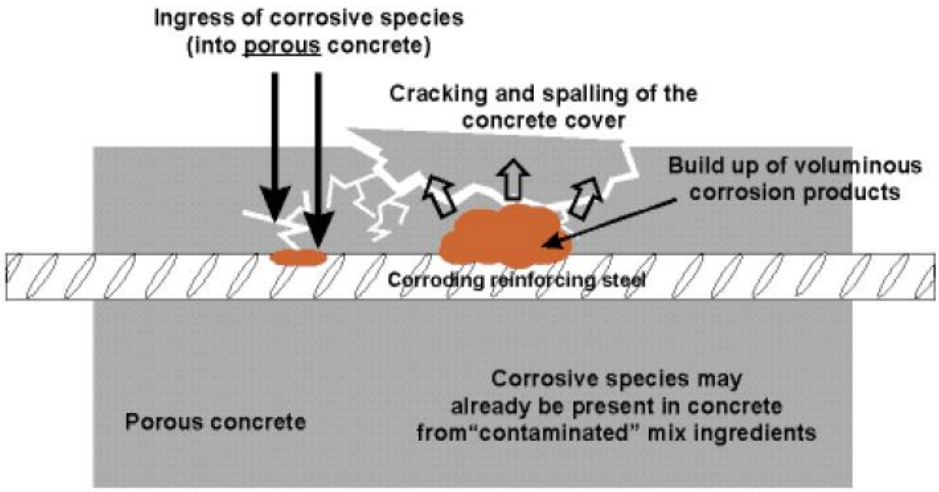

Fig. 1.1: Mechanism of reinforcement corrosion [98]

In the case of chloride corrosion, chloride ions react with iron and form soluble iron-chloride complex:

Anodic Reaction: $\mathbf{Fe + 2Cl^- \longrightarrow (Fe^{2+} + 2Cl^-) + 2e^-}$ (1.6)

This complex reacts with water to form ferrous hydroxide

Cathodic Reaction: $\mathbf{(Fe^{2+} + 2Cl^-) + 2e^- + 2H_2O \longrightarrow Fe(OH)_2 + 2H^+ + 2Cl^-}$ (1.7)

This ferrous hydroxide results in the formation of rust in presence of oxygen and water. The formation of corrosion products and the other processes such as cracking, spalling and delamination of steel bar is similar to that of oxide corrosion. However, the rate of corrosion is very slow in oxide corrosion than chloride corrosion.

The phenomenon and mechanism of corrosion process of steel in extreme marine environments, often referred to as phenomenological model of steel corrosion, given by Melchers [7] divides the corrosion process into four phases as shown in **Fig. 1.2**. The initiation of corrosion is represented by Phase 1 which is marked by the breakdown of passive layer of

iron oxides. The amount of water and oxygen that penetrates through the concrete dominates the rate of corrosion in steel. After a certain amount of corrosion has occurred, the corrosion loss starts to decrease. This may be due to the layer of rust formed around steel, thereby blocking the flow of oxygen and water. This state of lesser corrosion loss, known as calm phase, is represented by Phase 2. Due to further expansion of corrosion products, there is an increase in the mass loss of reinforcing steel. This state is represented by Phase 3. After this stage, the corrosion progresses at a more uniform rate, represented by Phase 4. Eventually, corrosion of reinforcement leads to the following events: fracture through cracking, delamination and spalling of concrete cover [5, 14, 13], reduction of concrete and reinforcement cross-sections, loss of bond between reinforcing steel and concrete ultimately leading to collapse. Hence, it is important in corrosion monitoring methodology to be able to pick up different phases of corrosion-induced damage in a systematic manner much before it reach the alarming levels. It is proposed in this work to investigate wave based techniques of UGW and AE for detecting corrosion-induced damages in RC structures.

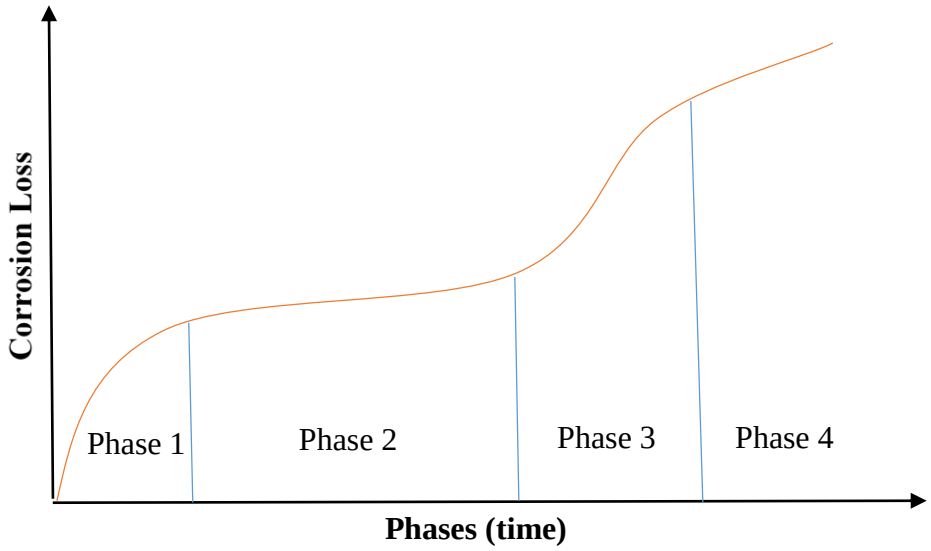

Fig. 1.2 Phenomenological model of corrosion loss in steel under sea water conditions [7]

1.3 WAVE PROPAGATION TECHNIQUES

There have been promising technological advancements in the wave based technologies for corrosion monitoring in RC structures. Initially, ultrasonic bulk waves were used by researchers but they suffered from the limitation of bulk attenuation leading to smaller sensing capabilities. Recently, ultrasonic guided wave monitoring has gained popularity. The method involves the introduction of high frequency wavelet packet or pulse into the structure using reinforcing bars as waveguides and then observing the transmission and subsequent reflection

of these waves [45]. The rebar acts as the waveguide assisting its propagation. The characteristics of transmitted or reflected waves change due to deterioration in the bar because of corrosion. Since ultrasonic guided waves involves monitoring the changes in a structure just by transmitting the signal through the structure to be tested, it is considered an active monitoring tool.

On the other hand, AE technique has been suggested as a passive monitoring tool that listens and records the changes occurring in a structure due to stress redistribution as a result of damage inside the material, using surface mounted sensors. The received signals are known as AE events, which are transient elastic waves originating from sudden outburst of energy from localised sources within a material [52]. The main factors which influence the AE signals are source characteristics, path between the source and transducer, transducer characteristics and measuring system. AE is used for detecting and localising the cracks arising from the initiation and progression of corrosion [60, 75]. Since AE monitoring involves the recording of signals generating inside the structure itself passively with surface mounted sensors, it can be termed as passive monitoring tool.

1.4 MOTIVATION FOR RESEARCH

A lot of research has been reported for monitoring corrosion in different RC structural elements using a variety of NDT techniques. Among the various techniques, wave based techniques of UGW and AE have started gaining popularity amongst researchers. But use of active UGW and passive AE needs to be investigated in detail for monitoring different aspects of corrosion initiation and progression in RC structures. This forms the motivation of research by utilizing active UGW and passive AE for corrosion monitoring in RC structures. It is also proposed to investigate the efficacy of these tools for monitoring passively protected FRP wrapped RC structures from corrosion.

1.5 OBJECTIVES OF THE RESEARCH

The aim of this research work is to investigate the efficacy of both active and passive wave propagation techniques utilizing ultrasonic guided wave and acoustic emission respectively for monitoring corrosion mechanism in RC structures subjected to chloride and oxide exposure. The focus is to investigate the applicability and effectiveness of monitoring different stages of corrosion in RC structures viz. initiation, progression and concrete cracking. The major objectives of the work are as below -

1. To study the effectiveness of Ultrasonic Guided Wave and Acoustic Emission techniques for monitoring initiation of corrosion in RC structures.
2. To monitor the progression of damage due to corrosion in RC structures at varying rates and different environments using Ultrasonic Guided Wave and Acoustic Emission techniques.
3. To investigate the efficacy of FRP wraps to corrosion impediment using Ultrasonic Guided Waves and Acoustic Emission techniques.

1.6 THESIS OUTLINE

The thesis is organised in the following manner:

Chapter 1 introduces the problem of corrosion and corrosion monitoring techniques. Gaps in the research area are identified and the objectives and scope of this study is outlined.

Chapter 2 includes the literature review in two parts. The first segment covers various studies carried using ultrasonic guided waves for damage monitoring in RC structures. In the second study, efficacy of acoustic emission technique for damage monitoring in RC structures has been presented.

Chapter 3 focusses on the monitoring of corrosion initiation in reinforced concrete structures using active ultrasonic guided wave and passive acoustic emission technique.

Chapter 4 focusses on UGW and AE monitoring of RC structures subjected to accelerated corrosion at advance stages of corrosion including the effects of varying environments and varying rates with the proposed two non-destructive techniques.

Chapter 5 presents the efficacy of UGW and AE techniques for monitoring passively protected reinforced concrete structures for corrosion impediment.

Chapter 6 presents the conclusions on various studies undertaken and provides a few recommendations for further study.

1.7 CLOSING REMARKS

In this chapter, a discussion on the importance of corrosion monitoring of RC structures is given. The advantages of non-destructive testing techniques over destructive testing techniques for corrosion monitoring are highlighted. Finally, the significance of wave propagation techniques viz. ultrasonic guided wave and acoustic emission is highlighted for complete assessment of RC structure subjected to corrosion induced damages. Aims and objectives of the research work are outlined. The succeeding chapter brings out a review of recent works done utilizing UGW and AE for damage monitoring in RC structures.

CHAPTER 2

ULTRASONIC GUIDED WAVE AND ACOUSTIC EMISSION TECHNIQUE – A REVIEW

2.1 INTRODUCTION

Quality control of engineering structures for prolonging the service life, safety by detecting deteriorations and deformations, and taking corrective measures in time, is of paramount importance. Non-Destructive Testing is widely used for monitoring structures such as steel in aerospace industry etc. without even disturbing the structure. The most commonly used NDT methods are visual inspection, eddy current testing, electrochemical testing, ultrasonic testing, infrared and thermal testing, acoustic emission and other methods. Most of these methods have been used for monitoring homogenous materials and therefore, their application in RC structures is still in its early stages.

Among various NDT techniques, wave propagation techniques have recently been exploited for damage monitoring in RC structures. They include ultrasonic guided wave and acoustic emission techniques. Ultrasonic guided wave technique works as an active monitoring technique wherein the signals are injected into the structure to be monitored and then from the variation of the received signal, the deterioration or deformation in the structure is assessed. On the other hand, acoustic emission technique works as a passive method wherein the sensors mounted on the structure passively listens to any activity which may be due to deterioration or deformation of the structure itself and relates to the extent in damage in the structure.

The chapter throws light on the two techniques and review the latest works done using the two techniques with focus on monitoring corrosion-induced damage.

2.2 ULTRASONIC GUIDED WAVE TECHNIQUE

This section provides an insight into the ultrasonic guided wave approach for damage monitoring.

2.2.1 Ultrasonic Testing

2.2.1.1 Basic Principle

Ultrasonic technique is based on the principle of physics that govern the propagation of sound waves in any medium. According to this principle, sound waves travel at a specific velocity through a given medium in a predictable direction, and when they encounter a

boundary with a different medium, they get reflected. Since 1940's, the laws of physics for the propagation of sound waves through solid materials have been used to detect internal discontinuities in metals such as hidden cracks, voids, porosity, etc. Sound waves above the audible frequency of 20 kHz are designated as ultrasonic. The wavelength of ultrasonic waves is of the same order of magnitude as visible light, and therefore these waves exhibit many properties similar to light, such as focussing, reflection and refraction. Ultrasonic waves are transmitted through solid materials such as steel by high frequency particle vibrations. The transmission of these waves is similar to pointing a flash light in a room with various objects that reflect the light. The directed ultrasonic wave is reflected by internal defects of the material such as cracks or voids.

Ultrasonic testing is a safe and well-established NDT technique that involves the propagation of high frequency sound waves to predict material strength, and detect the presence of internal flaws such as cracking, voids, honeycomb, decay and other damage. The generation and detection of ultrasonic waves require a transducer that is made of piezoelectric ceramics, composites or polymer. The transducer has the capability of converting a high voltage electrical pulse to a burst of sound waves and vice-versa. There are five types of transducers commonly used for ultrasonic flaw detection: Contact Transducers, Angle Beam Transducers, Delay Line Transducers, Immersion Transducers and Dual Element Transducers. The current research uses Contact Transducers. As the name implies, contact transducers are kept in direct contact to the surface of material (**Fig. 2.1**). Sometimes good contact requires the use of a coupling gel between the transducers and structure. These transducers introduce a sound wave perpendicular to the surface that is guided by the geometry of structure. These transducers are typically used for detecting voids, porosity, cracks, or delamination, and measuring the thickness of the material.

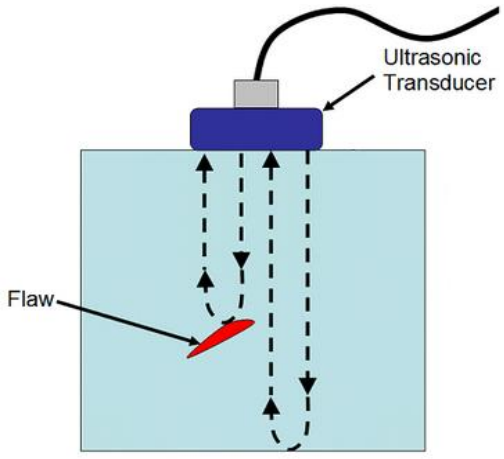

Fig. 2.1: Principle of Ultrasonic wave generation and detection [100]

The set up for ultrasonic flaw detection includes a function generator that generates an electric signal, an electro-acoustic transducer that converts the electric signal to sound wave, and a PC to display the initial and reflected pulses. Pulses of longitudinal, elastic stress waves are generated by an electro-acoustical transducer that is held in direct contact with the surface of concrete under test.

After traversing through concrete, the pulses are received and converted into electrical energy by a second transducer, or by the same transducer and is displayed on the screen. Two basic quantities are measured in ultrasonic testing; time of flight i.e., amount of time for the sound to travel through the sample, and amplitude of received signal. Based on the velocity of travel through the material and round trip time of flight through the material, thickness can be calculated as follows:

$$\mathbf{T = Vt/2} \tag{2.1}$$

where,

T is the material thickness

V is the material sound velocity

t is the time of flight

Measurement of the relative change in signal amplitude can be used in sizing flaws or measuring the attenuation of material. The relative change in signal amplitude is commonly measured in decibel. Decibel value is the logarithmic value of the ratio of two signal amplitudes. This can be calculated using the following equation:-

$$\mathbf{A_{dB} = 20\log_{10}(A_1/A_2)} \tag{2.2}$$

where,

dB represents Decibel

A_1 is the amplitude of input signal

A_2 is the amplitude of transmitted/received signal

2.2.1.2 Methods for Ultrasonic Testing

Most commonly used methods for ultrasonic testing are:

(a) Pulse Transmission method

(b) Pulse Echo method

(a) Pulse Transmission method

In the pulse-transmission method, an ultrasonic transmitter is used on one side of the material while a detector is placed on the opposite side. One unit acts as transmitter and the other unit as receiver. The beam from transmitter T travels through the material to its opposite

surface where the receiving transducer R is placed. Scanning of the material using this method will result in the location of defects, flaws, and inclusions in X-Y plane (**Fig. 2.2**). By measuring the relative change of amplitude of input and received signals, the relative severity of flaw is assessed.

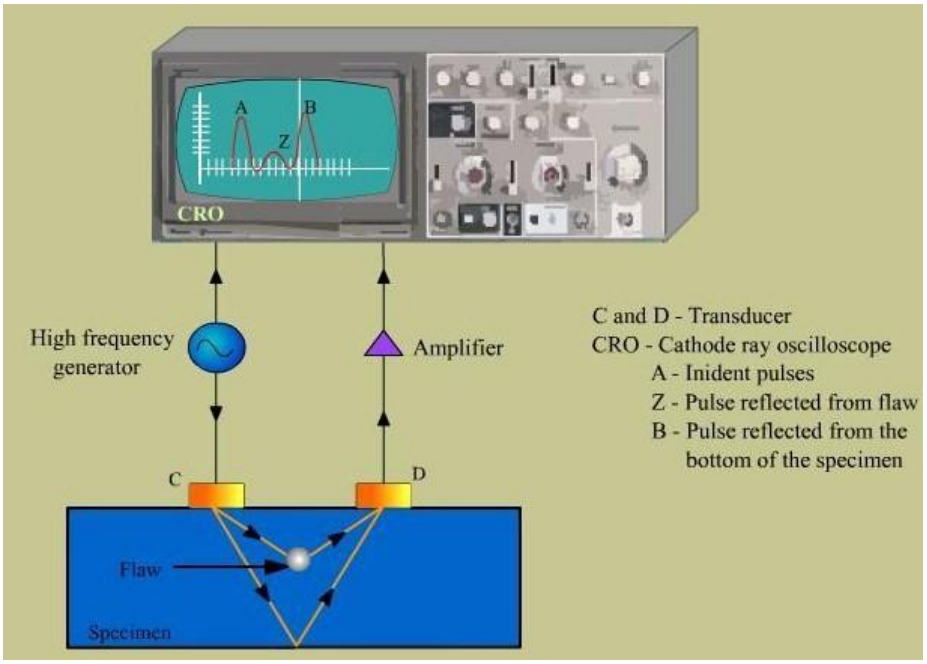

Fig. 2.2: Pulse Transmission method of testing [100]

(b) Pulse Echo method

In the pulse-echo (PE) method, a piezoelectric transducer with its longitudinal axis located perpendicular to and mounted on or near the surface of test material is used to transmit and receive ultrasonic energy (**Fig. 2.3**).

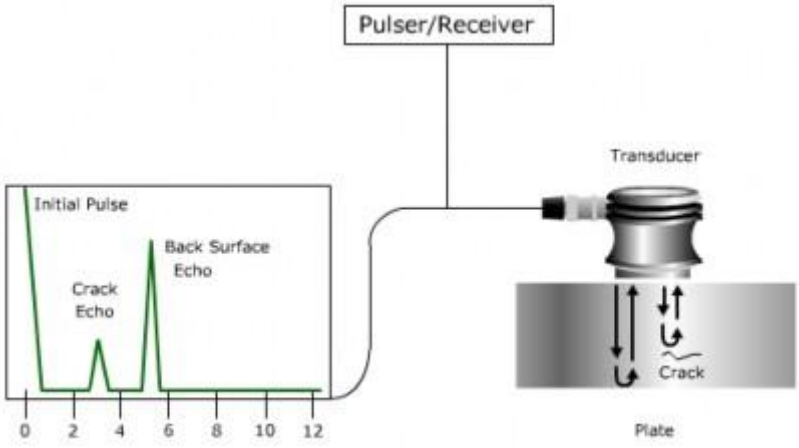

Fig. 2.3: Set-up for pulse echo method [41]

The ultrasonic waves are reflected by the opposite face of material or by discontinuities, layers, voids, or inclusions in the material, and received by the same transducer where the

reflected energy is converted into an electrical signal. The electrical signal is computer processed for display on a video monitor or TV screen. The display can show the relative thickness of material, depth into the material where flaws are located, and (with proper scanning hardware and software) where the flaws are located in the X-Y plane.

When there is an interface such as a crack, void or flaw in the wave path, part of the energy is reflected back from the interface and received by the same transmitting transducer. The reflected energy is converted into an electrical signal which is processed in a computer and digitized for display. The most commonly used method to analyse the reflected ultrasonic wave is time-of-flight (TOF) display, or A-scan. The discontinuities closer to the ultrasonic transducer are detected sooner than those farther away from the transducer. **Fig. 2.4** depicts TOF display.

In TOF display, x-axis is not typically units of time but is converted to distance. The time of flight between the excitation and reflected pulse is measured from the display. Knowing the velocity of wave, the location of defect can be calculated as follows:

$$\mathbf{D = Vt} \tag{2.3}$$

where,

D is the distance of defect from transducer end,

V is the velocity of wave, and

t is the time of flight

Thus, pulse-echo technique of ultrasonic testing can be efficiently used for detecting the extent of damage caused by corrosion in RC Structures. The current research uses pulse-echo technique for ultrasonic monitoring.

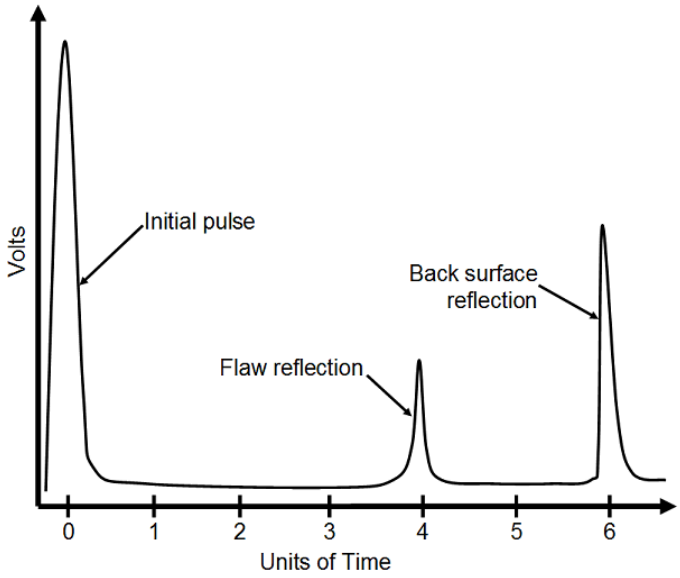

Fig 2.4: Pulse Echo method of testing [100]

2.2.2 Ultrasonic Guided Waves

Elastic waves in all frequency ranges-ultrasonic, sonic and subsonic, can be classified into two groups: Body Waves or Bulk waves and, Surface Waves or Guided Waves (**Fig. 2.5**). Body waves travel through the bulk material while surface waves propagate along the surface. Sound waves travel as a bulk wave in any elastic material where sound does not interact with the edges of material, therefore, acting as infinite extent of material. The velocity of sound in materials varies with its elastic properties which can be calculated by measuring the time of flight between two points.

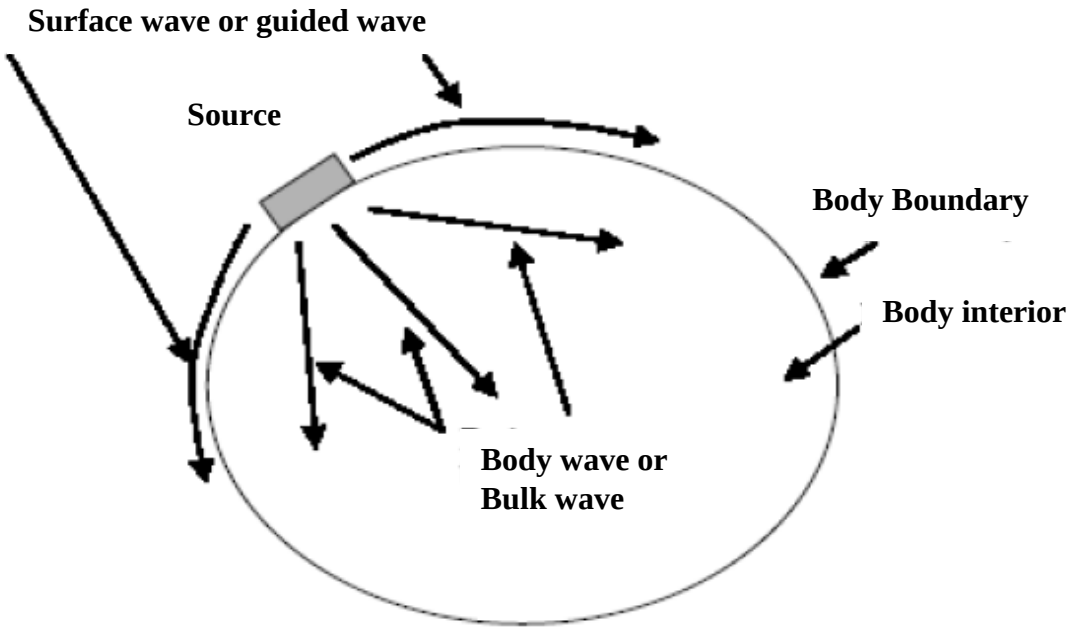

Fig. 2.5: Body waves and Surface waves generated by an ultrasonic source [38]

Velocity can be related to a variety of different material properties and conditions and is often used as a test of concrete uniformity, where velocity is usually displayed on a contour map. Large cracks and voids can be detected by an increase in travel time. However, when ultrasonic wave is constrained within the boundaries and is guided by the geometry of structure, it becomes a guided wave, that has the ability to travel long distances with minimum loss of energy. The structure that guides the wave is termed as 'waveguide'. Surface waves are often called guided waves because of the geometry of the boundary which guides them. The basic requirement for an ultrasonic wave to be a guided wave is that the thickness of waveguide must be comparable to the operating wavelength (**Fig. 2.6**). However, if the thickness of material is much greater than the operating wavelength, then bulk waves and surface waves exist (**Fig. 2.7**).

Major advantages of guided waves include quickness, low cost and improved sensitivity to a variety of defects. For a well-conditioned rebar, guided wave can propagate at least 300 feet and have the whole rebar tested in seconds based on the received time-domain signals.

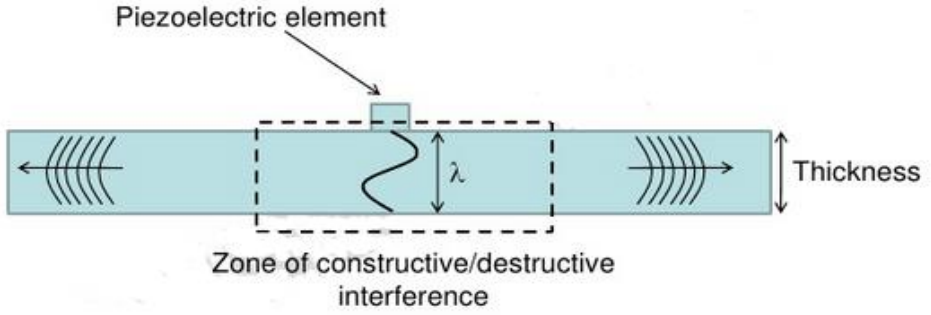

Fig. 2.6: Propagation of guided waves through a structure [101]

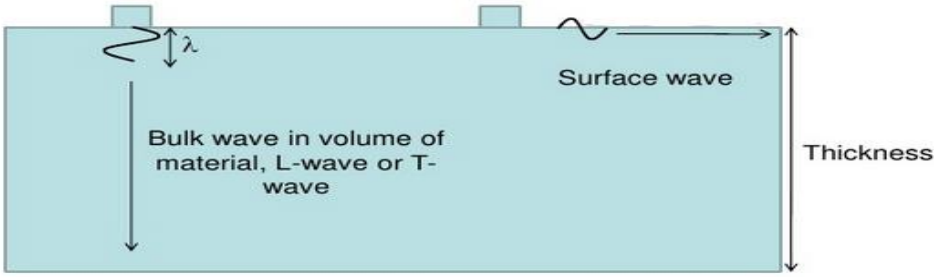

Fig. 2.7: Wave Propagation when thickness of material >> wavelength [101]

Another advantage of guided wave is that it only needs access to a small area of specimen for source loading, such as rebar end or some small area of the structure. Moreover, guided waves can propagate in the structure as a whole, and therefore, have the potential to inspect the entire structure from a single point. Thus, a guided wave excited at the exposed end of a rebar would be reflected from any defect in the bar, allowing defects to be accurately located. Guided Wave (GW) testing is one of the latest methods in the field of non-destructive ultrasonic monitoring for flaw detection. There are numerous advantages of Ultrasonic Guided Wave testing such as:

- High sensitivity, enabling the detection of small flaws
- High penetrating power, enabling the detection of flaws that are deep inside the structure
- Testing is possible through the accessibility of only one surface
- Capability of testing over long distances
- Some capability of estimating the size, orientation, shape and nature of defects
- Greater accuracy than other NDT techniques
- Easily portable

- Non-hazardous to the surrounding materials

Moreover, with this technique, frequency and mode tuning can be done to evaluate different types of deterioration or damage in structures.

2.2.2.1 Types

There are different types of ultrasonic guided waves based on the geometry of structure (waveguide) through which ultrasonic guided wave travels (**Fig. 2.8**).

(a) Plate wave or Lamb wave
(b) Bar wave
(c) Rod wave or bar wave
(d) Cylindrical guided wave
(e) Rayleigh wave
(f) Generalized Rayleigh-Lamb wave

If the structure of waveguide is a homogenous half space, then the guided wave propagating along the surface of half space is called Rayleigh wave, named after its inventor. Waves propagating through a plate like structure with two parallel stress free boundaries are known as Lamb waves. Elastic waves propagating through a hollow cylindrical or pipe structure are called cylindrical guided waves. When the guided waves propagate through a solid rod or bar, they are known as bar waves.

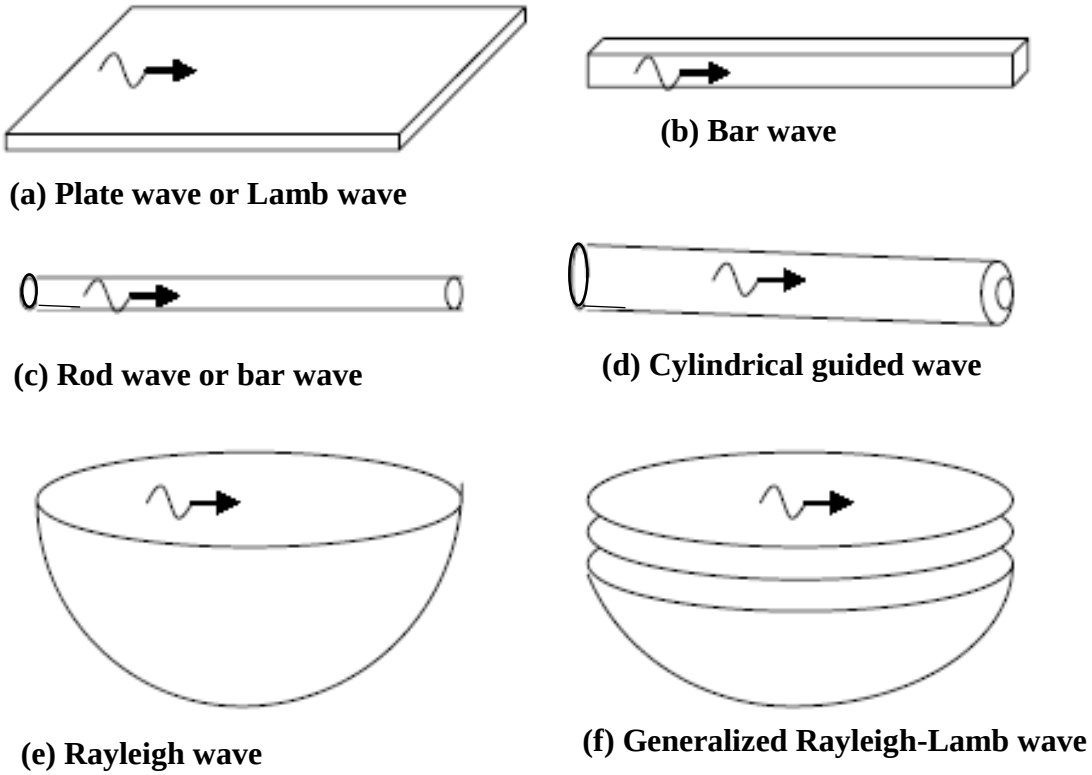

Fig. 2.8: Different types of ultrasonic guided waves [38]

2.2.2.2 Modes of propagation

A sound wave usually spreads out through the material as a bulk wave for an infinite bulk of perfectly elastic material and further decays in amplitude due to the spread of wave front. In case of a perfectly elastic steel bar, waves propagate in the form of guided waves. This is primarily due to the fact that sound waves get reflected from the structural boundaries, and energy remains in the bar as a guided wave. Due to the complex effect of the boundaries, it could be surmised that energy propagation occurs in modes with predictable properties such as mode shapes and frequencies. These mode shapes and frequencies can further be calculated from the solution of wave propagation equation. Hence, continuous propagating modes can be yielded from the solution of wave propagation equation.

The current research uses cylindrical guided waves as the test specimens are cylindrical steel bars. There are three types of propagating waves, or modes in a cylindrical waveguide:

(a) Longitudinal mode (L)
(b) Torsional mode (T)
(c) Flexural mode (F)

Longitudinal modes have radial and axial displacements, torsional modes have angular displacements and flexural modes have axial, radial and angular displacements. These modes are represented by the notation L (m, n), T (m, n) and F (m, n) respectively. In this notation, 'm' represents the circumferential displacement and is a function of cos(mθ), and 'n' represents the sequential order of mode. For longitudinal modes, the variable 'm' is zero as they are axially symmetric. For flexural modes, the variable 'm' varies as cos(mθ) around the circumference of steel bar. The other variable 'n' refers to the modes being numbered sequentially as they appear with increasing frequency. For example, L(0,1) is the notation for first longitudinal mode. In order to excite a particular mode, the appropriate frequency band is selected and these velocity-frequency relationships could be plotted as dispersion curves.

In order to describe the guided wave behaviour, the properties of the wave number, phase velocity and group velocity are studied using the dispersion curves for a free, perfectly elastic bar.

For a free elastic system such as steel bar in vacuum, the relationship between velocity of guided waves and their frequency is usually shown through dispersion curves. Two commonly used parameters for free elastic systems are phase velocity and group velocity. Phase velocity, V_{ph} is the velocity of monochromatic wave i.e., the velocity of a wave at a particular frequency.

$$\boldsymbol{V_{ph} = \frac{\omega}{\xi}} \tag{2.4}$$

where, ω is the angular frequency of wave which is related to frequency as $\omega = 2\pi f$; $\boldsymbol{\xi}$ is the real wavenumber which is related to wavelength as $\xi = 2\pi/\lambda$.

On the other hand, group velocity is the velocity of entire group of waves traversing through the structure. Group velocity, V_{gr} is related to angular frequency ω and real wavenumber $\boldsymbol{\xi}$ as

$$\boldsymbol{V_{gr} = \frac{\partial \omega}{\partial \xi}} \tag{2.5}$$

The structure of waveguide gets complicated when further layers (e.g. concrete layers) are added around the steel. The complication in structure is due to the leakage of energy from the waveguide into the embedding concrete due to a close match in the acoustic properties of steel and concrete. In such a case, the propagation of ultrasonic guided waves through the structure is dependent on elastic and damping properties of the layers. Therefore, it is essential to satisfy the stress and displacement boundary conditions. Further, the energy that is leaked into the concrete traverses as bulk waves and contributes to attenuation of the guided wave. The commonly used parameters to analyse the leaky waves are attenuation and energy velocity. Attenuation is due to two factors-leakage of energy into embedding concrete and damping effect in the waveguide material. Damping is because of non-perfect elastic nature of real materials and visco-elastic losses. Both bulk and guided waves experience damping effect, which is calculated using the damping properties of material.

- ***Attenuation***

  This section introduces the concept of wave attenuation through leakage into an embedding material. There is also another mechanism of sattenuation that occurs due to damping inherent in the waveguide material. This effect occurs because real materials are not perfectly elastic, and some attenuation of sound waves occur bevause of visco-elastic losses. This effect will occur in a bulk wave and a guided wave, and can be calculated if the damping properties of the material are known. The standard model of damping used bu Disperse assumes a constant attenuation per wavelength, which in a bulk wace means that attenuation generally increases with frequency. Although this effect has some influence on guided wave, the frequency-attenuation relationship of guided waves is much more complex and is controlled by many other factors, including leakage.

- ***Energy Velocity***

  The group velocity calculation is not valid for waves which are attenuating. The speed at which a wave packet will propagate along a structure is known as the

energy velocity, and can be obtained from data derived from the mode shapes (stress and displacement fields). The energy velocity is defined as the ratio of the power flowing along the structure to the strain energy stored in the structure as it passes. In cases such as the perfectly elastic steel bar in a vacuum, the energy velocity is equal to the group velocity. However, in leaky or attenuative systems, there are differences between group and energy velocities.

For ultrasonic testing of bars embedded in reinforced concrete, first step is to select the ideal frequency and mode of testing. Since longitudinal modes are easiest to invoke and are least attenuative out of the three modes of wave propagation, they are chosen for excitation. The different longitudinal modes at the ends of the bar are excited by varying the excitation frequencies. The selection of frequencies is done based on the phase velocity dispersion curves which are further validated by experimentally confirming the signal fidelity. High frequency low attenuative modes are found to be the best. Dispersion curves for 25 mm bar embedded in concrete are shown in **Fig. 2.9** [33]**.** The material properties of steel and concrete used for modelling in Disperse are given in **Table 2.1** [33]**.**

From **Fig. 2.9(a) and (b)**, it can be observed that the fundamental L(0,1) mode starts at zero frequency and is the fundamental low frequency lesser attenuative mode and hence preferred for ultrasonic investigation. The remaining higher modes start from a higher cut-off frequency with a plateau kind of region around the steel longitudinal bulk velocity line. Only L(0,7) mode exhibits a distinctive pattern as it links the subsequent plateau regions to form a low leakage mode that propagates close to the longitudinal bulk velocity of the steel. Hence, L(0,1) at 0.1 MHz and L(0,7) at 1 MHz are selected for ultrasonic investigations on 25 mm bar in concrete. From the attenuation dispersion curves in **Fig. 2.9(c)**, it can be confirmed that L(0,7) mode is the least attenuative mode for 25 mm bar embedded in concrete. These two modes are primarily used for corrosion monitoring in this entire study.

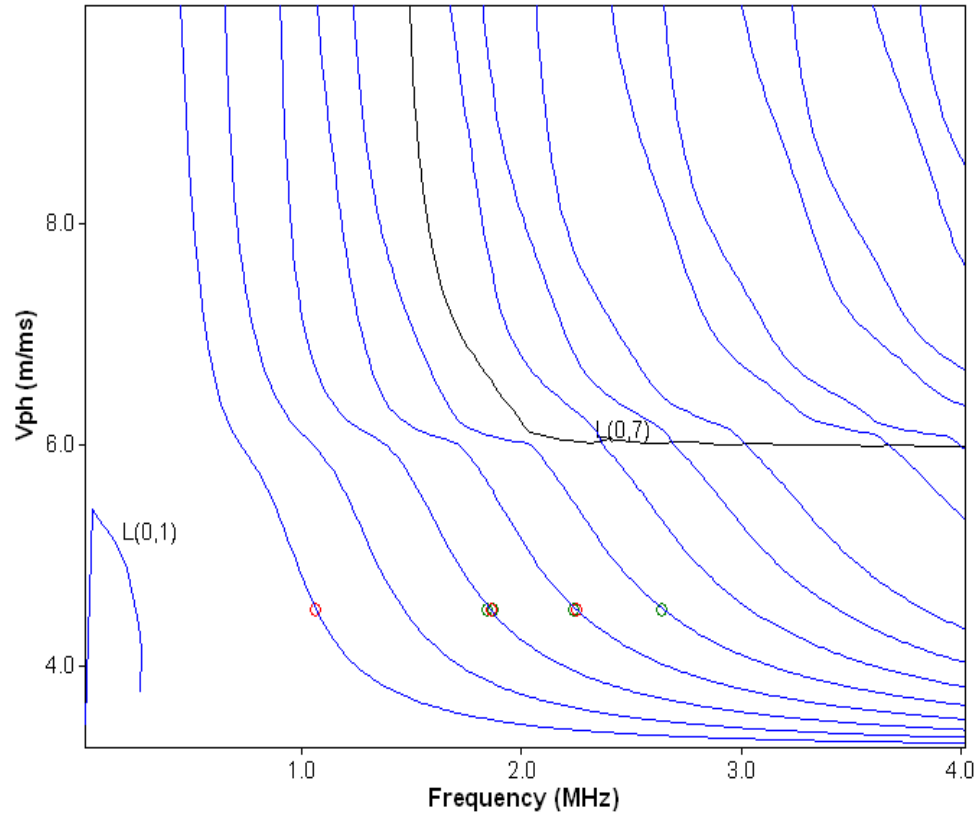

(a) Phase velocity dispersion curve

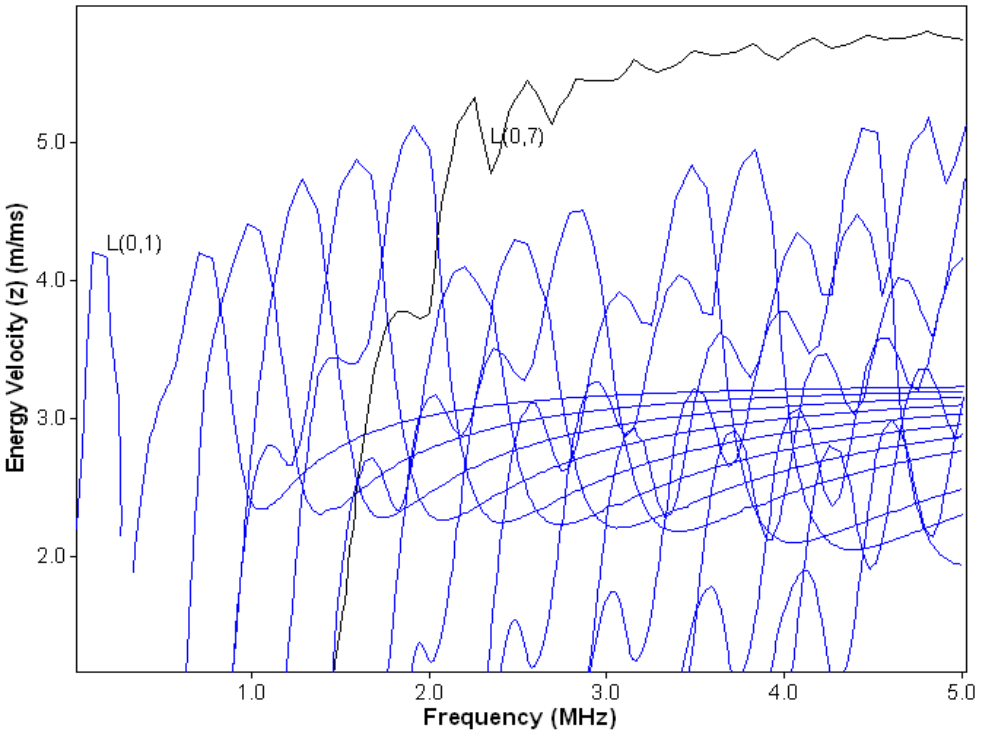

(b) Energy Velocity (z) vs frequency

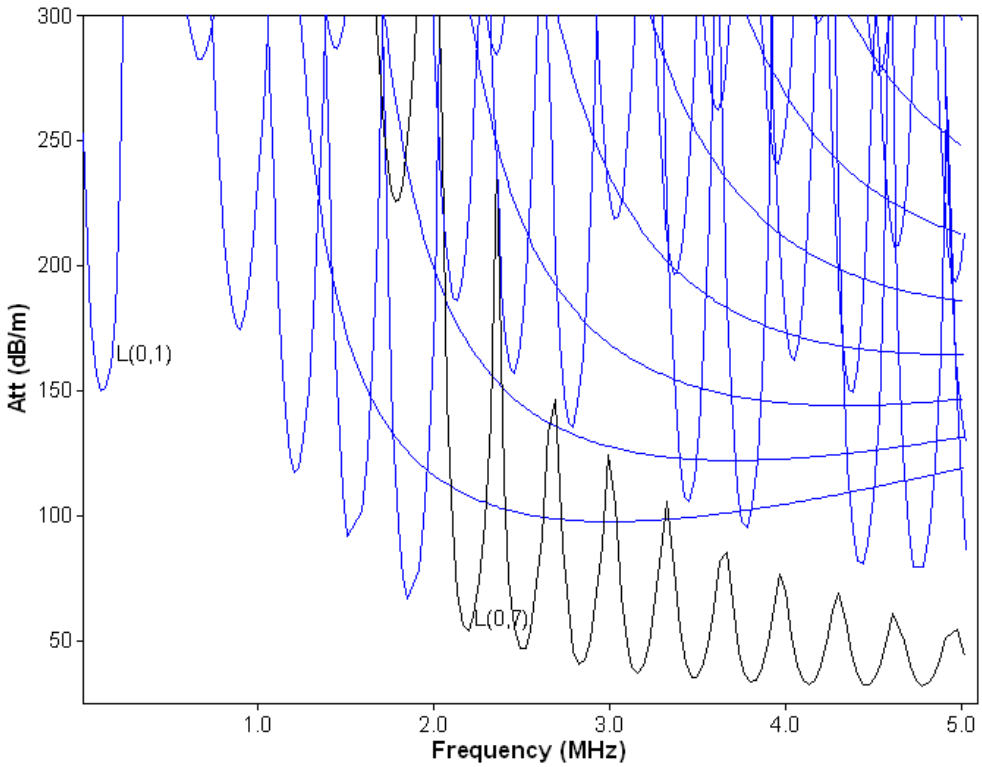

(c) Attenuation dispersion curves

Fig. 2.9 Dispersion Curves for 25 mm bar in concrete [33]

Table 2.1 Material Properties of steel and concrete [33]

S.No.	Material Property	Steel	Concrete
1	Modulus, E (GPa)	210	29.6
2	Density (ρ), (kg/m^3)	7932	2200
3	Longitudinal Attenuation (dB/m)	0.003	0.2
4	Shear Attenuation (dB/m)	0.008	0.5
5	Longitudinal Velocity (m/s)	5960	4100
6	Shear Velocity (m/s)	3260	2300
7	Poisson's Ratio	0.2865	0.27

For exciting the longitudinal guided waves in bars, a typical ultrasonic testing system is used. It consists of a pulser/receiver (DPR 300, JSR Make), transducers (Karl Deutsch Make), and display devices. Driven by the pulser, the compression transducer generates ultrasonic

pulse that propagates through the bar in the form of longitudinal waves. Ultrasonic testing of the bar can be done in both Pulse Echo and Pulse Transmission modes. A single contact transducer is used to generate and receive wave signatures in the Pulse-Echo method. Two contact transducers are used for sending and receiving the waveforms in pulse transmission method. For generating L(0,1) mode and L(0,7) mode in 25 mm steel bar, the transducers(Karl Deutsch Make) with a central frequency of 0.1MHz and 1 MHz respectively, are used. The transducers are driven by a Pulser/Receiver system with a particular gain (0-66dB) and maximum input voltage if 475 V. A computer digitizer card (Acquiris Make- 12 Bit resolution) is used to capture the received signal and its processing. The transducer is mounted in a holder and attached to the specimens using an industrial coupling gel**.** The excitation signal consists of a compressive spike pulse with duration ranging from 10-70 ns. The received signals are further analysed using origin software and the value of peak amplitude is noted from each signal. The peak amplitude values obtained from all signals are then normalised and thereafter plotted as peak to peak voltage ratio against time.

2.2.2.3 Limitations

One disadvantage of ultrasonic guided waves for monitoring corrosion in reinforced concrete is the limitation of inspection range for certain modes and frequencies. Unlike ultrasonic guided wave propagation in other multi-layered systems, such as a metal pipeline in air, wave energy in steel bars embedded in concrete is lost (i.e. attenuated) at high rates due to leakage into the surrounding concrete. Apart from leakage of ultrasonic guided waves, the reflection coefficient of defects such as breaks and patches also causes a problem. The recent discovery of high frequency, low-leakage guided modes [33] has the potential to reduce the attenuation due to leakage, although the reflection coefficients from defects need to be determined. In addition, lower frequency modes may offer an alternative to the high frequency modes for detection of surface/interfacial damages. Hence, in the present work, it is proposed to use high and low frequency ultrasonic guided wave modes for corrosion detection in steel embedded in concrete.

Another disadvantage of ultrasonic guided wave technique is the difficulty to find flaws in complex sized or shaped structures, where reflections from multiple features are not resolved in time, and it becomes impossible to detect an individual reflection or an extra reflection from a defect. Hence, a reliable structural health monitoring system for complex structures requires a great deal of research to find a method that can compensate the benign changes such as temperature variations, moisture uptake, ageing, etc. [42]. Some other limitations of ultrasonic

guided wave technique are extensive technical knowledge required for efficient monitoring, difficulty to inspect materials that are rough, irregular in shape, very small or non-homogenous and requirement for couplants to provide effective transfer of ultrasonic wave energy between transducer and the inspected structure.

In this research work, it is proposed to use longitudinal ultrasonic guided waves to pick up corrosion damage in rebars in concrete.

2.2.3 Review of Ultrasonic Guided Waves for Corrosion Monitoring

A review of the latest works utilizing ultrasonic guided waves for corrosion monitoring in concrete is briefed below.

Pavlakovic *et al.* [33] investigated the behaviour of ultrasonic guided modes of minimum attenuation with a steel bar embedded in low impedance grout, acting as a waveguide. This was done in order to maximise the inspection range of tendons. Two test specimens were constructed, comprising of a mild steel bar at the centre of a plastic pipe filled with grout. Both pulse-through and pulse-echo tests were carried out. It was found that the dispersion curves of circular steel bar imbedded in lower impedance medium exhibited a series of modes having attenuation minima at higher frequencies. The results were reported to be useful for inspection of tendons in post-tensioned bridges at locations close to the anchor points at the ends of the bridge. Another important point made was that the non-leaky mode that exists in the case of a flat plate imbedded in cement grout does not exist in the corresponding case of a circular bar imbedded in grout although it may exist for other material combinations.

Na *et al.* [34] investigated the feasibility of detecting and quantifying delamination at the steel-concrete interface using ultrasonic guided waves. The experiments were performed on three sets of specimens. Specimen sets 1 and 2 comprised of four cylindrical structures each with different amounts of separation (0, 25, 50, 75 % of concrete steel interface). Specimen set 3 comprised of three concrete beam structures- specimen with different amounts of separation without stirrups, specimen with different amount of separation with stirrups and, specimen with same amount of separation at different positions with stirrups. Ultrasonic testing was conducted in through transmission mode. Two experimental set ups were devised for both relatively high and low frequency transducers and four Transmitter/Receiver arrangements (TRA1, TRA2, TRA3, TRA4) were designed to generate, propagate and receive guided waves through steel bars and concrete. Two annular solid couplers of different dimensions were used to launch flexural cylindrical guided wave modes along the steel bar, and an angular solid coupler holder was used to launch lamb waves in concrete beams when steel bar was not accessible. Petroleum

jelly was used as a couplant. Experiments were conducted 4-8 times with every arrangement to investigate the consistency of results. The experimental investigation showed that the efficiency of annular shaped holders used for exciting flexural cylindrical guided wave modes was comparatively more than other holders. It was observed that though signals generated by relatively larger angles of incidence were more sensitive to discontinuities, however the propagating signal strength for a large incident angle was not always higher than the signals generated by smaller incident angles. It was concluded that the ultrasonic guided wave technique can be applied to predict or quantify the degree of separation or delamination using pulse through transmission mode. However, other techniques such as pulse-echo method are required to predict the exact location of separation.

Miller *et al.* [37] investigated the changes in delamination between reinforcing steel bar and concrete due to corrosion, using ultrasonic guided waves. Electromagnetic acoustic transducer (EMAT) and piezoelectric transducer (PZT) were used for corrosion monitoring. They reported that ultrasonic guided waves have the capability of distinguishing corrosion and delamination. The study confirmed the reliability of ultrasonic guided wave for health monitoring of reinforced concrete structures. It was suggested that ultrasonic guided waves are sensitive to the type of steel used and to the rib patterns on the reformed steel bars.

Na *et al.* [38] investigated the feasibility of ultrasonic guided wave testing technique for detecting delamination at GFRP rod-concrete interface. The experimental investigations involved ultrasonic testing in through transmission mode for both glass fibre reinforced polymer and steel bars embedded in concrete to study the effect of high attenuation shown by GFRP. Two transmitter-receiver arrangements with transducer's center frequency of 50 kHz, 150 kHz and 1 MHz, were applied to propagate ultrasonic guided waves through the specimens, and ultrasonic tests were carried out. It was observed that the testing sensitivity was not affected by the high attenuation of GFRP bar and therefore, ultrasonic guided wave technique can be applied equally well for detecting delamination at GFRP/Concrete and Steel/Concrete interface. The dispersive behaviour shown by the ultrasonic guided waves was also studied. The specimens were modelled as GFRP bars of finite diameter embedded in an infinite concrete medium, for wave mode identification. Ultrasonic testing was done to obtain the material properties, and these were used to plot energy velocity curves and attenuation dispersion curves. The experimental observations from the curves conclude that ultrasonic guided wave technique can be used for GFRP-concrete interface testing.

Beard *et al.* [39] proposed a method using guided ultrasonic waves to inspect grouted steel tendons, anchors and rock bolts for corrosion and fracture. Two types of reinforcing tendons

were constructed- single wire (5 or 7 mm in diameter) and 15 mm seven wire strands. A pulse-echo technique was carried out from the free end of structure to measure the attenuation experienced by the wave in short lengths of grouted tendons. The amount of attenuation that the wave experienced because of leakage into the embedding material and material losses, was used to evaluate the reflection coefficient of modes from different geometry breaks. The measurements of attenuation and reflection coefficients were used to determine the maximum length of tendon that can be inspected using this method. The experimental results illustrated that the inspection range for a complete break was limited to about 1.2 and 0.8 m for 7 and 5 mm dia wires respectively. For 15 mm stranded tendons, the inspection range was limited to about 1.5 m for the center wire and about 0.5 m for the six outer wires. This indicate that the use of ultrasonic guided waves for the inspection of small diameter tendons would be limited to provide confirmation of defects in localized areas, due to high level of attenuation and poor reflection of modes. However, it was seen that with an increase in tendon diameter (25-30 mm), the attenuation reduces considerably. The rebars and grouted bolts with a large steel diameter, generally have flat ends which are good reflectors of low-leakage modes.

He *et al.* [41] investigated the use of ultrasonic guided waves in a two-layered structure (composed of solid steel and semi-infinite layer of concrete) to measure the length of steel rod embedded in concrete and to estimate the amount of delamination between a steel rock bolt and concrete. A Semi-Analytical Finite Element Method (SAFEM) model was used to calculate the high frequency theoretical wave structures for a rod embedded in concrete. The ultrasonic testing was conducted on six specimens with different amounts of delamination (0, 25, 33, 50, 75 and 100% of the entire rod length) using pulse-echo technique. The experimental results illustrate that, in order to determine the length of an embedded rod, one must use guided wave modes at higher frequencies. A transducer with a center frequency of 1 MHz or higher was found to be suitable for length determination. For most frequencies above 1 MHz, there was a little amplitude difference between a completely bonded interface and a 33% delaminated specimen. The lower frequency ultrasonic guided wave modes showed better results while estimating delamination at the steel-concrete interface. It was concluded that any transducer with a center frequency larger than 2 MHz is not suitable for delamination estimation. It was also concluded that ultrasonic guided wave pulse-echo technique can be applied to inspect large lengths of embedded rods.

Cawley [42] studied the application of ultrasonic guided waves for long range inspection of large structures such as airframes. The problem of overlapping of reflections from different features in complex structures was highlighted. An increase in feature density made it

impossible to analyse an individual reflection or, an extra reflection from a defect. This problem was resolved by subtracting the current response from a baseline measurement taken when the state of structure was known and this made it possible to monitor the changes in the response of structure. However, this method required a high degree of signal stability with time in the absence of damage, or a scheme that could correct benign changes such as temperature variations. One such scheme, 'temperature compensation' was implemented and considerable results were obtained. It was emphasized that some other benign changes such as moisture uptake in adhesives are also a matter of concern and a great deal of research is required to realise a reliable health monitoring system for complex structures.

Ervin *et al.* [43] investigated ultrasonic guided wave modes in both low and high frequency ranges capable of monitoring corrosion in reinforced concrete. The fundamental longitudinal modes L(0,1) and L (0, 9) were chosen for experimental testing at low and high frequency respectively. L(0,1) mode was chosen because it shows negligible signal loss due to material absorption. It was used to access interfacial damage between steel and mortar. L (0, 9) mode was selected because it is the fastest and lowest attenuating mode in the system. Experiments were conducted to examine the effect of reinforcing ribs, water and mortar on low and high frequency ultrasonic guided waves. Ultrasonic testing was carried out in a through transmission mode on rebar in air, rebar immersed in water, rebar embedded in mortar, corroded rebar in air and reinforced mortar specimens undergoing accelerated corrosion. Testing showed that reinforcing ribs has an attenuative effect on ultrasonic guided wave propagation only in certain frequency ranges. Ultrasonic guided wave was less affected at higher frequencies, and negligibly affected when the wavelength is much longer than the characteristic dimension of the rib. Testing confirmed that L(0,1) mode has some sensitivity to water over the frequency range tested. It was observed that the lowest frequencies of L (0, 9) mode show sensitivity to water while the higher frequencies show diminished sensitivity. For the bars embedded in mortar, testing showed that the low frequency mode was highly attenuated, resulting in monitoring of relatively short distances (e.g. 1 m). The attenuation shown by L (0, 9) mode was much smaller than L(0,1) mode. For rebar specimens extracted from accelerated corrosion tests, testing showed that L(0,1) was not substantially affected in the lowest range. However, interesting results were seen for L (0, 9) mode. It was observed that there was no frequency content between frequency domain peaks when the corrosion damage frequency was low. As the corrosion level increased, the frequency content between frequency domain peaks, referred to as 'web' frequencies started to increase. For rebar specimens undergoing accelerated corrosion, testing showed that L(0,1) was highly attenuated such that it was not detected until

after corrosion had initiated and corrosion product accumulation caused mortar cracking. Once detected, L(0,1) mode was sensitive to the combined effect of bond deterioration and mortar stiffness reduction. The results indicate that the signal strength of L(0,1) mode was increasing as the mass loss was advancing. L (0, 9) mode was relatively insensitive to the surrounding interface conditions at high frequencies. This allowed the monitoring of steel cross sectional area and bar topography, from the onset of corrosion to severe pitting.

Sharma and Mukherjee [45] discussed the use of longitudinal ultrasonic guided waves to monitor notch and debond defects in steel bars in concrete simulating pitting and delamination phenomenon caused by corrosion. The low and high frequency ultrasonic pulse echo and pulse transmission technique was used for early detection of damages in steel in RC beams. The exact location and magnitude of damage was indicated by efficient combination of the two ultrasonic monitoring techniques. Ultrasonic guided wave monitoring utilizing specific core and surface seeking modes was applied to identify corrosion mechanism in a bar embedded in concrete. In general, huge pitting and non-uniform area loss highlighted by severe signal attenuation marks chloride corrosion, which was well unravelled by core seeking mode. It began with delamination shown by signal rise with surface seeking mode. It was concluded that through judicious selection of ultrasonic modes, the complete corrosion mechanism in RC structures can be successfully identified.

Sharma and Mukherjee [20] investigated the type of corrosion mechanism in chloride and oxide environments in RC beams. Ultrasonic guided waves with specific core and surface seeking modes were used for monitoring rebar corrosion in beams. It was observed that in case of chloride corrosion in beams, when core-seeking mode was propagated, the signal was highly attenuated, thus indicating pitting and non-uniform area loss. When surface seeking mode was propagated, there was an initial rise in the signal strength and then a fall, thus indicating delamination followed by local loss of material. In case of oxide corrosion in beams, it was observed that when core-seeking mode was propagated, there was a slow fall in signal strength, indicating the absence of pitting. When the surface-seeking mode was propagated, there was an initial drop in the signal due to the pressure build up by the formation of corrosion products, indicating a slow corrosion rate and localized corrosion and eventually, a gradual rise in signal strength was observed, indicating slow bond deterioration. The ultrasonic voltage trends of the received signal in both chloride and oxide corrosion specimens using surface-seeking and core-seeking mode were analysed to successfully monitor the mechanism and rate of rebar corrosion. Simultaneous destructive tests were also carried out on RC beams, and it was found, that non-destructive Ultrasonic technique correlate well with the destructive technique.

Sharma and Mukherjee [47] reported non-destructive evaluation of reinforcing bars that are corroding in the presence and absence of chlorides utilizing ultrasonic guided waves. Ultrasonic guided wave monitoring utilizing specific core and surface seeking modes to identify the type, rate, and mechanism of corrosion in a reinforcing bar in concrete subjected to different exposure conditions was discussed. The experimental investigation involved monitoring of RC beams undergoing accelerated impressed current corrosion. In general, huge pitting and non-uniform area loss highlighted by severe signal attenuation marks chloride corrosion, which was well picked up by core seeking mode. It began with delamination shown by signal rise with surface seeking mode. In oxide corrosion, the rate of corrosion was slow, localized, and marked by slow bond deterioration as depicted by signal strength rise in surface seeking mode. Pitting was insignificant in core seeking mode in oxide corrosion (OC). Thus, it was observed that through a judicious selection of ultrasonic modes, different types of corrosion in RC structures can be successfully identified. Bars at different stages of corrosion were ultrasonically monitored in both oxide and chloride environments to explore the ability of ultrasonic guided waves to predict the level of deterioration of bars. It was done successfully by correlating ultrasonic voltage ratio with destructive parameters of mass loss, tensile strength and bond strength in the two common corrosion environments. It was concluded that, although the use of ultrasonic guided waves is effective in identifying the presence of corrosion in rebar in widely varying environments, the method needs access to the ends of rebar. At site, bars that are most susceptible to corrosion need to be exposed at the ends to perform the test. Also the signal-to-noise ratio should be above the ground noise level.

Sharma and Mukherjee [48] reported a non-contact, in-situ and non-destructive methodology for monitoring corrosion in submerged plates using ultrasonic guided waves. Two modes at different frequencies i.e., L(0,1) and L(0,7) modes at 0.1 MHz and 1 MHz were used for monitoring corrosion-induced damage in plates. Along with the ultrasonic signals, mass-loss, stress-strain behaviour and tensile strength of the plates were also monitored. It was observed that the study could be highly useful in developing a non-destructive technique for monitoring progressive corrosion in plates and assessing their deterioration in strength, stiffness and mass loss that would ultimately aid in estimation of the residual life.

Moustafa *et al.* [49] studied the corrosion monitoring of post-tensioned concrete structures using fractal analysis of guided ultrasonic waves. Piezoelectric were permanently mounted on the steel tendon and were used to transmit and receive guided ultrasonic waves. The corrosion monitoring was performed through the examination of the fractal dimension of ultrasonic guided wave measurements over time. The corrosion was accelerated on two 7 wire steel

strands embedded in concrete blocks. A new outlier detection algorithm has been proposed to enhance the sensitivity of the technique to the corrosion-induced damage.

Farhidzadeh *et al.* [50] investigated the corrosion-induced damage in steel strands using guided ultrasonic waves. A reference free algorithm based on the dispersion curves, continuous wavelet transform and wave velocity measurements, was proposed in order to estimate loss of cross-section of the strand. It was clearly exhibited that the diameter of the wire could reasonably be estimated without any baseline as a reference.

Beena *et al.* [51] proposed a non-contact damage monitoring methodology using guided ultrasonic waves for the detection of corrosion-induced damage in Concrete filled steel tubes (CFST) sections. The specimens were monitored in pulse transmission mode. It was reported that ultrasonic guided waves clearly picked up the notch and the debond defects in CFST sections due to corrosion. The loss-of cross-sectional area and pitting due to accelerated corrosion, was also well picked by ultrasonic guided waves. It was suggested that non-contact ultrasonic guided wave approach could be effectively used for degradation monitoring in CFST sections.

2.3 ACOUSTIC EMISSION TECHNIQUE

Acoustic emission outshines the existing NDT techniques with its ability of monitoring dynamics process of deformation. The material deformation can be due to minor or major cracks, bond failure, yielding, etc. The deformation of structure leads to release of energy which generates transient elastic wave, known as ‘acoustic emission’ that traverse through the structure [50]. The acoustic waves vary with the rate and size of structural deformation and can be easily recorded by placing sensors on the surface of structure.

The following sub-sections provide an explanation of AE mechanism, terminology, equipment, signal analysis and its application in corrosion monitoring of RC structures.

2.3.1 Principle of AE

The deformation in any structure which may be due to localized sources such as cracks, change in stress planes etc. release acoustic emissions in form of transient elastic waves. These transient elastic waves/acoustic emission traverse through the structure and are finally recorded by piezoelectric transducers that are mounted on the structure itself. The mechanical acoustic emissions are converted into electrical AE signals which is further converted into an electronic

data set. This data set is further analysed and the recorded data is plotted into graphs. **Fig. 2.11** shows the process of generation and recording of acoustic emissions.

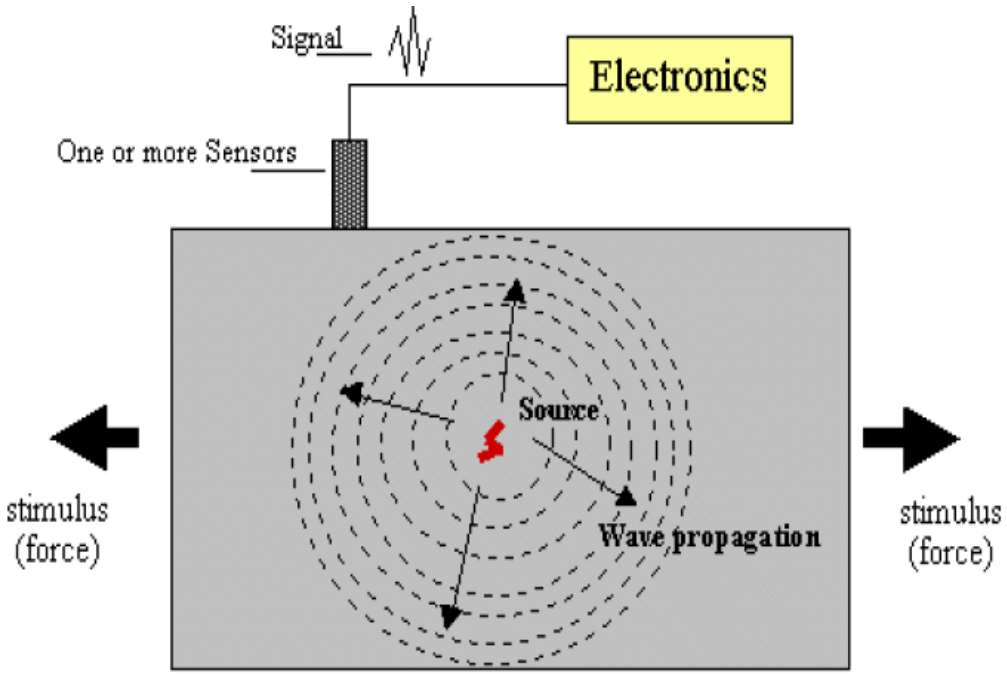

Fig. 2.11: Principle of Acoustic Emission [71]

Broadly, an AE signal is classified into two types – continuous signal and transient signal. A continuous signal, as shown in **Fig. 2.12**, is the one whose amplitude varies continuously for a long duration and it can occur due to movement or dislocation. A transient signal, as shown in **Fig. 2.13**, occurs for a short time duration and is usually called a 'burst' signal. It can occur due to onset or propagation of cracks.

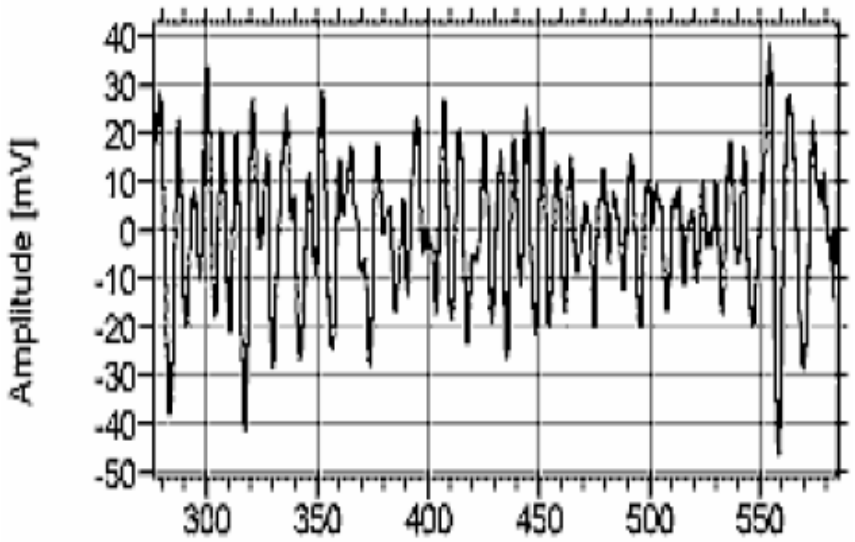

Fig. 2.12: Continuous Signal [71]

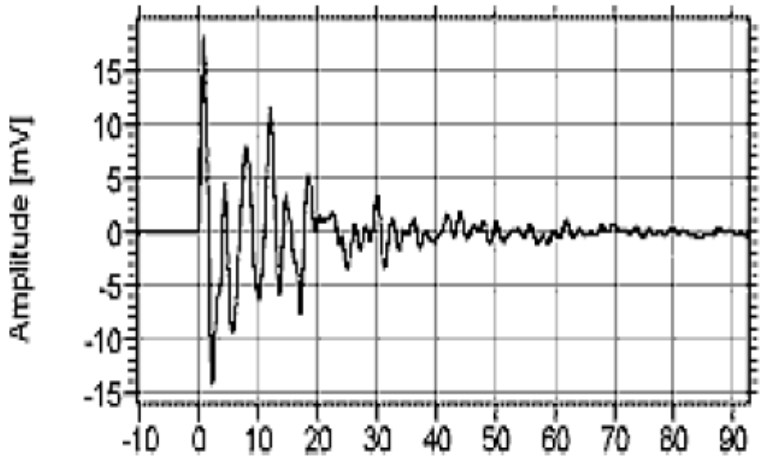

Fig. 2.13: Transient Signal [71]

The detection of dynamic process of damage of structures with the help of consequent release of energy (acoustic emissions) distinguishes AE testing from all other NDT methods. AE testing can be used for all kinds of materials and structures subjected to some loading. AE testing can effectively prevent some catastrophic failures of system with hidden or unknown discontinuities. However, signal attenuation, noise material heterogeneity are few limitations of AE testing.

Acoustic emission monitoring is believed to be very old and is reported to be used by artisans for quality assessment of their manufactured pottery [54]. Fuyuhiko Kisinouye carried out the first experiment using acoustic emission testing in 1933 and later in 1936, some AE experimentation was carried out by Friedrich Forster and Erich Schhil. In 1948, Warren Manson, Herbert Mcsimin and William Shockley used AE testing for measuring dislocation of 0.1 nm displacements.

The first substantial research work on AE phenomenon was reported by Josef Kaiser in 1950, popularly known as the Kaiser effect. In 1954, Bradford H. Schofield concluded that AE is mostly a volume effect and not a surface effect. Finally, in 1960, AE testing was categorised as a unique NDT technology.

2.3.2 AE Parameters and their significance

Primarily, AE monitoring has two aspects 1) to detect and record the acoustic emission generating from a damage source 2) to locate the origin of damage. After acoustic emissions are recorded, the detected waveforms are analysed to understand the characteristics of source of acoustic emissions both qualitatively and quantitatively. The characteristics of damage source, distance between the source and AE sensor, characteristics of AE sensors etc. are the principal factors that influence the recording of AE signals.

The AE test set-up involves mounting of AE sensor on the surface of the material with the help of an adhesive or a tape. The sensors record the signals originating from the deformation inside the material. The sensors are further connected with the pre-amplifiers and the amplified signal is displayed on the display device. The various properties of recorded AE signals such as amplitude, counts, measured area under the rectified signal envelope (MARSE), duration, and rise time (**Fig. 2.14**) are studied. The discussion of the parameters is given below:

1. *Threshold*- It is the voltage level that is set to eliminate the noise. During the AE testing, a large no. of acoustic emission signals are generated and are recorded by the sensors. In order to effectively discern the useful AE signals from the recorded signals, threshold value is set. The set-threshold value allows the user to discard the unwanted noise at the testing site. The AE sensors record AE signals only when it reaches the threshold value. The threshold value is set in the hardware set-up. Usually, all the AE sensors are set with the same threshold value but if an AE sensor develops a noise problem during the test, the threshold value could be raised so that only the useful data is recorded.
2. *Hit*- A hit may be defined as a transient signal recorded by the AE sensor which is above the threshold value. It indicates that an AE wave is detected by a sensor mounted on the surface of structure. The entire AE data is recorded in terms of AE hits. It directly indicates some kind of changes undergone by the structure.
3. *Arrival time*- It is the time when the recorded signal exceeds the already set-threshold value.
4. *Peak Amplitude*- It is the maximum absolute voltage value of AE signal expressed in decibels.

   $$\boldsymbol{V_{dB} = 20 \log\left(\frac{V_{max}}{1\mu V}\right) - (\text{Preamplifier gain in dB})} \quad (2.6)$$

   Since they are represented on the logarithmic scale, they are considered to be the best indicators of how strong the emissions are. The threshold values are set in terms of amplitude only. The values of recorded amplitudes truly indicates the nature of the source of acoustic emissions

5. *Rise time*- It is the time interval from arrival time to peak-amplitude time of AE signal. Rise time is usually used to filter out the correct acoustic emissions. For example, if rise time is short i.e. from 10 to 15 seconds, this further implies that the AE sensor got triggered in the middle of a signal and the registered arrival time for that sensor could be wrong. The entire data related to this acoustic emission could be discarded. If the recorded rise time is very long for a particularly recorded signal (specifically when it is greater than half the signal strength), this negates the transient nature of the signal. Such a recorded AE signal could

also be ignored. Hence, the signal rise time could clearly indicate whether the received signal is coming from a real source of stress change or it is distorted and hence, may be extraneous.

6. *Duration*- It is the time for which AE signal remains above the threshold value. This parameter could also reveal important information about the intensity of damage. For example, if the source of emission is strong, duration of the hit will be more and vice-versa.
7. *Counts*- It is the number of times AE signal exceeds the threshold value within the duration. It is the first parameter to be used for the analysis of acoustic emission. A count is collected every time a signal crosses the threshold. The plot of count versus time gives the entire history of acoustic emissions from the material. The parameter primarily depends on threshold amplitude, type of AE sensor, the gain and bandwidth of the pre-amplifier, the quality of acoustic adhesives and the arrangement of sensors. If a single count is registered for a particular signal, it is discarded for electronic noise. It is considered a single acoustic emission signal contains many oscillations.
8. *Signal Energy*- It is defined as the integral of the voltage squared versus time plot. Signal energy is very difficult to measure with an analog circuit because of the dynamic nature of the signals. With an analog circuit, only if the signals have same characteristics, signal energy could be measured. Therefore, instead of signal energy, absolute energy is calculated. It is generally expressed in the form of absolute energy or measured area under rectified signal envelope. Absolute energy is obtained from the integral of squared AE signal voltage divided by reference resistance over the duration. The only limitation of absolute energy is that it covers only digitized signal length such that if the signal length is longer, the total recorded energy will be far lesser than the actual energy.
9. *Event*- It is the group of AE hits recorded by a number of sensors from the same place of material deformation. The AE event is primarily utilized for source location. With the help of time of arrival and the known geometry of the structure, the location of the course of acoustic emission can be figured using triangulation.
10. *Signal Strength*- Signal strength is usually used for damage evaluation of structures. As per the Physical Acoustic Corporation (PAC), signal strength is defined as the integral of the rectified voltage signal over the duration of the AE waveform packet. It is also referred to as relative energy i.e., the amount of energy released by the material or a structure. It is a direct function of amplitude and duration of the recorded AE signal. It is calculated over the entire dynamic range of the AE signal and is totally independent of the gain.

Fig. 2.14 shows the basic features of an AE signal.

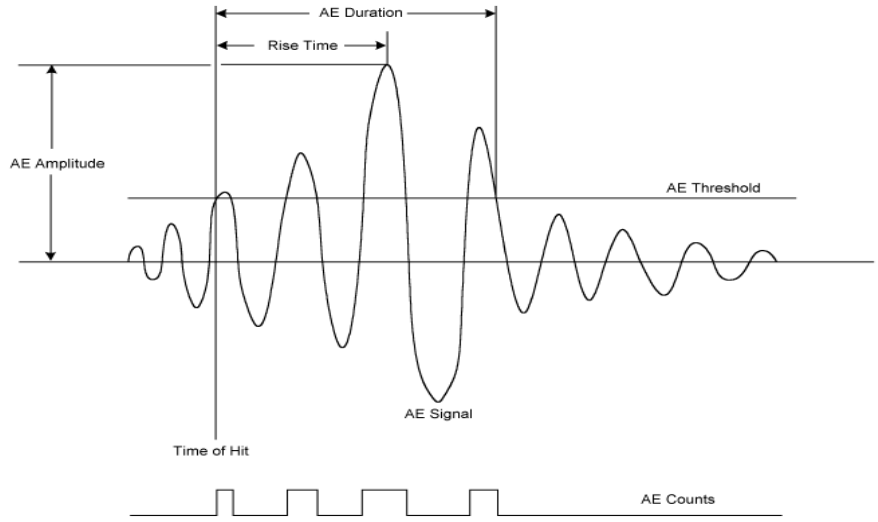

Fig. 2.14: Basic features of AE signal [75]

The other component of AE testing is locating the areas of active damage and mapping of entire cracking process. Time of arrival (TOA) approach is most commonly used for source locations and comes as an inbuilt in the AE win software. This approach involves multiple sensors mounted on the surface of concrete in an array and using the time delay between the pairs of sensors within the array.

Arrival time is the instant a signal crosses a pre-set threshold value. This threshold amplitude is an important parameter in AE studies as it describes the point at which the system starts recording the signal waveform. It is to be noted that threshold values are often set in order to remove as much low amplitude noises as possible, but care must be taken so that no genuine signals are missed. A simple illustration for linear source location is given in **Fig.**

Fig. 2.15. Linear source location [75]

If the distance between two sensors S_1 and S_2 is known (D), the distance between the source and sensor S_1, L_1 can be calculated as:

$L_1 = c.\ T_1,\ L_2 = c.\ T_2,\ L_1 - L_2 = c(T_1 - T_2) = -c.\Delta t$ (2.7)

$L_1 + L_2 = D,\quad L_1 = 0.5(D - \Delta t.c)$

Where T_1 and T_2 are the times of arrival of signal at two sensors, Δt is the time difference $T_2 - T_1$ and c is the speed of AE waves.

An illustration of two dimensional source location is shown in **Fig. 2.16.** Three sensors S_1, S_2 and S_3 are placed on the surface of a structure at locations(x_1, y_1), (x_2, y_2) and (x_3, y_3). The location of the source to be determined, is (x_s, y_s). The distance between the sensors are D_1, D_2 and D_3 (which are known), and the distances between the source and the sensors are d_1, d_2 and d_3 (need to be solved). t_1, t_2 and t_3 are the times the signal reached sensors S_1, S_2 and S_3 respectively.

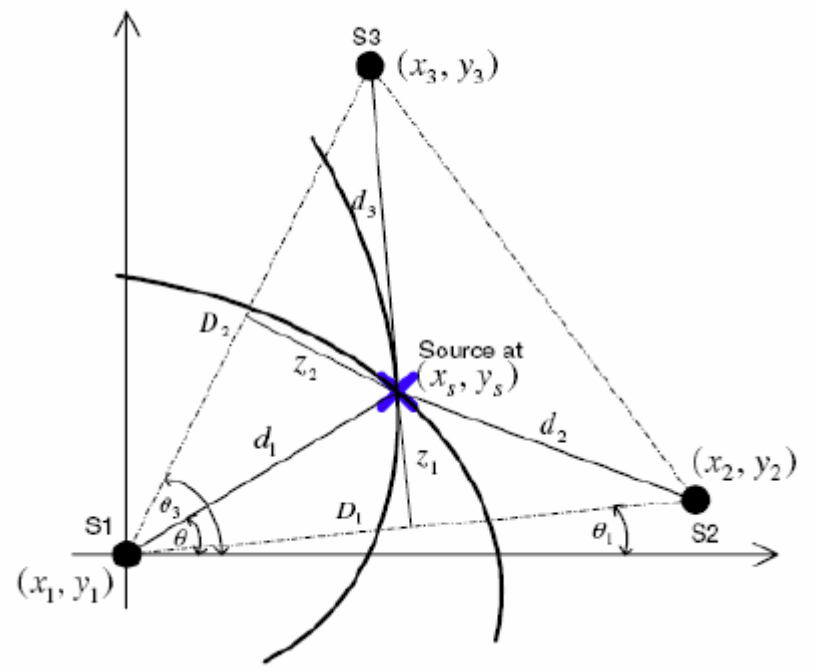

Fig. 2.16 Two dimensional source location [75]

The distance d1 can be calculated using the following equation:

$$d_1 = \frac{D_1^2 - \Delta t_1^2 . c^2}{2(\Delta t_1 . c + D_1 \cos(\theta - \theta_1))} \quad (2.9)$$

$$d_2 = \frac{D_2^2 - \Delta t_2^2 . c^2}{2(\Delta t_2 . c + D_2 \cos(\theta_3 - \theta))}$$

Where angles θ, θ_1 and θ_3 are marked in Fig. 2.16

D2-d1 = $c(t_2 - t_1) = c.\Delta t1$

D3-d1 = $c(t_3 - t_1) = c.\Delta t2$

Δt_1 and Δt_2 are the time differences $(t_2 - t_1)$ and $(t_3 - t_1)$ and c is the wave speed.

The location of the source is given by

$x_s = x_1 + d_1 \cos\theta$

$y_s = y_1 + d_1 \cos\theta$

Using a suitable iteration scheme, the values of θ are varied and the value that minimises the error between two calculated source locations is used to identify the location.

TOA method has been in use for a long time, but a number of studies have reported that complications can arise when used in larger structures: as mode conversions, dispersion and attenuation of waves may result in sensors recording the arrival of different wave modes that have travelled with different velocities [75]. With the help of AE software, the origin of acoustic emissions can be located in 1-D, 2-D and 3-D as well.

2.3.3 Basic Components of AE Equipment

The AE equipment comprises of following basic components in order to monitor the AE signals generated from deformations in RC structure.

1. *Sensor*- It is mounted on the surface of RC structure to record AE signals. Generally, a piezoelectric transducer is used that converts mechanical AE waves to electrical signal. The sensors must be mounted carefully at the appropriate location in order to effectively detect the source location.
2. *Couplant*- It is used to mount the sensor on the surface of RC structure for reliable transmission of AE signals. Generally, vacuum grease, solvent soluble resins, water-soluble glycols, and ultrasonic couplants are used. In order to ensure that sensors remain stationary, holding devices like rubber bands, tapes, springs, etc. are used.
3. *Preamplifier*- Since, AE signal recorded by the sensor is too weak for monitoring purpose, therefore, it is passed through a preamplifier that magnifies the AE signal before further processing.
4. *Data acquisition system*- It is used for storing and analysing the data generated from AE signal monitoring. The data is in the form of AE signal parameters and waveforms.

2.3.4 AE Signal Analysis

There are two approaches of analysing an AE signal to detect the deformations or damage in RC structure- Parametric Analysis and Waveform Analysis. Parametric analysis is about extracting the parameters from AE signal and estimating the damage based on signal parameters. This technique has high recording and data storing speed since it deals with only parameters with respect to certain threshold voltage and not the entire signal. However, this technique can be misleading in certain situations such as the case where it is difficult to differentiate between AE signal parameters and noise. Waveform analysis technique is about recording the AE signal directly and estimating the damage based on signal behaviour. This

technique is capable of differentiating between AE signal waveform and noise and can provide reliable results. However, this technique needs a lot of system memory for storage and requires temporary shut-down of recording system while storing AE signals which generates a delay.

Therefore, in practical applications where large RC structures need to be monitored, recording of AE signal parameters is recommended. At the same time, it is suggested that technician should ensure the proper working of monitoring system by recording and analysing some AE signals [75].

Parametric Analysis

It involves the recording of AE signal parameters to provide qualitative as well as quantitative assessment of damage in RC structures. Some of the commonly used parameters for qualitative damage assessment are hits, counts, energy, signal strength and amplitude.

- **Cumulative hit activity** can be used to estimate the regions of cracks. The regions of higher AE activity or where larger number of hits are recorded correlates to the regions of high crack growth rate.
- **Cumulative Signal Strength (CSS)** refers to the addition of signal strength of each hit over time and focus on the total amount of AE activity generated. This curve can be used to detect the sudden and major damage in a RC structure. The height of spikes or knee formed in CSS curve indicates the presence of micro or major cracks.
- **Amplitude of AE hits** varies with the intensity of damage in RC structure. Micro-cracks, usually produced in larger numbers, generate acoustic emission with lower values of amplitude. On the contrary, macro-cracks produced in small numbers, generate acoustic emission of higher amplitude. However, amplitude values can sometimes be misleading. In order to analyse the deformation in RC structure in a quantitative manner, researchers have proposed the methods of 'Intensity Analysis' and 'Ib-value Analysis'.
- **Intensity Analysis** of damage quantification utilize the parameter 'signal strength' to compute historic index and severity index. The historic index at a particular time is the ratio of average signal strength of recent hits to average signal strength of all the hits till that time. It is represented as

$$\mathbf{HI(t)} = \frac{\sum_{\mathbf{i=K+1}}^{\mathbf{N}} [\mathbf{S_i}/(\mathbf{N-K})]}{\sum_{\mathbf{i=1}}^{\mathbf{N}} (\mathbf{S_i}/\mathbf{N})} \tag{2.7}$$

where, HI(t) is the historic index at time *t*, K is a certain number of past hits, N is the total number of hits, S_i is the signal strength at *i*-th hit.

- **Severity Index** is calculated by taking the average signal strength for a certain number of hits having maximum signal strength. It is represented as

$$\mathbf{SI(t)} = \sum_{\mathbf{j=1}}^{\mathbf{L}} \left(\mathbf{S_j/L}\right) \quad (2.8)$$

where, SI(t) is the severity index at time *t*, L is the certain number of hits with maximum signal strength and S_j is the signal strength at *j*-th hit.

- **Ib-value Analysis** involves the amplitude distribution of AE signals for damage quantification. The variation and diversification in the types of cracks (micro-macro-cracks) engenders different types of acoustic emission of variegating frequency and amplitude [102]. Since, the study of amplitude alone is not sufficient as the cumulative damage may lead to signal attenuation which varies the amplitude values prior to the recording of values by sensors [74]. Therefore, the statistical analysis of distribution of acoustic emission of lower as well as higher amplitudes need to be performed in order to understand the damage severity undergone by the structure.

The Ib-value is one such AE indicator that bridges the weak AE hits (hits with lower amplitude values as a result of micro-cracks) and strong AE hits (hits with higher amplitude values as a result of macro-cracks). Therefore, micro-cracking leads to higher Ib-values indicating the stress accumulation due to crack propagation, and macro-cracking results in lower Ib-values indicating the release of stress by opening of cracks**.**

It has been reported that as the cracking phenomenon becomes acute, higher percentage of strong hits are produced in comparison to weak hits amongst the total number of hits recorded. This brings a sudden fall in the slope of distribution (Ib-value) [68,76,102,103]**.** Shiotani *et al.* [68] developed a model to categorise the degree of damage in concrete as per the following criterion:

I. *Serious Damage*: Ib-values vary around 0 to 0.1
II. *Intermediate Damage*: Ib-values are between 0.1 and 0.2
III. *Intact or minor damage*: Ib-values are larger than 0.2

Ib-value analysis, proposed by Shiotani *et al.* [68,74] , is given as

$$\mathbf{Ib} = \left[\frac{\mathbf{\log_{10} N(\mu+\alpha_1 \sigma) - \log_{10} N(\mu+\alpha_1 \sigma)}}{(\boldsymbol{\alpha_{1+}\, \alpha_2})\boldsymbol{\sigma}}\right] \quad (2.9)$$

where, $\alpha_1 \, and \, \alpha_2$ are constants such that $N(\mu - \alpha_2 \sigma)$ and $N(\mu + \alpha_1 \sigma)$ represent the number of hits with amplitude higher than $(\mu - \alpha_2 \sigma)$ and $(\mu + \alpha_1 \sigma)$ respectively. In order to calculate Ib value, AE hits can be taken in the range of 100 considering an overlap of 80 (for example, in the first cycle, Ib value is calculated for AE hits ranging from 1-

100; in the second cycle, Ib value is calculated for AE hits ranging from 21-120 and so on) [80].

Waveform Analysis

Waveform Analysis involves the recording and analysis of AE signals for damage assessment. The recorded signal can be analysed by applying processing methods such as fourier transform, short-time fourier transform and wavelet transform.

- **Fourier transform** converts the signal from time-domain to frequency domain and as a result, able to identify the frequency components of AE signal. But, during this transformation, it loses the information containing the time of occurrence of AE signal. Fourier transform of a signal is given by-

  $$\mathbf{F(\omega) = \int_{-\infty}^{\infty} f(t) e^{-j\omega t}\, dt} \quad (2.10)$$

  where, ω is the angular frequency, f(t) is the AE signal in time-domain, and $F(\omega)$ is the AE signal in frequency-domain.

- **Short-time fourier transform (STFT)** and **Wavelet transform (WT)** overcome the limitation of fourier transform by retaining the time information along with frequency components of AE signal. STFT is about computing the fourier transform of product of AE signal and a window function. Firstly, the fixed-size window is placed over AE signal at a certain time and its fourier transform is calculated. Secondly, this fixed size window is moved to the subsequent portion of AE signal and its fourier transform is calculated. This procedure is followed for the entire AE signal. Due to fixed window size, STFT has a fixed time as well as frequency resolution. STFT of a signal is given by-

  $$\mathbf{S(\omega) = \int_{W} f(t) s(t-\tau) e^{-j\omega t}\, dt} \quad (2.11)$$

  where, $s(t-\tau)$ is the window function centered at time τ and $S(\omega)$ is the short-time fourier transform of AE signal $f(t)$.

  WT overcomes the limitation of STFT by using variable window size for fourier transform. The size of window depends on the frequency components of AE signal. Low frequency components require a window with long time interval and high frequency components require a window with short time interval. This is accomplished by splitting the AE signal into different levels of variegating frequency and multiplying each level with suitable window size. The continuous wavelet transform of a signal is given by-

  $$\mathbf{CWT(a,b) = \frac{1}{\sqrt{a}} \int_{-\infty}^{\infty} f(t) \Psi\left(\frac{t-b}{a}\right) dt} \quad (2.12)$$

where, *a* and *b* are scaling and shift parameters of wavelet function of (t) and CWT(a,b) is continuous wavelet transform of AE signal $f(t)$.

The discrete wavelet transform of a signal is given by-

$$\mathbf{DWT_{j,k}} = \frac{\mathbf{1}}{\sqrt{\mathbf{2^j}}} \sum_{\mathbf{n}} \mathbf{f(n)} \boldsymbol{\Psi} \left(\frac{\mathbf{n-k}}{\mathbf{2^j}} \right) \quad (2.13)$$

where, j is scaling coefficient, k is shifting coefficient, $1/\sqrt{2^j}\ \Psi\left[(n-k)/\sqrt{2^j}\right]$ are the scaled and shifted version of wavelet function (t) and $DWT_{j,k}$ is discrete wavelet transform of AE signal $f(t)$.

It is proposed to use AE technique for monitoring corrosion-induced damage in concrete by mounting sensors on concrete surface. The following section reviews the state of art of AE technique used for corrosion monitoring in RC structures.

2.3.5 Review of AE for damage/corrosion monitoring in concrete

Weng *et al.* [52] investigated the applicability of acoustic emission technique for detection and characterization of damage due to corrosion of reinforcing steel in RC structures. Three experiments were performed i)AE monitoring of RC specimens undergoing polarization scans ii) AE monitoring of RC specimens undergoing impressed current tests iii) AE monitoring of freely corroding RC specimens. The first experiment involved AE analysis by studying the behaviour of potential with counts. The acoustic noise was found to increase when the potential is greater than ~0.95V and lower than ~1.10V. The second experiment involved AE analysis by studying the behaviour of counts with time of exposure and distance along specimen. The AE counts and impressed current were initially low and then suddenly increased with the onset of cracks on the surface of specimen. AE source was located by mounting multiple sensors on the surface. The third experiment involved the study of AE counts with time of exposure. The AE counts were found to be greater for corrosively active specimens than the passive specimens on the basis of potential values. It was reported that AE activity can be used effectively for detecting and characterizing damage in laboratory experiments. However, its effectiveness in practical applications need to be investigated.

Dunn *et al.* [53] developed a relationship between AE characteristics and corrosion damage to structures. The RC specimens undergoing accelerated corrosion were analysed using AE parameters - counts and cumulative amplitude distribution. The AE counts were found to vary with the severity of damage. They increase with an increase in the degree of cracking due to greater extent of corrosion. The slope of cumulative amplitude distribution, known as b-value,

was found to decrease with the increase in the degree of cracking. It was concluded that AE counts and b-value are indicative of the extent of corrosion damage.

Maji and Shah [55] studied the localization of cracks and movement of the fracture process zone using acoustic emission techniques. Plain-mortar and model-concrete specimens were loaded in direct tension and the rate of AE events and sources of acoustic emission activity was studied. It was reported before peak load was reached, all the recorded events were located near the notch. Furthermore, the acoustic emission activity progressed during the strain softening region with an increase in loading. The fracture-process zone was located using AE events and the location of the zone was confirmed with the location of the crack tip evaluated by a modified linear-elastic fracture mechanics model for concrete as well as by the microscopical observations.

Quyang *et al.* [56] studied the mode I and mixed mode failure in pre-notched plain concrete beams using AE technique. AE activity in plain concrete beams loaded in flexure using four point loading. The AE activity was represented using AE seismic moment tensor representation and characterized as mode I, mode II and mixed mode. This was compared with the observed visual cracking on the surface of the beams. It was reported that most micro-crack planes were in a direction normal to the tensile stresses for a mode I macro-crack (center-notched), whereas micro-crack were relatively uniformly distributed for a mixed mode macro-crack (off center notched). It was concluded that AE could be used as a powerful technique for assessing the damage in concrete.

Zdunek *et al.* [57] determined the feasibility of AE monitoring for corrosion detection of rebar in concrete. RC specimens, exposed to cyclic salt exposure in order to initiate corrosion, were monitored using AE technique. It was observed that the number of AE events increase with the micro-cracking of concrete due to build-up of corrosion products on rebar. Also, high amplitude AE events were observed due to micro-cracking. Furthermore, when AE signals recorded by the two transducers were analysed, a shift of ~10 μsec was observed which can help in finding the source location of AE events. The AE results were compared with the galvanic current measurements, half-cell potential measurements and electrochemical impedance spectroscopy measurements. It was observed that AE is able to detect the early onset of rebar corrosion.

Hearn and Shield [58] investigated crack propagation in conventionally and prestressed concrete beams under cyclic loading under three point bending, using AE. The recorded acoustic activity was compared with visual observations to validate the source location data. The Kaiser effect was studied and felicity ratios were calculated as a function of load. It was

reported that AE behaviour for conventionally and prestressed concrete under loading was distinctive, indicating the potential of AE technique.

Austin *et al.* [64] studied the suitability of impressed current method to accelerate corrosion in RC structures using AE technique. The gravimetrical and theoretical mass loss was also calculated. Different prisms with varying characteristic strengths as well as the cover thickness were subjected to accelerated corrosion between 3 days and 17 days. The localised nature of the chloride-induced corrosion was reported. A sudden increase in AE hits and AE energy was observed after a certain span of time indicating AE technique that AE clearly detected the onset of corrosion-induced damage and on the basis of these results, a modified Faraday's law was proposed for relating variation of impressed current with loss of mass. It was also reported that the thickness of concrete cover increased the time of onset of corrosion and the strength of concrete had very less effect on it. The results were verified using destructive test which involves breaking of specimens to expose the corroded reinforcement. Finally, it was reported that impressed current method is the most effective and quick to accelerate chloride-induced corrosion.

Uddin *et al.* [65] investigated the crack propagation due to corrosion of reinforcement in concrete both analytically and experimentally. A two domain BEM based on circumferential stress criterion, was applied to mixed-mode crack extension. Very small surface cracks, the longitudinal-diagonal cracks and the diagonal cracks in the arbitrary direction were evaluated. An expansive agent was used to generate these cracks. The results were confirmed with AE Simplified Green's functions for moment tensor analysis (SiGMA) with 3D VRML. It was finally reported that reinforcement corrosion induces mode-I fracture with a very less contribution of the mixed-mode and the mode II fractures.

Assouli *et al.* [66] investigated the concrete cracking due to reinforcement corrosion utilizing AE and half-cell potential technique. The concrete samples were subjected to both chloride-induced and carbonation-induced corrosion. It was found that carbonation process was very severe with chloride ions. The disappearance of the passive layer corresponded to high carbonation and a very high acoustic activity. It was reported that acoustic activity has a perfect correlation with corrosion of reinforcement in concrete.

Ing *et al.* [69] investigated the influence of cover zone factors on the release of acoustic emission with the progression of chloride-induced corrosion in RC structures. Corrosion was accelerated using impressed current method. The effect of rebar diameter, cover thickness and compressive strength on AE signals using normalised mass loss was reported. The onset of corrosion was detected by an increase in the cumulative absolute energy of AE signals. There

was no significant effect of cover thickness on absolute energy of AE signals. A small increase in the absolute energy of AE signals was observed with an increase in rebar diameter. On the other hand, a significant effect of compressive strength of concrete on AE was observed. The absolute energy of AE signals was found to vary exponentially with the compressive strength which indicates that AE can pick up the sudden release of strain energy in concrete.

Lyons *et al.* [70] investigated the corrosion of RC using AE and the influence of diurnal and seasonal temperature variations on corrosion detection. The chloride rich RC prisms were coupled with chloride-free prisms. They were then exposed to diurnal and seasonal temperature cycles. Both AE and galvanic current were measured to keep a track of evolution of corrosion-induced damage. No clear relationship between both the AE data and the galvanic recording was reported. However, both of them were reported to be able to emulate the evolution of the corrosion and temperature in the diurnal cycles. The seasonal variations had a greater impact on the galvanic reading whereas it was found to have no influence on the AE. It was also reported that AE detected the damage induced in concrete by the expansive oxides even when the very low galvanic currents were recorded.

Ohtsu and Tomoda [73] investigated the corrosion process in reinforced concrete slabs subjected to a wet-dry cycle test using acoustic emission. The increase in cumulative AE hits was observed at two instants and these were further distinguished into shear cracks as well as tensile cracks using RA-Average frequency value plot. The first instant of high AE activity was attributed to the development of shear cracks and the second with the developing tensile cracks. Scanning Electron Microscope (SEM) was also used to confirm the results. FEM analysis confirmed that the onset of corrosion may occur a bit earlier than that is estimated by the design code. The reinforcing bars were removed from the specimen and it was reported that corrosion of rebars occurs only after the chloride concentration in concrete reached a certain threshold value. SEM analysis was done on a rebar skin in order to evaluate the deterioration of the rebar. The disappearance of the ferrous ions was reported and it was suggested that 1st period of high AE activity could correspond to the onset of corrosion.

Kawasaki *et al.* [78] investigated corrosion-induced damage of a number of RC structures. The RC specimens were subjected to cyclic wet-dry test. The high AE activity confirmed the onset of corrosion and the nucleation of concrete cracking due to expansion of corrosion products in the corrosion process. From the SEM analysis, it was observed that passive film on the surface of the rebar was disappeared. Ib-value analysis was also performed and it was concluded that high AE activity and low Ib-values indicate transition from the onset of corrosion to the micro-cracking of concrete. It was reported that Ib-value could easily confirm

the transition between the transition periods from initiation to micro-cracking and from micro-cracking to major cracking stages. Since very few events were located during the initial stages, the results from SiGMA analysis were reported to be significant. However, in the later stages, the kinematics of the corrosion-induced cracks are clarified by the SiGMA analysis.IT was further reported that tensile cracks are developed around the rebar and then the shear cracks are nucleated.

Shah and Kishen [77] utilized AE technique to evaluate the fracture behaviour of concrete-concrete interface. The reinforced concrete specimens were cast with and without the interface present and were tested under 3–point loading in flexure. Eight AE sensors were used to monitor the entire crack propagation process. An increase in compressive strengths of concrete on both sides of the interfaces with the decrease in maximum load carrying capacity and the fracture energy of interface beams was reported. The fracture process zone and the damage zone was analysed with recorded number of events. A correlation between AE energy and fracture energy was attempted. It was reported that a similar behaviour as that of the fracture energy.

Shah and Kishen [81] studied the acoustic emission activity due to the fatigue crack growth in plain concrete beams under three-point beams. Six acoustic emission sensors that were mounted on the surface of the beam were used to record the crack propagation. Variations in load and the corresponding displacement, crack mouth opening displacement and activity were simultaneously recorded during the entire duration of the test. A Paris law type relationship between the rate of acoustic activity per cycle and the stress intensity factor range was reported. It was further suggested that this relationship could be exploited to compute the crack length and hence damage during in-service monitoring of engineering structures using AE. The b-value analysis on recorded AE data was also performed with an objective to track the different stages of fatigue crack growth. It was observed that AE could aid in identifying the sudden failure in fatigue tests.

ElBatanouny *et al.* [83] investigated characterization of the corrosion-induced damage in cracked concrete with pre-stressing strand using AE. The corrosion of strand embedded in concrete was accelerated by supplying a constant potential between the strand and the copper plate. The specimens were kept immersed in a 3 % NaCl solution. Half-cell potential measurements, steel section-loss, and visual inspection results were compared with AE results. The characteristic wave speed was used to determine the location of active corrosion which was found to be in the midsection. One the AE parameters i.e., Cumulative Signal strength was used to characterize corrosion and is found to relate well with the measured potential values.

Intensity analysis was used to evaluate the deterioration of steel due to corrosion-induced damage. It was finally concluded that AE is useful, non-intrusive technique for the detection and quantification of corrosion damage and may be developed as a structural prognostic tool for maintenance purposes.

Benedetti *et al.* [86] studied the corrosion progression in small scale, pre-notched and pre-cracked RC specimens representing areas near the clear cover in typical RC members. Corrosion was accelerated at 10 V under the influence of 3% NaCl solution. AE sensors with a resonant frequency of 55 kHz were used to record AE data continuously for the entire duration of corrosion-induced damage. The objective of the study was to investigate the initiation of corrosion in RC structures. The knee observed in cumulative signal strength plot was in coherence with measure potentials. Since the majority of the AE signals were recorded after the onset of the corrosion, it was suggested that corrosion in RC could be studied as a continuous phenomenon. The time driven and absolute energy data was found to be compatible with cumulative signal strength plot. Fromm the statistical analysis, it was confirmed that a wider notch will lead to an earlier initiation of corrosion-induced damage. The cumulative signal strength results were found to be more useful for identifying the nucleation of cracking whereas time driven data could not be used for the same purpose due to the burst nature. The study demonstrated that time driven data approach of AE to characterize the onset of corrosion was effective and most suitable.

Kawasaki *et al.* [84] investigated corrosion monitoring in RC beams subjected corrosion using AE. Corrosion was accelerated using a cyclic dry and wet process. The two stages i.e., onset of corrosion in rebar and the nucleation of corrosion-induced cracks in concrete were identified. The decrease in the RA value and the increase in the average frequency value was observed at the onset of corrosion. The Ib-value plot also exhibited a sharp decrease during the same period. It was confirmed that AE could identify the onset of corrosion in RC structures. The locations of the AE sources by the SiGMA analysis were reported to be in agreement with those of the corrosion-induced cracks in concrete. This further implied that AE sources were of tensile cracks mostly. SEM and Electron Probe Microscope Analyse (EPMA) picture were compared with AE activity and it was confirmed that first transition in the AE activity was surely related to the onset of corrosion. The second transition was also confirmed to be associated with corrosion-induced cracks in concrete.

Elfegani *et al.* [82] monitored the corrosion-induced damage in small-scale pipe samples due to pre-stressing wire corrosion using AE technique. It was reported that AE technique could easily detect macro-cracks and the propagation of cracks. In order to aid appropriate

maintenance, nature of cracks was studied and cracks were classified using a novel analysis approach. The Kernel Density Estimation function was used to locate the origin of cracks effectively. The results confirmed the effectiveness of AE to detect early corrosion and macro cracks in pipe structures**.**

ElBatanouny *et al.* [83] investigated early corrosion in prestressed T-girders measuring using AE technique. Corrosion was accelerated using wet/dry cycles in 3% NaCl solution in four prestressed girders out of which two were pre-cracked. The specimens were pre-cracked to study the effect of the already present crack. Along with AE, half-cell potential (HCP) measurements and Linear polarization resistance values were also recorded periodically in order to make sure that deterioration in concrete is due to corrosion of reinforcement. Further, the specimens were loaded under flexure and the visual inspection of the corroded strands were made. Cumulative signal strength was found to be very effective for detecting the onset of corrosion. It was reported that intensity analysis could be used to classify corrosion damage using empirical charts for corrosion levels. The residual capacity of the specimens were measured and they were to be indicative of AE's ability to detect corrosion-induced damage before it incurs major damage in the structure itself.

Velez *et al.* [89] investigated the effectiveness of AE to detect and classify early corrosion-induced damage in prestressed concrete pile exposed to salt water. In order to simulate the realistic corrosion mechanisms, impressed anodic current method was utilized. Several Ae sensors were mounted on the surface of large –size concrete strips reinforced with seven –wire steel strands and also electrochemical measurements were taken. The results were then compared with visual observation of decommissioned models. From the visual observations, cracks were found on the surface of specimens. AE signal strength and cumulative signal strength clearly identified the steel depassivation during the early stages of corrosion. IA analysis was performed for discriminating between the corroding and non-corroding specimens. Also, a refined IA-based criteria for corrosion assessment was proposed and it was found to be less sensitive to wave attenuation and dispersion.

Benedetti *et al.* [86] studied AE activity in small scale RC specimens subjected to accelerated corrosion based on the increase in the capillary suction of concrete. The frequency spectrum of AE signals and the effectiveness of the historic index to identify the corrosion onset was reported. The acoustic emissions that were recorded during the onset of corrosion was reported to range between 35 to 50 kHz. The historic index *H(t),* was reported to be very effective parameter in identifying the onset of corrosion in RC specimens. The frequency spectrum of AE signals before and after the initiation of corrosion is investigated to isolate the

frequency components associated with corrosion. It was shown that AE signals generated by an early corrosion excite a well-defined narrow band of frequency spectrum.

Kawasaki *et al.* [87] evaluated the seismic capacity of the damaged RC beams from corrosion of reinforcement using AE technique. AE activity was recorded continuously during the flexure testing on RC members exposed to a cyclic wet and dry method corrosion. A comparison between the recorded AE parameters with mechanical properties such as flexural capacity, toughness and quantity of energy absorption was reported. The corrosion state of acceleration stage was also compared with that of dormant stage. A correlation between the concentration of chloride ions and the AE activity was indicated. AE activity clearly indicated a significant difference between the fracture process amongst low chloride and high chloride concentrations. It was also reported that the number of shear cracks are very high for high chloride specimens.

Zaki *et al.* [91] assessed the corrosion of RC beams under three point load testing using acoustic emission technique. The RC beams were subjected to accelerated corrosion using a direct current (DC) power supply with 5 % sodium chloride (NaCl) solution. The RC beams were corroded upto 0, 4.55, 16.86 and 32. 37%. The recorded AE hits indicated the three levels of damage (I, II, III) level. It was reported that damage level I, where the percentage of tensile cracks increased drastically, could provide an early indication for assessing of corrosion damage of RC beams.

Li *et. al.* [92] studied the corrosion-induced damage in a steel reinforced mortar block using a combination of acoustic emission technique and fiber Bragg grating strain measurements. Corrosion was accelerated using a constant current. Acoustic emission tracked the cracked propagation in mortar whereas the expansion of mortar with the formation of rust was monitored using fiber Bragg grating strain sensors. The results demonstrated three different types of sources of acoustic emissions such as evolution of hydrogen bubbles, generation of corrosion products and crack development. A correlation between the recorded AE activity and strains measured on the surface of specimen was reported as well.

2.4 CLOSING REMARKS

In this chapter, the mechanism as well as fundamentals of ultrasonic guided wave and acoustic emission propagation are explained in detail. The basic set-up of UGW and AE testing techniques are also discussed. Additionally, an extensive literature review was carried out on UGW and AE techniques for monitoring corrosion in RC Structures independently. The review established the efficacy of UGW and AE for damage monitoring specially related to corrosion

in concrete structures. But still need to be investigated before it can be practically employed in civil engineering structures.

CHAPTER 3

MONITORING INVISIBLE CORROSION

3.1 GENERAL

Corrosion of reinforcement in RC structures is considered to be one of the major durability problem costing billions of dollars to global economy. Hence, an early diagnosis and prognosis of corrosion can be hugely beneficial. Initially steel remain passivated owing to high pH (around13) of pore solution in concrete, preventing the anodic reaction to occur. However, the Cl^- ions (about 700 ppm) present in concrete pore water solution can impair the corrosion inhibitive properties of this passive layer. The entire mechanism of corrosion of steel in marine conditions has been observed to have four phases (**Fig. 1.2**). As already discussed, the phase 1 refers to the initiation of corrosion succeeding the depletion of the passive layer. Phase 2 corresponds to the calm phase where in micro-cracks build up and hence not much activity is visible. Phase 3 refers to active cracking phase where the micro-cracking take the shape of macro-cracking. Finally, in the last the phase 4 refers to more uniform progression of corrosion. Eventually, corrosion of reinforcement leads to the fracture of concrete, delamination and spalling of concrete cover, reduction of concrete and reinforcement cross-sections, loss of bond between reinforcing steel, ultimately leading to collapse of the structure. Hence, it is quite evident that corrosion detection can be most effective only if it is able to discern corrosion in the initial stages (when the corrosion-induced damage is not visible to the naked eyes) i.e., Phase 1.

This chapter reports simultaneous monitoring of corrosion in RC structures using well established half-cell potential (HCP) measurements and a combination of two NDT which are ultrasonic guided wave and acoustic emission. The aim is to observe corrosion damage before it is visible on the concrete surface. RC beams have been subjected to anodic current and the progression of corrosion has been monitored with all three technologies. The relative efficacy of the technologies for tracking corrosion, especially when it is at its initial stages and invisible on the concrete surface is reported.

3.2 EXPERIMENTAL INVESTIGATION AND METHODOLOGY

3.2.1 Specimen Details

RC beams of 150 mm square cross-section and 700 mm length were cast using the mix proportions of cement, sand and stone aggregates as 1:1.41:2.56 with a water-cement ratio of

0.45. The most popular mix used in practice was adopted. A single plain mild steel bar of diameter 25 mm and 1 m length was embedded at the centre of cross-section of beam and 150 mm length of the bar was projected at both ends of the beam. The average 28 days compressive strength of concrete was 25 N/mm^2.

3.2.2 Inducing Accelerated Corrosion

The RC beam specimens were subjected to corrosion using impressed current technique. The reinforcing bar was made anode by connecting it to the positive terminal of a constant voltage power supply. A stainless steel wire mesh wrapped on the cotton gauge in the middle 200 mm length of the beam was made cathode by connecting it to the negative terminal of power supply. A direct electric current was impressed between the reinforcing bar and the stainless steel mesh at a constant voltage of 20 V. In order to simulate marine conditions, 3.5% NaCl solution was used as a drip in the middle 200 mm of the wrapped beam. All the three beam samples were subjected to similar exposure of accelerated chloride corrosion. To observe initial corrosion under the accelerated condition, three samples were subjected to accelerated corrosion for 9 days and the nomenclature used is given in **Table 3.1.** Three samples were studied to ensure the repeatability of all NDT measurements.

Table 3.1: Nomenclature of specimens used for monitoring invisible corrosion

Specimen	**Details**	**Exposure Duration**
S-9-1	Sample 1	9 days
S-9-2	Sample 2	9 days
S-9-3	Sample 3	9 days

3.2.3 Ultrasonic Guided Wave Set-Up

For ultrasonic guided wave monitoring, an ultrasonic testing system consisting of an ultrasonic pulser/receiver DPR500 (Karl Deutsch make), cylindrical contact piezoelectric transducers of 0.1 MHz and 1 MHz frequency and display devices were used. Ultrasonic guided waves were produced in the embedded rebar in RC beams by Pulse Transmission (PT) mode of wave propagation by varying the exciting frequency. One cylindrical transducer acts as the transmitter and sends the ultrasonic waves from one end of the rebar into the RC beam and the other transducer at the other end of bar acts as the receiver. The comparison of change in the

transmitted signal amplitude and characteristics is used to quantify and relate the damage in the embedded bar because of corrosion.

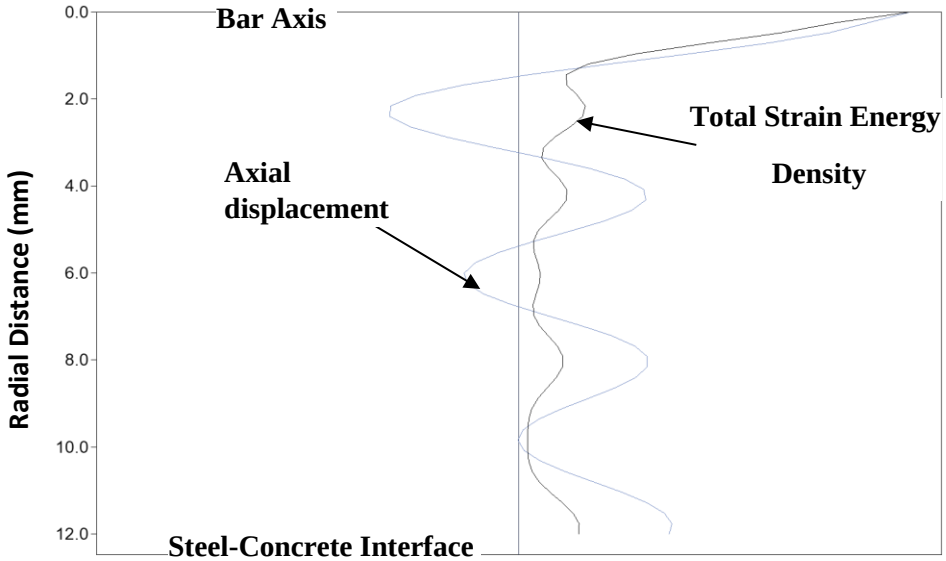

(a) Core Seeking Mode L(0,7) at 1 MHz

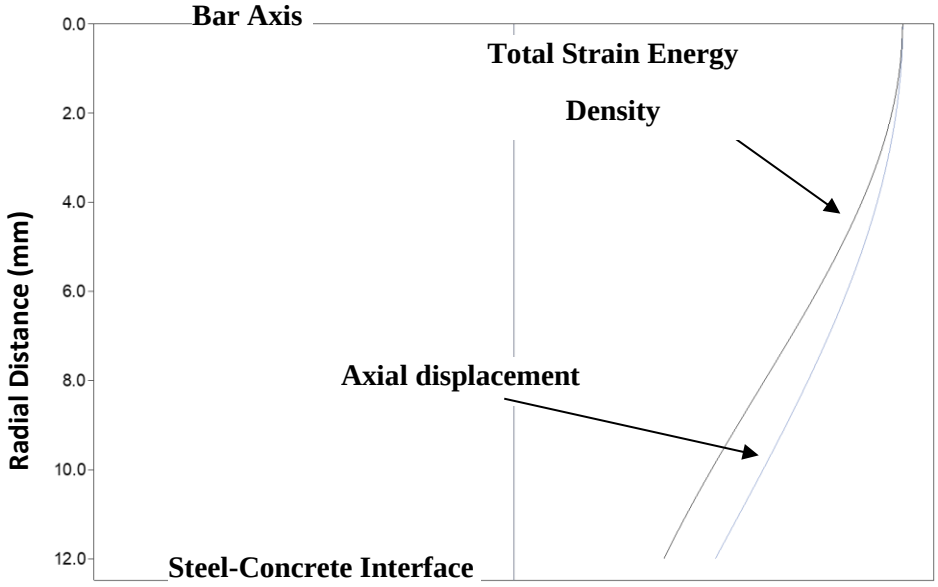

(b) Surface Seeking Mode L(0, 1) at 100 kHz

Fig. 3.1: Mode Shapes [45]

In the bars embedded in concrete, various ultrasonic guided wave modes are produced when the waveguide interacts with the bar. It also depends on how the ultrasonic waveguide is excited in the bar. Longitudinal guided wave modes experience minimum attenuation and are easiest to excite and hence are preferred modes. They can be easily produced by placing the compressional transducers along the two ends of the bar by means of a holder assembly. Different longitudinal modes can be produced by varying the excitation frequencies. The most

preferred longitudinal modes in steel embedded concrete are the ones with the lower attenuation at low frequency. The fundamental L(0,1) mode at low frequency of 100 kHz is chosen for ultrasonic investigations. Another high frequency mode L(0,7) at 1 MHz with displacement profile centred in the middle of the bar is found efficient for layered systems is chosen [33]. This mode experiences low attenuation and energy velocity maxima at 1 MHz. These frequencies were experimentally validated by confirming the signal fidelity. Transducers with longer waveform duration and a relatively narrow frequency bandwidth with centre frequency of 0.1 MHz and 1 MHz were hence, used for further experimental investigations. **Fig. 3.1** shows the mode shapes of L(0,1) and L(0,7) modes.

Another important feature for the selection of modes was the radial distribution of displacement and energy density of the mode shapes. It has been observed in the previous studies [33,45] that L(0,1) is a surface sensitive mode which is sensitive to the surface modifications in the reinforcing bars due to corrosion and picks up the initial delamination of the reinforcing bar from the surrounding concrete. Similarly, L(0,7) mode is a core-seeking mode which could pick up another major effect of chloride corrosion, pitting in the bar. This mode mainly progresses through the core of the bar and has negligible surface component and is sensitive to the local degradations such as pitting or crevice corrosion in the reinforcing bars. Hence, these two modes L(0,1) and L(0,7) at 0.1 MHz and 1 MHz respectively, were selected for ultrasonic guided wave monitoring of rebar undergoing corrosion in RC beams.

Compressional narrow band piezoelectric transducers of 25 mm diameter and central frequencies of 0.1 MHz and 1 MHz were used. The transducers were attached to the exposed ends of bar using a coupling gel and a holder assembly. The schematic and actual set-up used for ultrasonic guided wave investigations is shown in the **Fig. 3.2(a)** and **(b).** The ultrasonic guided wave readings were taken after every 24 hours throughout the exposure duration using both the modes of excitations. The AE monitoring system was paused when ultrasonic monitoring was conducted.

3.2.4 Acoustic Emission Set-Up

For acoustic emission monitoring, a Micro-II digital AE data acquisition system with 8 AE channels (Physical Acoustics Corporation, USA), AE sensors, pre-amplifiers, and filters was used. AE sensors detect signals and waveforms generated due to micro-cracks that occur as a result of corrosion of rebars embedded in concrete. It has been observed that AE signals produced due to corrosion of reinforcement in RC structures have a main spectrum band in the frequency range 20-80 KHz [75]. Another investigation suggested the use of 7 kHz, 15 kHz,

30 kHz and 60 kHz, resonant frequency sensors for concrete corrosion monitoring [63]. In this investigation, six AE sensors (with 30 KHz resonant frequency) were used for AE monitoring.

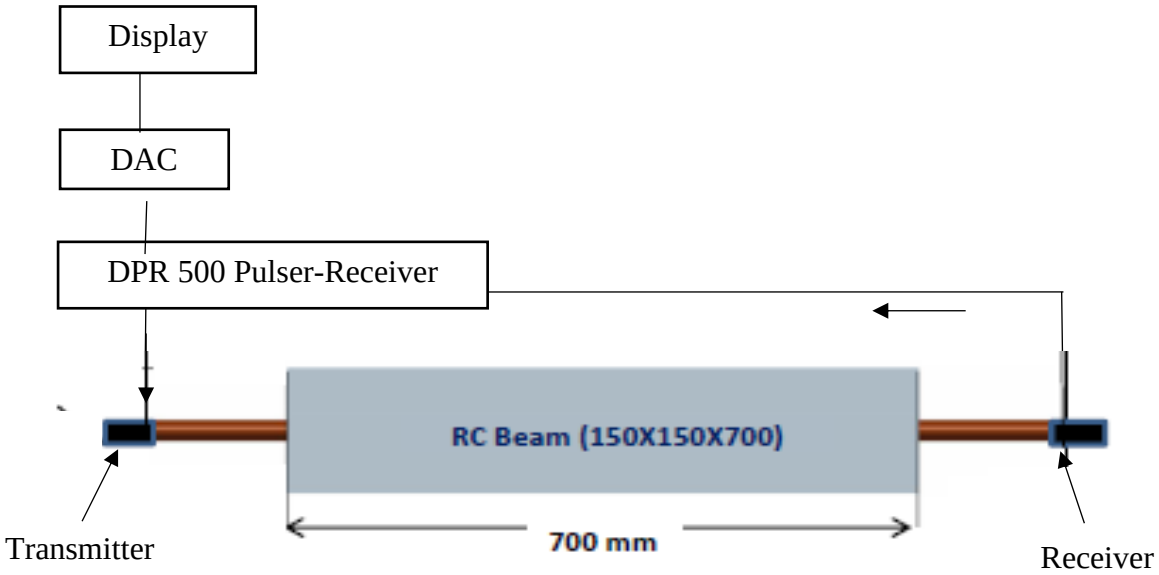

(a) Schematic

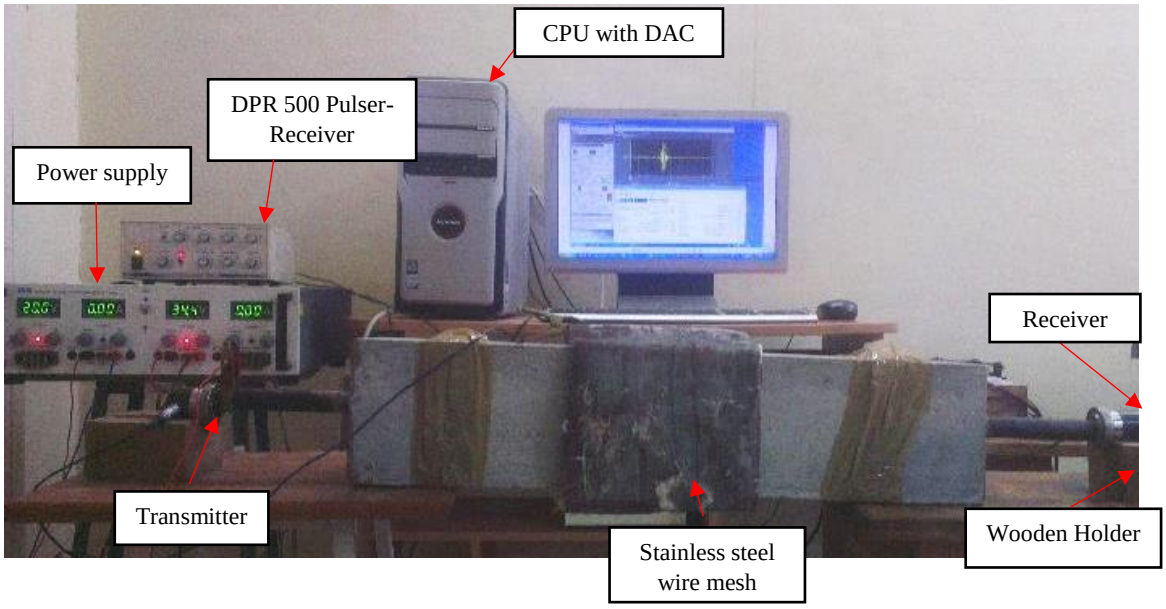

(b) Actual

Fig. 3.2 Ultrasonic guided wave monitoring set-up

As shown in **Fig. 3.3(a)**, three sensors were mounted on the front face of beam and the remaining three were mounted on the back face of beam**.** All AE sensors were mounted using a coupling gel and held in position using sticking tapes throughout the exposure period. A threshold of 45 dB was initially set to acquire significant AE signals originating due to corrosion of reinforcement. The experimental setup for AE data acquisition is shown in **Fig. 3.3(b)**. Acoustic emission signals were recorded continuously during the entire duration of

exposure to corrosion. AEWin software was used for extracting AE data providing various characteristics of AE signals such as amplitude, AE signal energy, duration, counts and rise time [47-49].

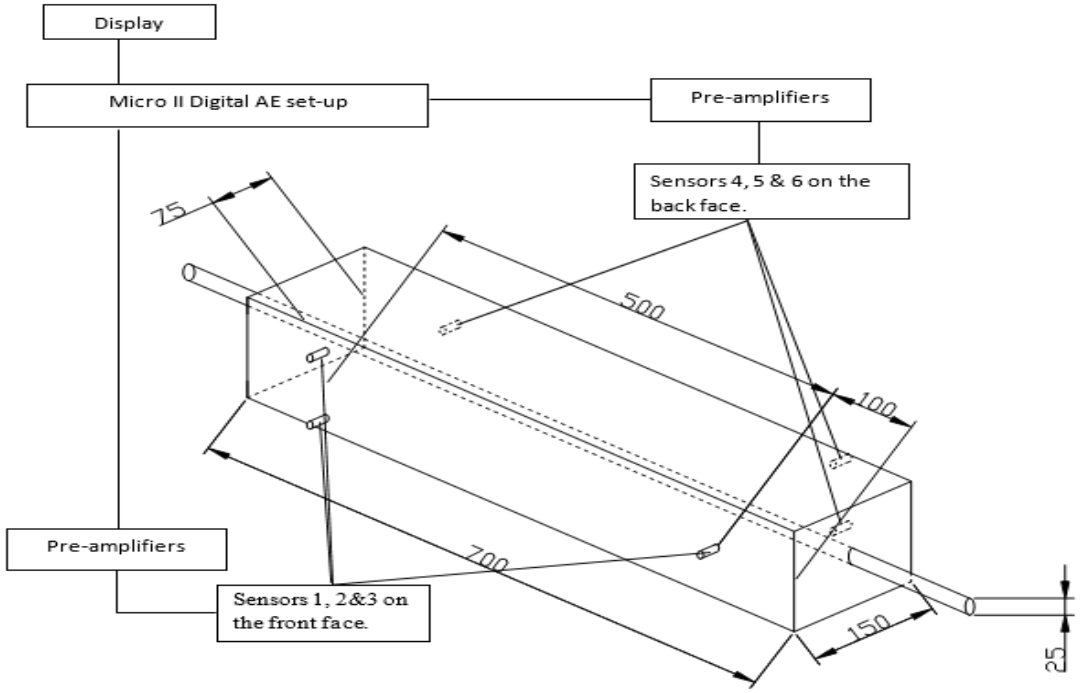

(a) Schematic

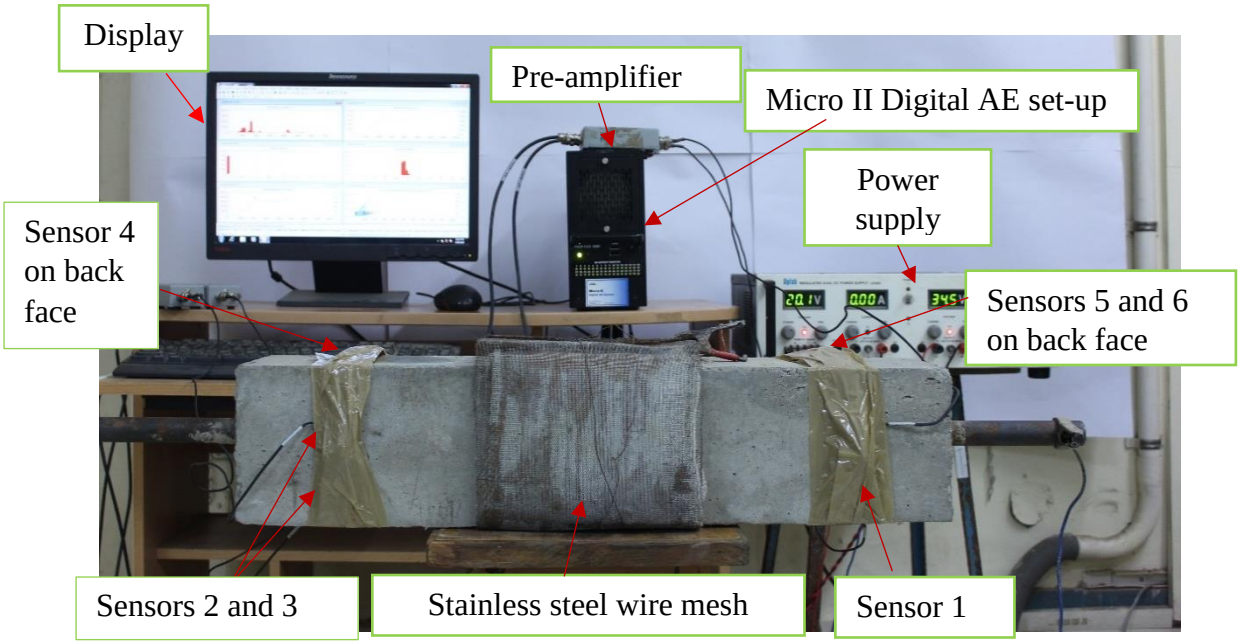

(b) Actual

Fig. 3.3 Acoustic emission monitoring set-up

Along with the corrosion monitoring by ultrasonic guided waves and acoustic emission, half-cell potential measurements (ASTM C876) were also done simultaneously to compare the proposed NDT methods with conventional techniques for corrosion monitoring. It should be noted that AE data acquisition was paused after every 24 hours for recording HCP. During this period, the impressed current power supply was also turned off. HCP readings were taken using a copper-copper sulphate (Cu-$CuSO_4$) reference electrode. In order to measure the potential difference, the negative terminal of a voltmeter was connected to the reinforcement and the positive terminal was connected to the reference electrode. The surface of concrete was scanned at various locations for detecting the probability of corrosion. The probability of corrosion is detected by the decreased potential difference. The well established that there is 90% probability of corrosion in the reinforcement when the potential drops below -350mV [104].

3.3 VISUAL OBSERVATIONS

Fig. 3.4(a)-(e) shows the condition of beam after every 0, 3, 5, 7 and 9 days of accelerated impressed current corrosion in chloride environment.

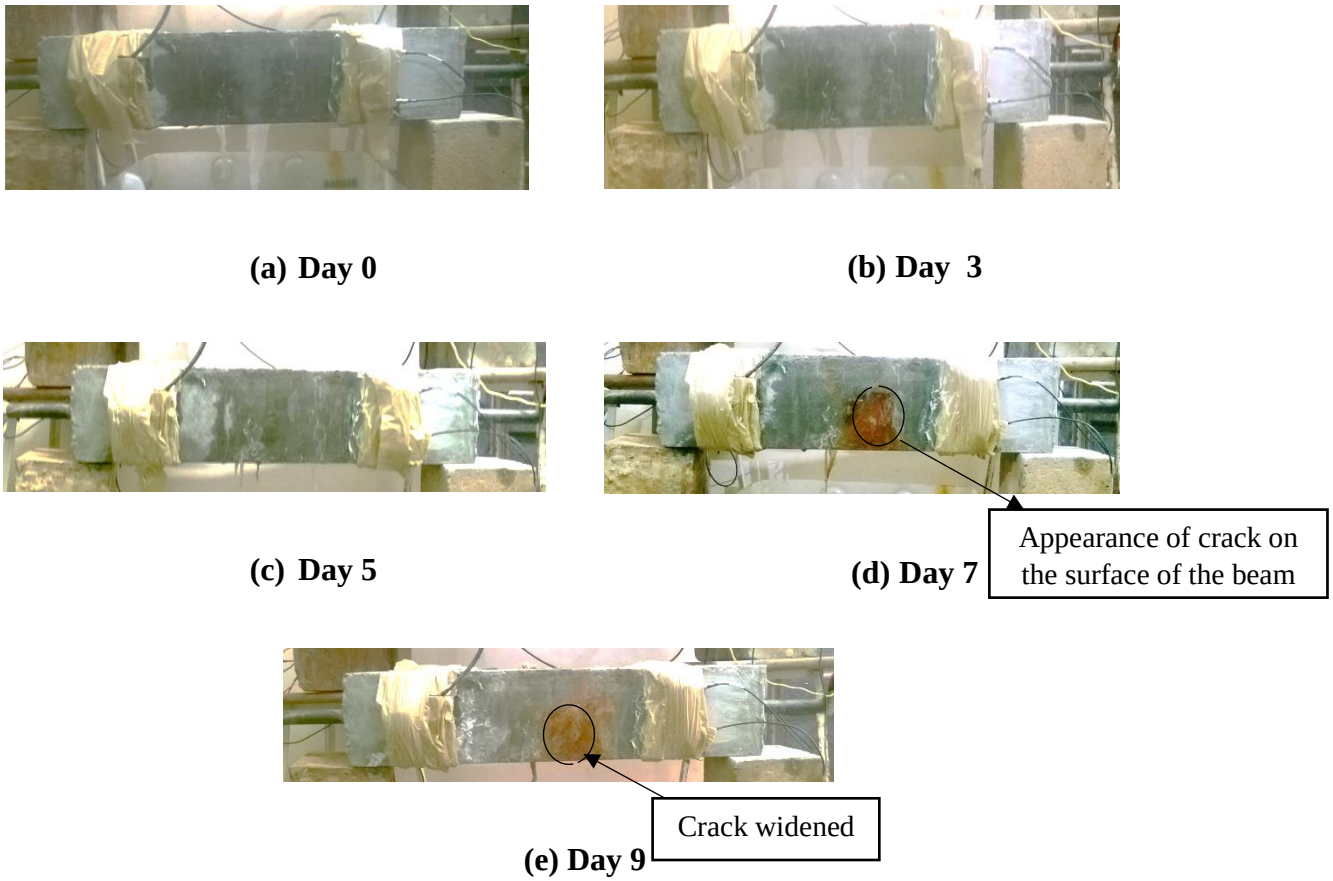

Fig. 3.4 Visual monitoring of RC beam

No damage was observed in RC beam during the initial five days of accelerated corrosion. After 5 days of exposure to chloride induced corrosion, a small transverse crack appeared on the surface of the RC beam at its middle portion and a reddish brown liquid started flowing out of the crack (**Fig. 3.4)**. Subsequently, the crack widened and increased in length followed by the increased flow of rust products and widespread rust stains. The appearance of transverse crack in the beam was observed in other RC beams as well which was between 5 and 7 days of exposure. It is possibly due to localised corrosion exposure in the middle 200 mm length of beam leading to pressure build up due to expansive rust product and subsequent cracking of concrete. All the beams had very wide cracks after 9 days of exposure.

3.4 HALF-CELL POTENTIAL MEASUREMENTS

Half-cell potential measurements were taken on RC beam specimens with increasing corrosion exposure after each day as shown in **Fig. 3.5**. Potentials above -350 mV were recorded in the first few days thereby indicating lesser probability of corrosion due to initial passive condition of rebar in concrete. However, as the corrosion progressed, the recorded potentials started decreasing rapidly and fell below -350 mV after 4-5 days. This points towards complete breakdown of passive layer and progression of corrosion into the rebar. Shortly after this time, formation of rust products and consequent cracking of concrete was observed, which further allowed easy permeation of electrolyte through the concrete cover and therefore, rapid reduction of the potential was noted.

The breaking down of resistance to corrosion is also observed in the variation of impressed current required to maintain a constant voltage (**Fig. 3.6**). The current flowing through the circuit was regularly monitored from the ammeter attached to constant voltage power supply after every 24 hours of exposure. **Fig. 3.6** shows the relationship between anodic current and the increasing corrosion exposure. It can be observed that there is a sudden drop in the current amplitude immediately after 24 hours of exposure to chloride corrosion. This may be due to the build-up of corrosion products that has higher electrical resistance. After this period, the current slowly starts increasing with time indicating the gradual breakdown of the passive layer and pointing towards corrosion initiation. Clearly, the electrochemical techniques indicate the likelihood of corrosion, but there is no clear indicator for discerning early corrosion.

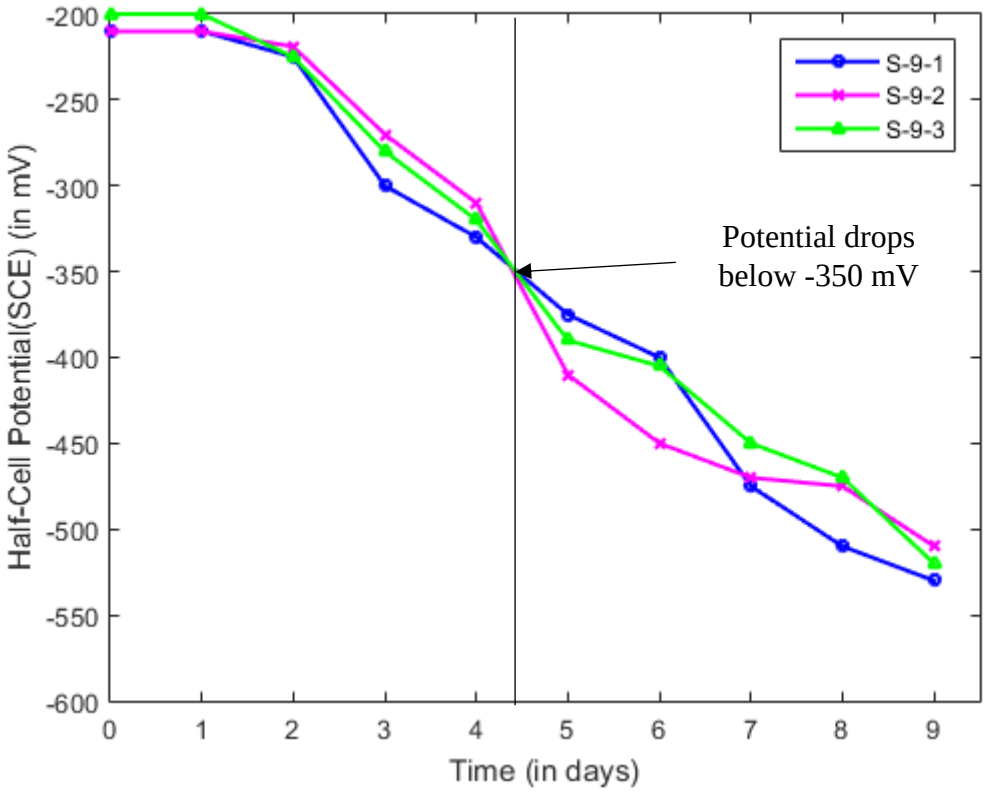

Fig. 3.5: Half Cell Potential measurements with increasing corrosion exposure

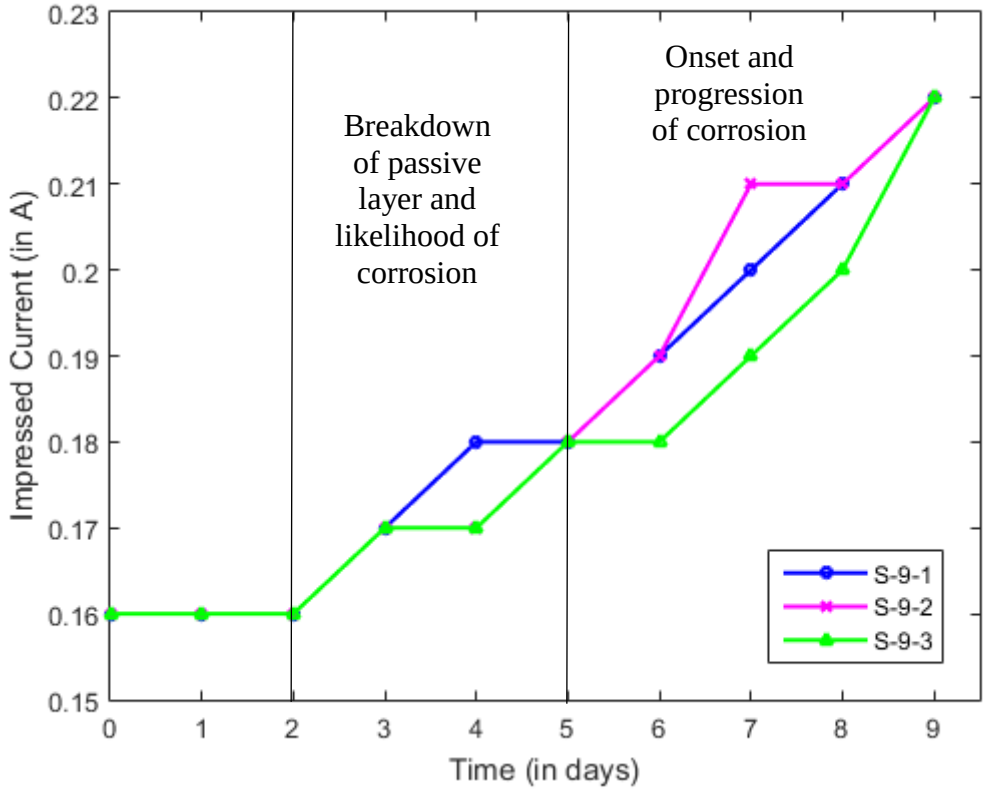

Fig. 3.6: Variation in impressed current with increasing corrosion exposure

3.5 ULTRASONIC GUIDED WAVE INVESTIGATIONS

3.5.1 L(0,7) mode at 1 MHz

From the transmitted signals obtained with increasing corrosion at different days of exposure (**Fig. 3.7**) and the normalized signal amplitudes vis-s vis fresh signal amplitude shown in **Fig. 3.8**, it can be observed that L(0,7) mode at 1 MHz there has no significant variation in the signal strength amplitude up to 7 days of exposure to corrosive environment. It is primarily due to core-seeking behaviour of selected mode and it is sensitive to corrosion damage in the bar only after the corrosion has penetrated into the bar in the form of pitting. Initially, during the process of corrosion initiation, the damage is not significant in the core of bar and hence the signal remains flat. However, after 7 days onwards, the signal starts falling indicating formation of pits. This core-seeking mode can be used to differentiate surface corrosion from pitting. From visual observation, it is clear that pitting starts to happen when clear signs of corrosion are visible on the concrete surface.

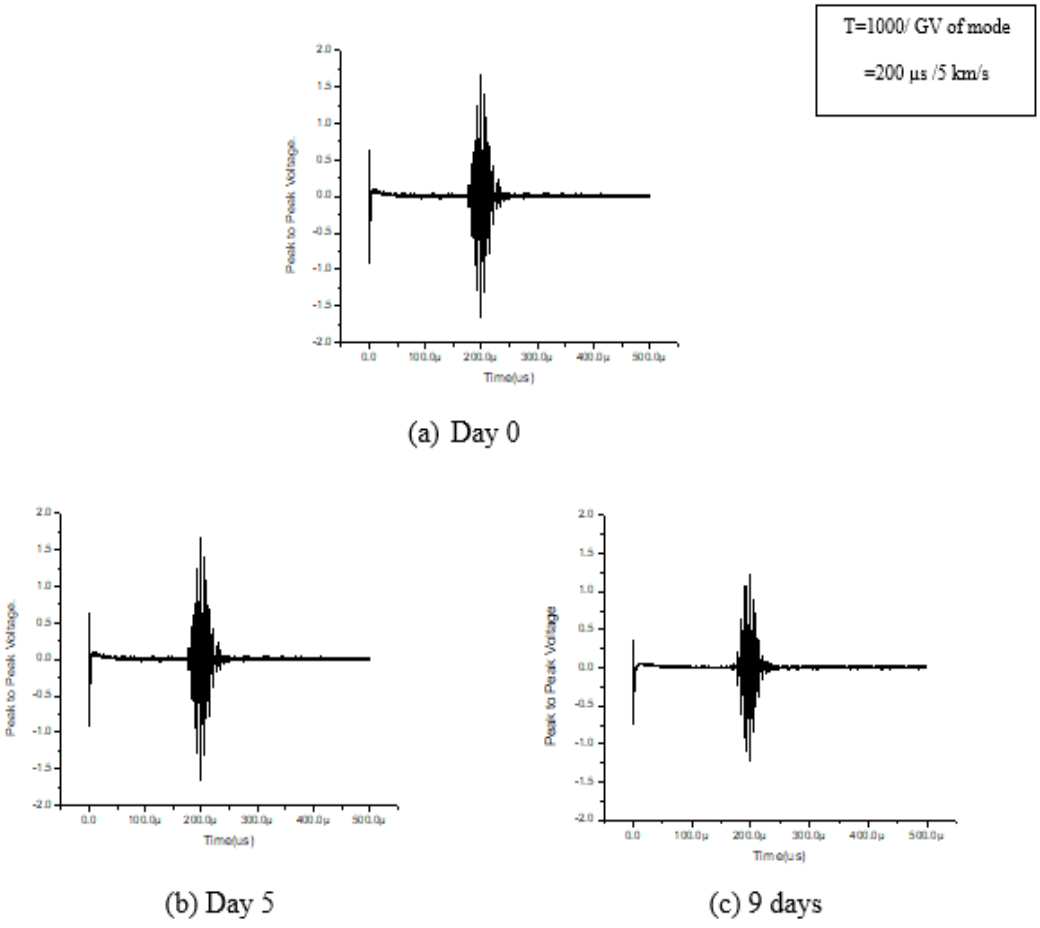

Fig. 3.7 PT signatures at different stages of corrosion using L(0,7) mode at 1 MHz

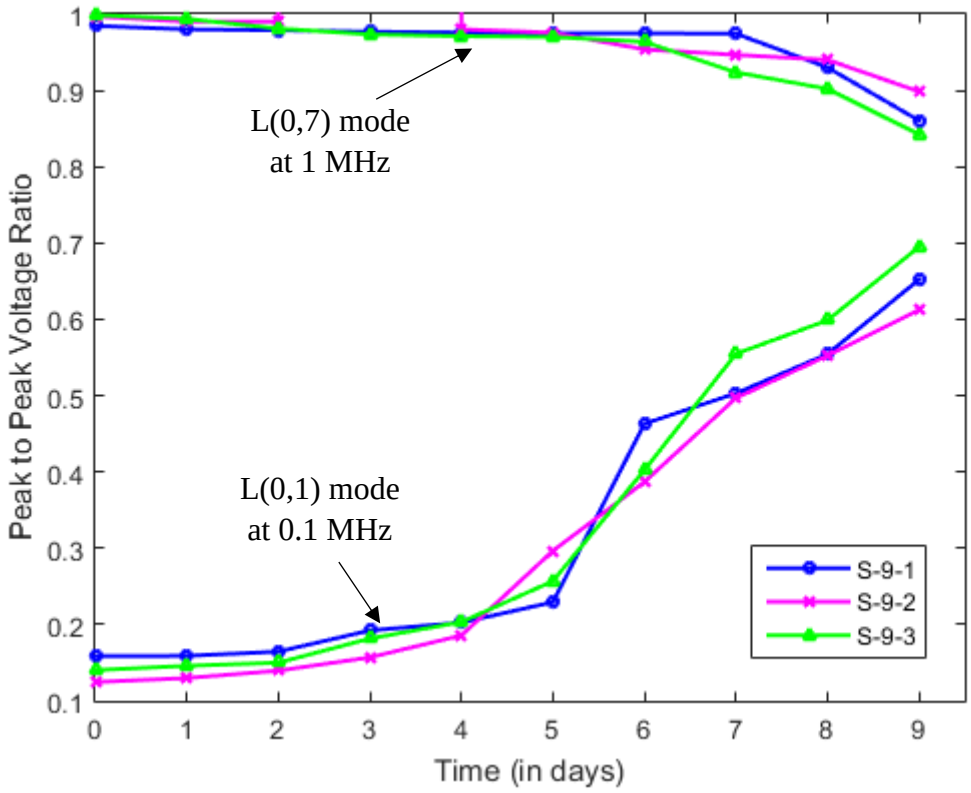

Fig. 3.8: Peak to Peak Voltage ratio trends using Core and Surface-seeking modes

3.5.2 L(0,1) mode at 0.1 MHz

The transmitted signal amplitudes obtained at different days of corrosion using L(0,1) mode are shown in **Fig. 3.9.** The trends of transmitted signal amplitudes normalized with respect to healthy beam ultrasonic guided wave signal amplitudes is shown in **Fig. 3.8** using L(0,1) mode. It is observed that there is a gradual rise in the signal up to five days. After 5 days, the rate of rise in the signal amplitude increases significantly. It is due to the initiation of corrosion in the bar after depassivation. The surface corrosion causes formation of rust products at the bar-concrete interface resulting in the loss of bond between the steel and the concrete. It separates the bar from the surrounding concrete by forming a softer layer of rust and impedes leakage of the pulse energy from the bar to concrete. Thus, higher energy reaches the other end of the bar resulting in the increase in signal amplitude. L(0,1) being a surface sensitive mode, detects the surface corrosion of the bar. Clearly, L(0,1) mode is able to detect when corrosion products are formed on the bar surface; in this case after 5 days.

T=1000/ GV of mode

=200 μs /5 km/s

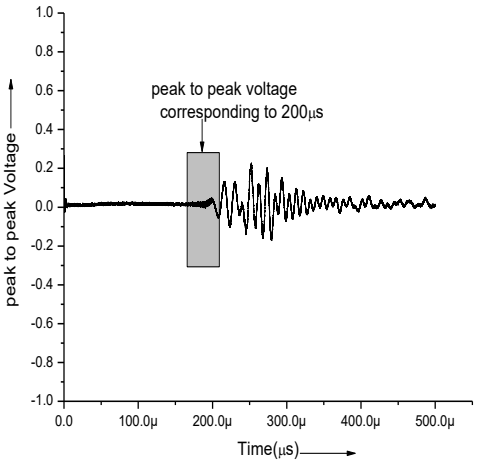

(a) Day 0

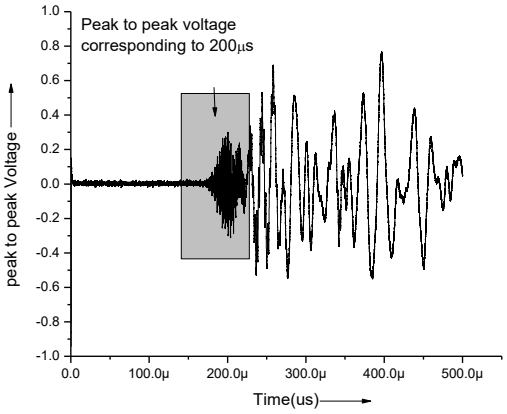

(b) Day 5

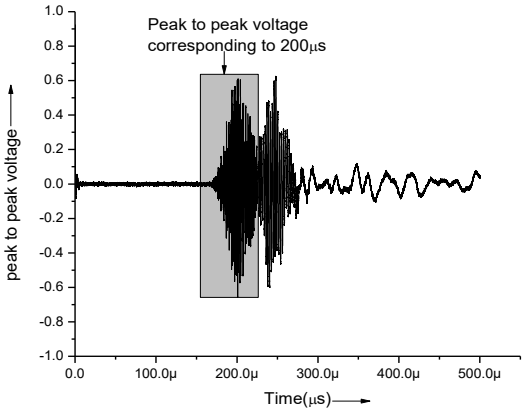

(c) Day 9

Fig. 3.9: PT signatures at different stages of corrosion using L(0,1) mode at 0.1 MHz

3.6 ACOUSTIC EMISSION INVESTIGATIONS

3.6.1 Cumulative AE Hits

AE signals generated as a result of corrosion in rebar were monitored by six AE sensors and digitized using AE win software. The results are displayed in various parameters such as amplitude of AE signals, AE hits, absolute energy and signal strength.

With increasing exposure, cumulative AE hits are plotted for total duration of exposure of 9 days of accelerated corrosion (**Fig. 3.10)**. It can be observed that there is high AE activity recorded during the entire duration of 9 days of accelerated corrosion. AE hits were observed from the first day of exposure and the number of hits continuously increased with time. There is a marked increase in the rate of hits between day 2 and 3. It may be recalled that corrosion

activity was discernible at day 5 with ultrasonic L(0,1) mode which has been related to surface corrosion (**Fig. 3.8**).

In case of L(0,7) mode the signal altered noticeably on day 7 which has been related to pitting (**Fig. 3.8**). In case of electrochemical methods, on the other hand, a sharp drop on day 2 was observed (**Fig. 3.5**). A sudden drop in impressed current was also noticed on day 2 (**Fig. 3.6**). The change of trend in HCP or impressed current is most likely to signify break down of the passive layer. There was no visual manifestation of corrosion on days 2 and 3 (**Fig. 3.4**). Clearly, acoustic events occur prior to the formation of corrosion products on the surface of the rebar. Thus, AE has the potential to detect early stage corrosion at a stage the passivation layer breaks down.

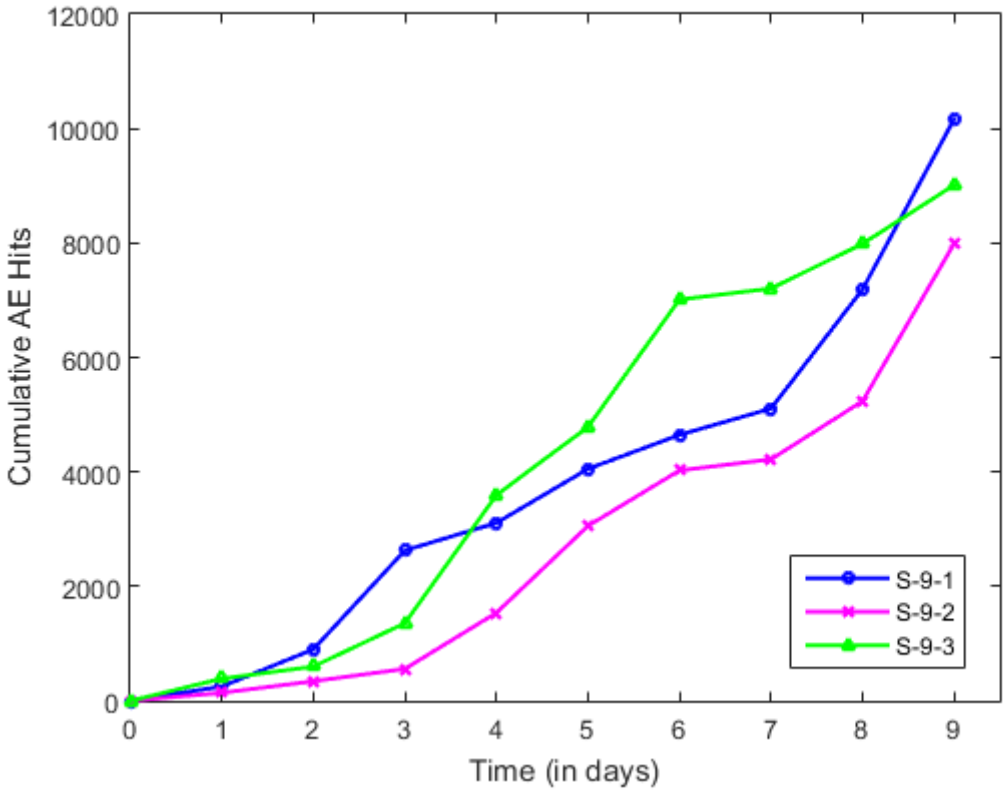

Fig. 3.10 Cumulative AE hits with increasing exposure to accelerated corrosion

3.6.2 Cumulative Signal Strength (CSS)

Cumulative signal strength is defined as the integral of rectified voltage signals over the duration of AE waveform packet**.** It is a parameter that is governed by two AE parameters of AE signals i.e., amplitude and duration [44, 47, 49]. The CSS curve (**Fig. 3.11**) is observed to have the same trend as in AE hits. However, the sudden rise in the AE hits on Day 2 is not so clearly visible in case of CSS curve. This indicates that the initial AE events, although in

substantial numbers, are of relatively smaller intensity. **Fig. 3.12** plots the AE events each day with their corresponding amplitudes. Clearly, while the number of events is more evenly distributed over the days, the intensity of the events increases with time. During the initial stages the cracking emits smaller energy, possibly signifying micro-cracking.

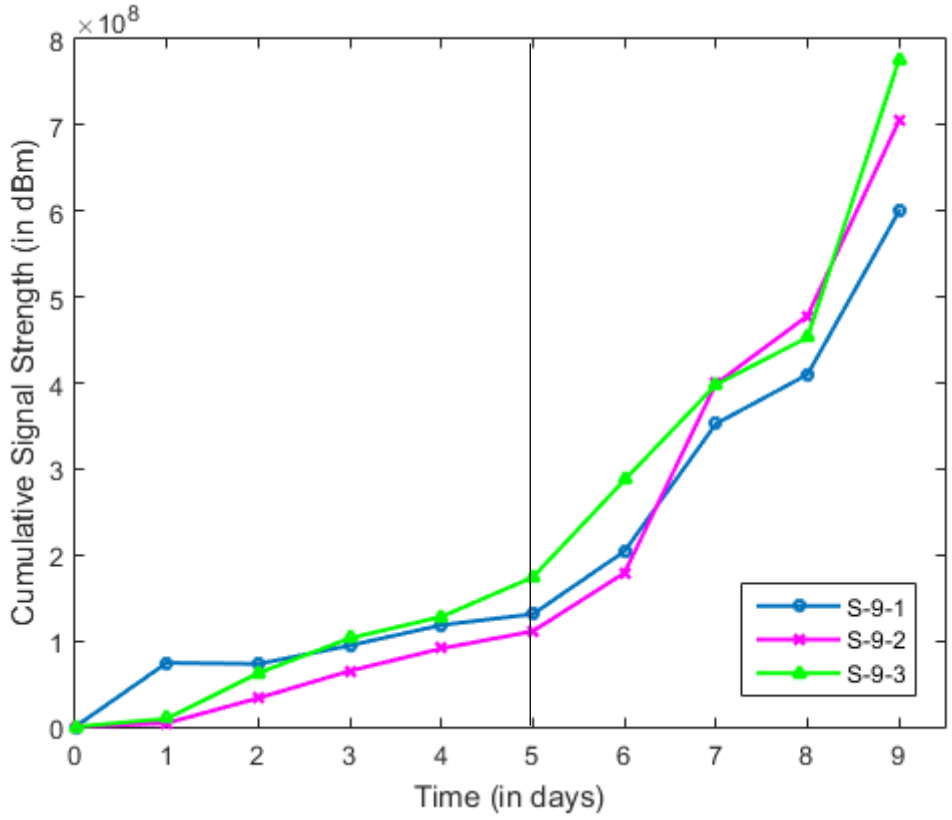

Fig. 3.11 Variation of Cumulative Signal Strength with corrosion progression

At later stages the cracks coalesce to form large cracks releasing much larger energy. During the 9 days of exposure, the amplitude of recorded AE hits also had a distinctive pattern (**Fig. 3.12**). During the first 5 days, the amplitude rose but remained within a relatively narrow range from 60 dB to 75 dB. On day 5, there has been marked increase in the amplitude. It may be recalled that from that point of time the delamination between concrete and the rebar was detected through ultrasonics. Ostensibly, the delamination is triggered through major acoustic events of large amplitudes, possibly due to coalescence of the micro cracks to form major cracks. From that point onwards the amplitude of the acoustic events remained relatively high and it rose from 75 dB to 95 dB. Once concrete starts to crack the cracking progresses until it relieves the bursting pressure created due to corrosion. This implies that the amplitude of recorded AE signals gives significant information about the type and extent of corrosion that an embedded rebar undergoes.

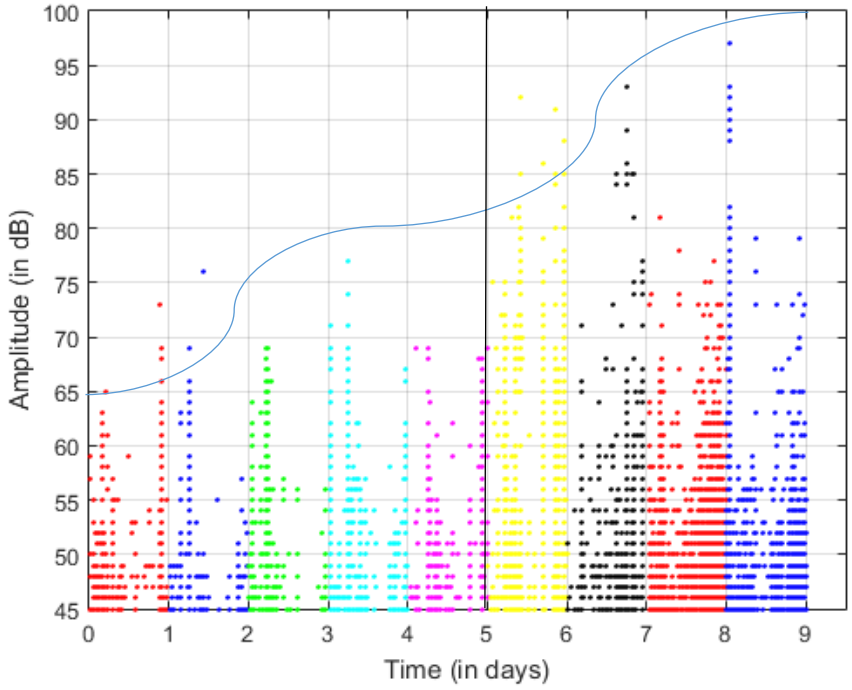

Fig. 3.12 Variation of amplitude of AE hits with time for (S-9-3)

3.6.3 AE Event Maps

The locations of AE hits can be determined from the recordings of events from a number of receivers that traces back the point of origin of event. The source location is based on Time of Arrival (TOA) approach and is extracted from the data using 3-D locate software tool. The discussion of the working of TOA is given in chapter 2. This section reports the chronological sequences of events recorded in this experiment (**Fig. 3.13**). It is important to note that the acoustic events that occur within the zone covered by the receivers are reliably tracked. Location of events occurring in other parts of sample is not reliably traced.

There are very few AE event records on day 1. The first events were near the central part of beam in the vicinity of where the rebar was placed. However, they were not exactly at the location of rebar. It is likely that the first events were triggered at a position of damage. On subsequent days, the events spread from their initial location. It may be noted that no visual manifestation of damage is observed at this time.

From day 3, a definite pattern in the spread of event locations was noted. They moved from the centre towards the surface of beam. The events had spread on both sides of reinforcement. By day 4, the events began to group together and started looking like a crack. From day 5, a vertical crack through the depth of beam is clearly discernible. It may be noted that on day 5 a small surface crack was noticed. On day 6, a brown liquid started oozing out in small quantities confirming that the crack has spread from the rebar at the centre to the surface. From that point

onwards the events had spread further in both directions. Evidently, the AE event maps agree well with visual observations.

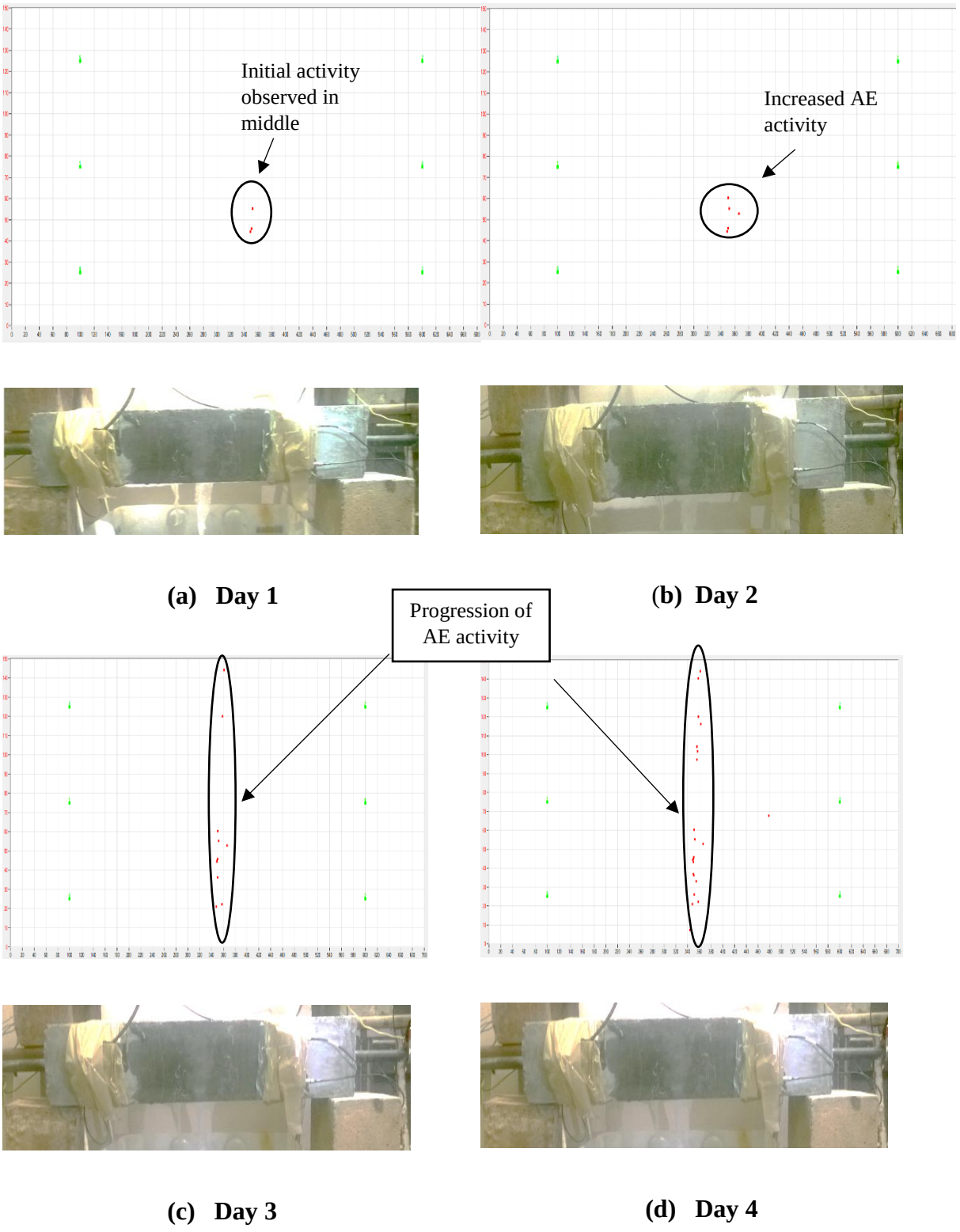

(a) Day 1 **(b) Day 2**

(c) Day 3 **(d) Day 4**

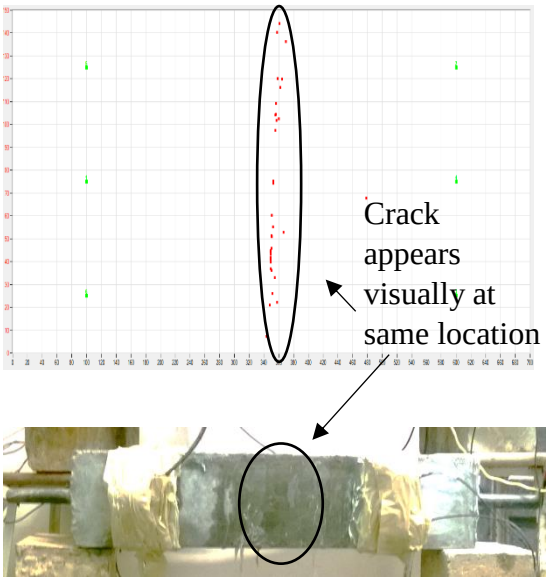

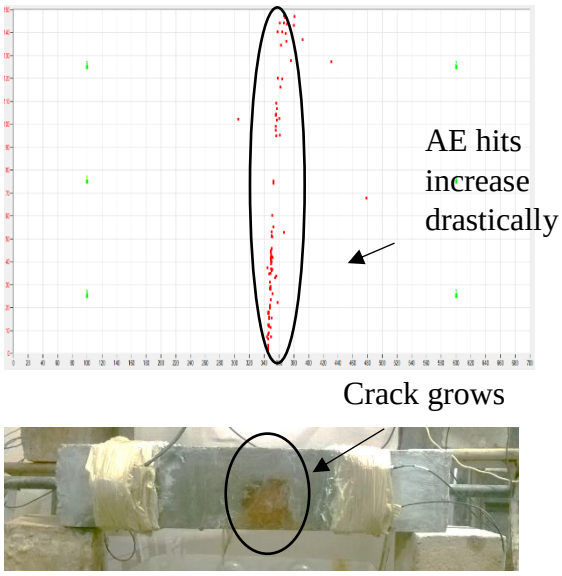

(e) Day 5

(f) Day 6

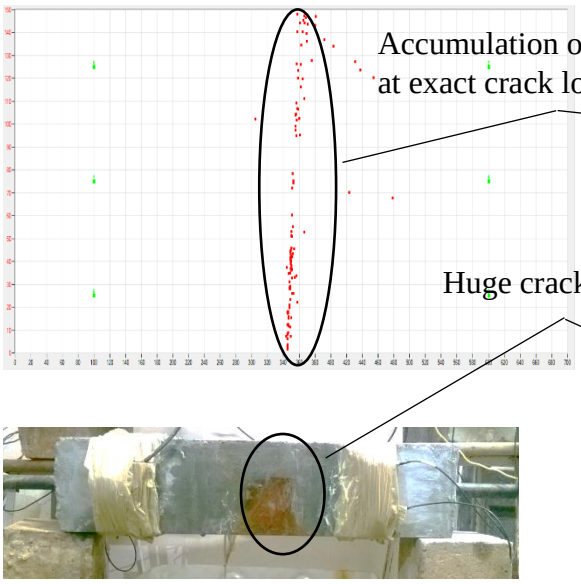

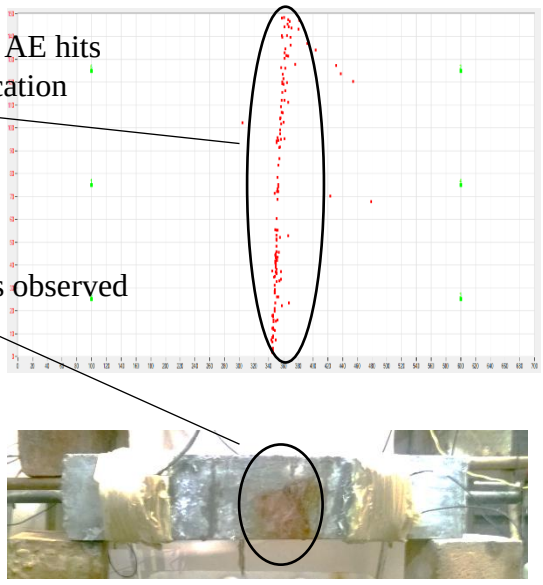

(g) Day 7

(h) Day 8

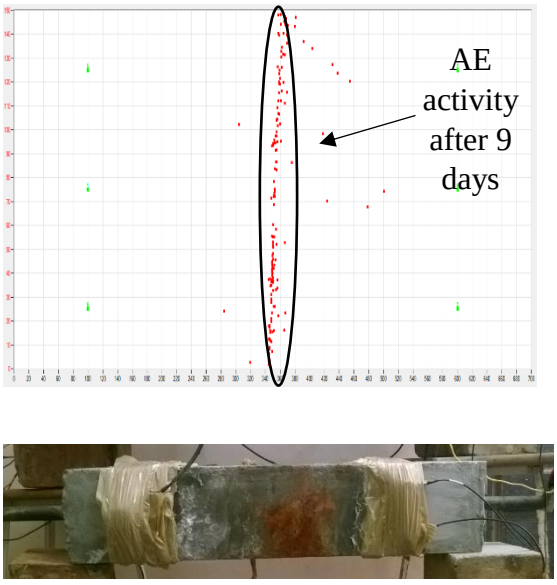

(i) Day 9

Fig. 3.13: AE X-Y plots with increasing corrosion exposure

This experiment demonstrates that the acoustic emissions due to corrosion start well ahead of the cracks are visible at the surface. Thus, invisible corrosion can indeed be monitored through acoustic emission. The growth of damage in concrete from the initiation of micro-cracks to the visible surface cracking can be reliably mapped through this technology. Precise information of the corrosion status can be obtained from the combination of event maps, cumulative AE hits and their corresponding strengths. At the onset of corrosion there is a sudden increase in the number of AE hits. The event amplitudes, on the other hand, increases suddenly when the micro-cracks coalesce to form major cracks. The event maps reveal the location of corrosion damage as well.

3.7 COMPARATIVE ANALYSIS OF NDT TECHNIQUES

Three NDT techniques have been used in this study, for monitoring impressed current corrosion in RC structures of HCP, UGW and AE. From the results (**Fig. 3.5** and **Fig. 3.6**), it can be clearly seen that HCP indicates the likelihood of corrosion through a sudden drop in half-cell potential. However, it does not provide any quantitative information about the onset or progression of corrosion. Moreover, it has been reported that the factors such as concrete cover, depth, surface conditions and electrical resistance are may influence HCP measurements. No information about the location of corrosion damage inside the RC structure is obtained through HCP measurements.

Propagating ultrasonic guided waves through reinforcing bar embedded in concrete using core-seeking mode and surface-seeking modes **(Fig. 3.8)** are capable of differentiating between delamination and pitting corrosion. However, they tend to be more sensitive to physical changes at bar-concrete interface. To discern early stage invisible corrosion prior to physical changes, one needs continuous monitoring using AE. It has shown a spurt of AE hits at the initiation of corrosion. There is a continuous and consistent increase in AE hits and AE signal strength which can be related to the acoustic activity occurring in concrete due to corrosion (**Fig. 3.10-3.12)**. By plotting AE event maps it is possible to locate the origin and track the progress of cracking in concrete (**Fig. 3.13**). It gives a pictorial view of the damage map in concrete structures. This implies that AE is highly effective in detecting the presence, initiation, localization, intensity and mapping of damage due to corrosion in RC structures.

Fig. 3.14 presents composite results obtained from all the three techniques i.e. half-cell potential measurements, ultrasonic guided wave measurements and acoustic emission for monitoring onset of corrosion and its initiation during the first five days. It can be clearly observed that AE hits are recorded increasingly in the first two days when the other recordings are relatively flat. AE signals possibly indicate when micro cracks coalesce to form large cracks through sudden increase in the strength of the signals. From AE event maps, the growth of corrosion cracks can be tracked.

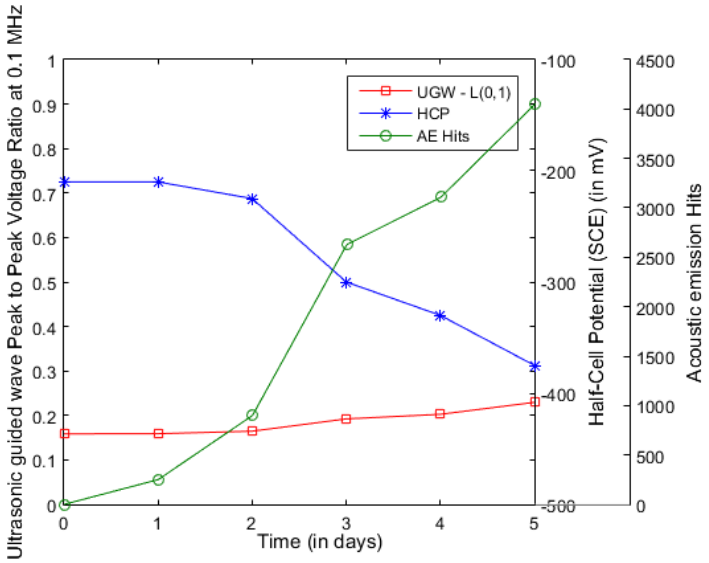

(a) S-9-1

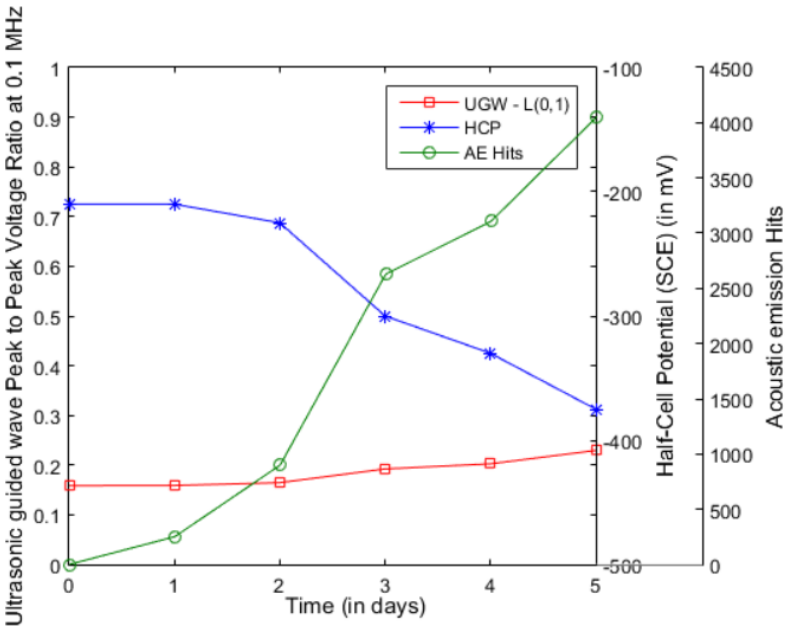

(b) S-9-2

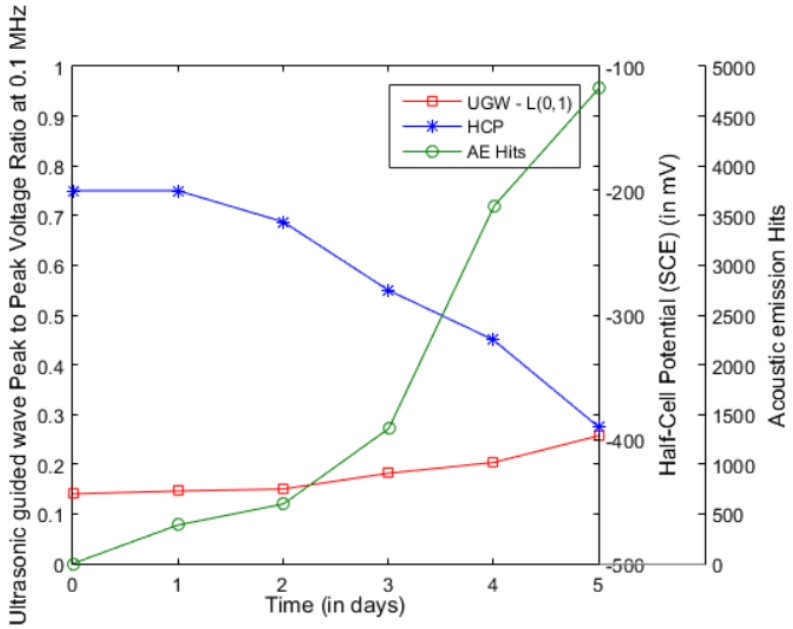

(c) S-9-3

Fig. 3.14 Comparison of HCP, UGW and AE for monitoring initial corrosion upto 5 days

Although AE technique seems to give more detailed information on corrosion, it may be borne in mind that the sensors must be installed at all times for AE. The other techniques offer the flexibility of monitoring the structure periodically with removable sensors. A combination

of active UGW and passive AE technique can be effectively used for monitoring corrosion phenomenon in concrete. While AE may be more efficient in monitoring the initial phases of corrosion, it may not be reliable in case of a profusely cracked structure as the cracks would resist the AE signals to reach the sensors. Moreover, ultrasonic guided wave techniques may be more suitable to monitor the manner of corrosion (surface or pitting). Thus, a combination of UGW and AE may be optimal for diagnosis and prognosis of corrosion.

3.8 CLOSING REMARKS

The chapter reports two non-destructive techniques based on wave propagation for monitoring onset of corrosion in concrete before it is visible. Reinforced concrete beam specimens were subjected to anodic corrosion at a constant voltage. The specimens were instrumented with surface mounted AE sensors to record acoustic events inside the specimens due to corrosion. They were also monitored using the Ultrasonic Guided Wave technique by passing an ultrasonic pulse through the bar. The results are correlated with well-established electrochemical techniques. From simultaneous monitoring of corrosion using the three technologies, pros and cons of each technology have been determined. It can be concluded that a judicious combination of electrochemical and wave technologies can reveal the state of corrosion from its early stages.

CHAPTER 4

MONITORING PROGRESSION OF CORROSION

4.1 GENERAL

The monitoring of initial stages of corrosion-induced damage corresponding to Phase 1 of the phenomenological model was studied in the preceding chapter, using electrochemical as well as suggested wave based active and passive monitoring techniques of UGW and AE respectively. The vis-à-vis efficacy of the three NDT techniques with respect to initiation of corrosion in RC structures was established. This chapter reports investigation of deterioration with considerable corrosion in RC structures. The focus is to investigate the applicability and effectiveness of monitoring different stages of initiation, progression and concrete cracking due to chloride induced corrosion in RC structures involving both active UGW and passive AE techniques. UGW measurements are reported directly on the embedded rebar by propagating waves through them, while the RC beams are undergoing corrosion. AE sensors were mounted on the concrete directly for recording the effect of corrosion on surrounding concrete in advanced stages as in Phase 2, 3 & 4 of the phenomenological model. The main factors that influence the AE signals are source characteristics, path between the source and transducer, transducer characteristics and the measuring system. The NDT investigations utilizing both UGW and AE are carried out in RC beams undergoing corrosion at advanced and progressive stages.

4.2 EXPERIMENTAL INVESTIGATION AND METHODOLOGY

4.2.1 Specimen Details

For non-destructive monitoring at advanced stages of corrosion, four small scale RC beams of similar dimensions 150 mm × 150 mm × 700 mm with three replicates of each, were cast using the mix proportions of cement, sand and stone aggregates as 1:1.49:2.59 with a water-cement ratio of 0.45. A single plain mild steel bar of diameter 25 mm and 1.0 m length was kept embedded at the centre of cross-section of beam and 150 mm length of bar was projected at both ends of beam. The methodology of UGW and AE used for corrosion remained same as reported in **Chapter 3** shown by **Fig. 3.2 & 3.3**. **Table 4.1** shows the nomenclature followed for specimens undergoing corrosion for 9, 19, 30 & 48 days. Three samples of each specimen were tested to ensure the repeatability of results. The statistical spread in the observations was small and hence, the mean values have been plotted for HCP, UGW & AE results.

Table 4.1 Nomenclature of samples used for monitoring advanced corrosion

Specimen nomenclature	Duration of exposure (days)
S9	9 days
S19	19 days
S30	30 days
S48	48 days

4.2.2 Inducing accelerated corrosion

Acceleration of corrosion in all samples was done by impressed current techniques as explained in **Chapter 3**. As outlined, the four beams were exposed to different durations of chloride exposure for 9 days (S9), 19 days (S19), 30 days (S30) and 48 days (S48).

4.3 RESULTS AND DISCUSSIONS

4.3.1 Visual Observations

RC beam undergoing accelerated corrosion showed formation of reddish brown corrosion products with the increasing exposure to corrosive environment. After 9 days of accelerated corrosion, cracks started appearing on the surface of beam as shown in **Fig. 4.1(a)**. A reddish brown liquid started oozing out of the crack. The length and width of cracks increased with the increasing exposure to corrosive environment which is very clearly visible in **Fig. 4.1(a)–(d)**. After 48 days of corrosion, RC beam was in a highly degraded condition. Long and wide cracks were visible parallel to the reinforcing bar throughout the length of beam. Visual observations confirmed that the longitudinal crack appeared after 6–7 days of accelerated corrosion and with further exposure, these cracks get widened and elongated and spread in the entire length in 48 days. Another distinguishing feature observed was the appearance of transverse cracks which started initiating after 18–20 days and were predominantly visible at 30 days (**Fig. 4.1(d)**). It was accompanied by widespread rust staining in the beam.

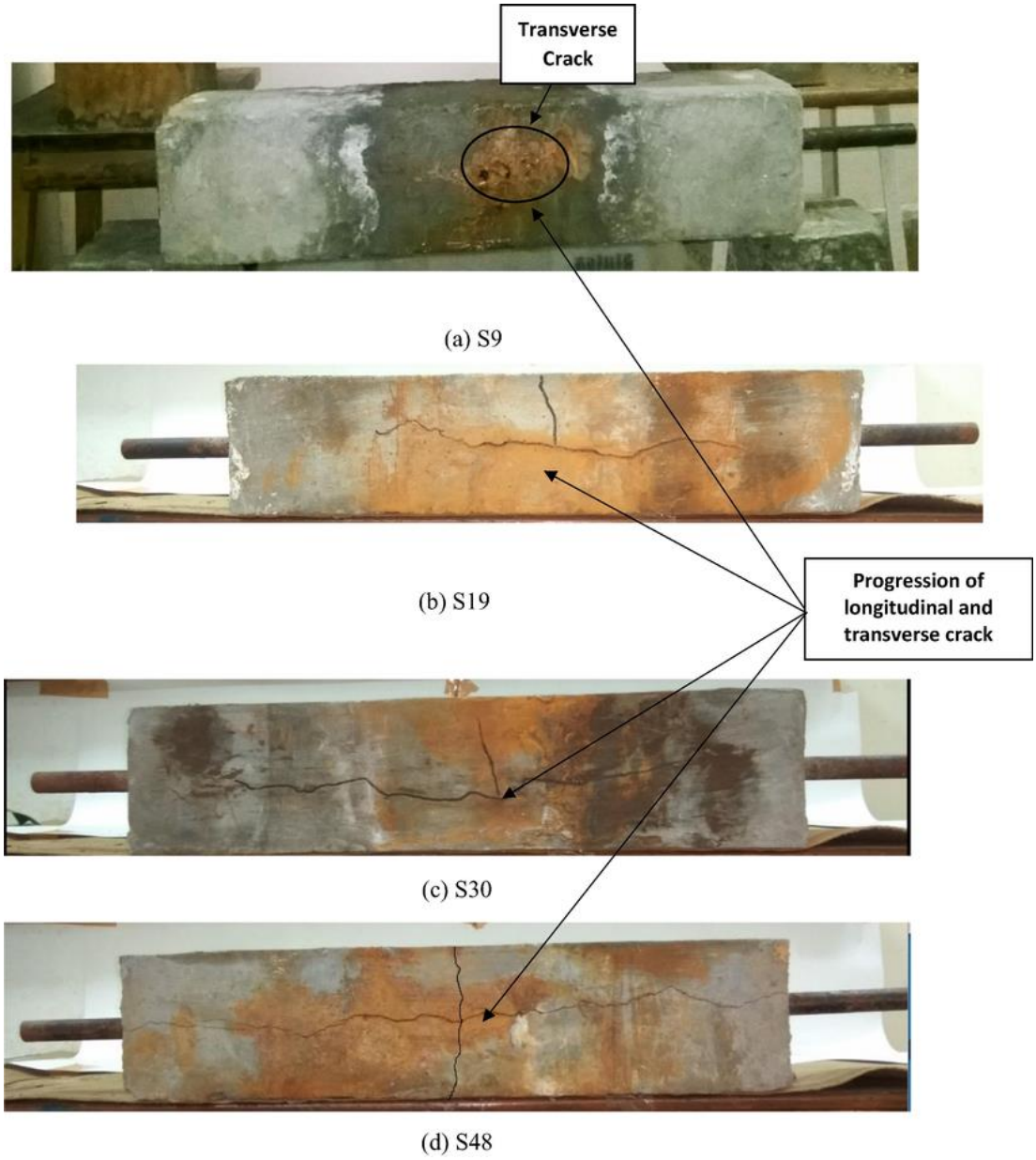

Fig. 4.1 Visual Observations in Beams corroded to different levels

4.3.2 Half-cell potential measurements

Half-Cell potential measurements were taken on RC beams as shown in **Fig. 4.2**. Low initial values (which were more positive in nature i.e., less than 200 mV) were recorded thereby indicating the initial passive conditions of rebar. However, as the corrosion progressed, the recorded potentials started decreasing rapidly and fell below −350 mV after 5–6 days. This indicates depassivation of protective layer and progression of corrosion into rebar. It is well supported by the formation of rust products and consequent cracking of concrete after 6–7 days. This further allowed easy permeation of electrolyte through the concrete cover and therefore, rapid reduction of potential was noted.

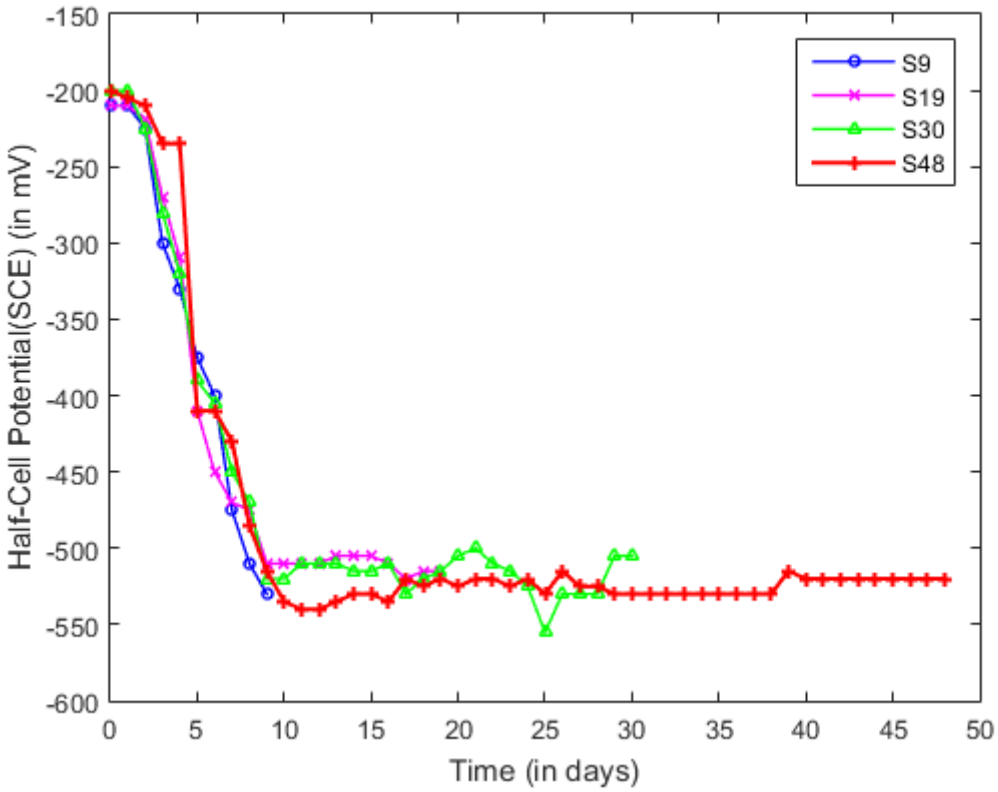

Fig. 4.2 Half-cell potential measurements with progressive corrosion

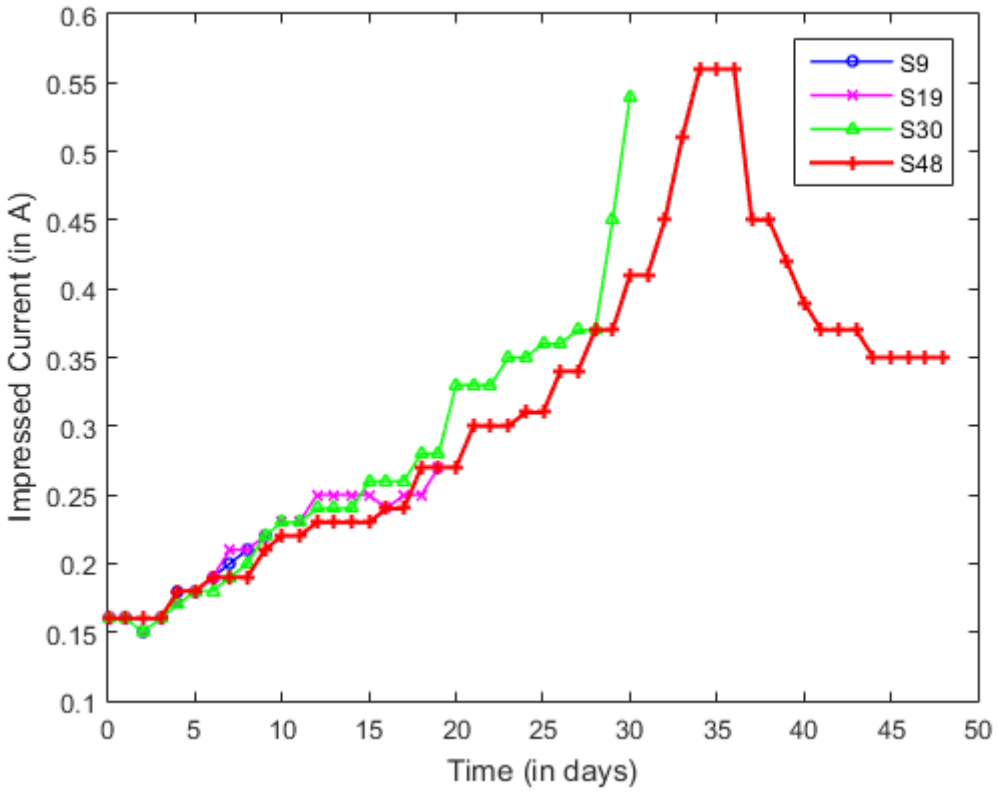

Fig. 4.3 Variation in Impressed Current with time for different specimens

The propagation of corrosion was also estimated through the measurement of anodic current through bar while the voltage was kept constant. At the constant voltage from power supply, the current was noted after every 24 hours (**Fig. 4.3**). It was observed that for initial 2 days of exposure, there is a marginal drop in the current. It can be considered as the period during which the passive layer forms. This may be due to the build-up of corrosion products that has higher electrical resistance. After this period, the current starts increasing with time indicating gradual breakdown of the passive layer due to ingress of chloride ions leading to initiation of corrosion. The current continued to increase until 30 days when the corrosion had progressed extensively. This indicates that the effective resistance of the system comes down due to corrosion. Progressive cracking of concrete provides easier access of chloride ions affecting lower electrical resistance.

4.3.3 Effect of corrosion on rebar with UGW

The embedded rebar in RC beam specimens undergoing corrosion is monitored periodically using selected ultrasonic guided wave modes of L(0,1) at 0.1 MHz and L(0,7) at 1 MHZ respectively in pulse transmission mode. Ultrasonic pulse transmission signals were recorded after every 24 hours for the total duration of exposure of 48 days. For S48 sample, **Figs. 4.4** and **4.5** show the transmitted peaks obtained with L(0,1) mode at 0.1 MHz and L(0,7) mode at 1 MHz through the embedded bar at different stages of corrosion in S48 sample. Damage experienced by the rebar due to corrosion at any instance can be studied by measuring the relative change in the amplitude of transmitted signal vis-à-vis the maximum signal strength. The received signals are normalised with respect to the peak signal to obtain the normalised peak to peak voltage ratios in the corresponding modes (**Fig. 4.6**).

In L(0,1) mode at 0.1 MHz, there is a steep rise in the transmitted signal for first 10 days. The rise is moderate from days 11 to 20. The rise in signal is due to the debonding of rebar from the surrounding concrete. Due to the formation of rust products on the surface of bar, a soft layer is created. It leads to reduction in leakage of signal into the surrounding concrete and hence, rise in signal. L(0,1) being a surface seeking mode is sensitive to surface modifications in the rebar due to corrosion. A gradual drop in the transmitted signal is observed after 24 days which continues till the end of the experiment (48 days). This points towards corrosion reaching the inner parts of rebar causing pitting and local area loss. The pits create a barrier to the ultrasonic waves and as a result, the signal strength falls.

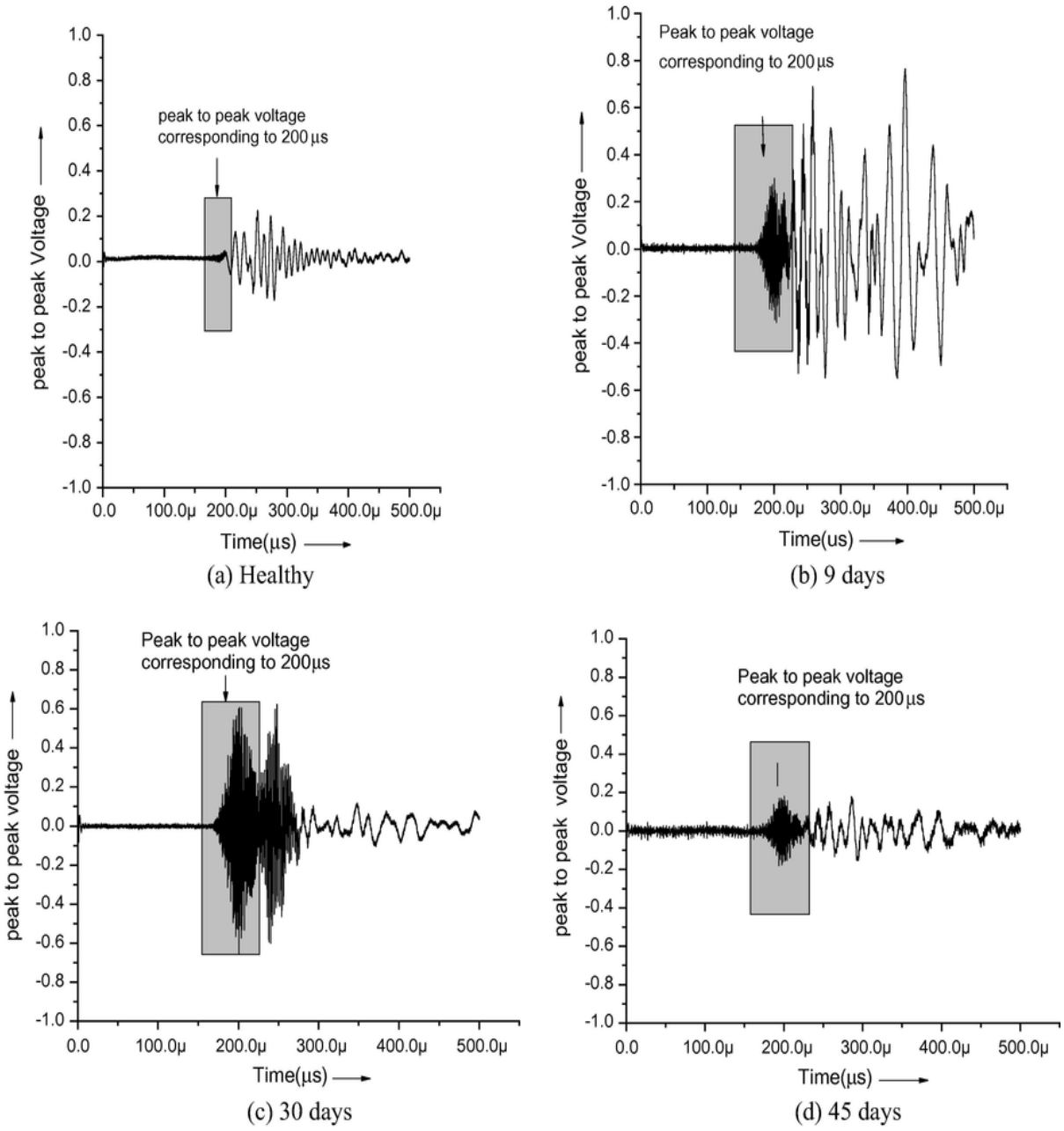

Fig. 4.4 PT signatures for S48 specimens undergoing progressive corrosion with L(0,1) mode at 0.1 MHz

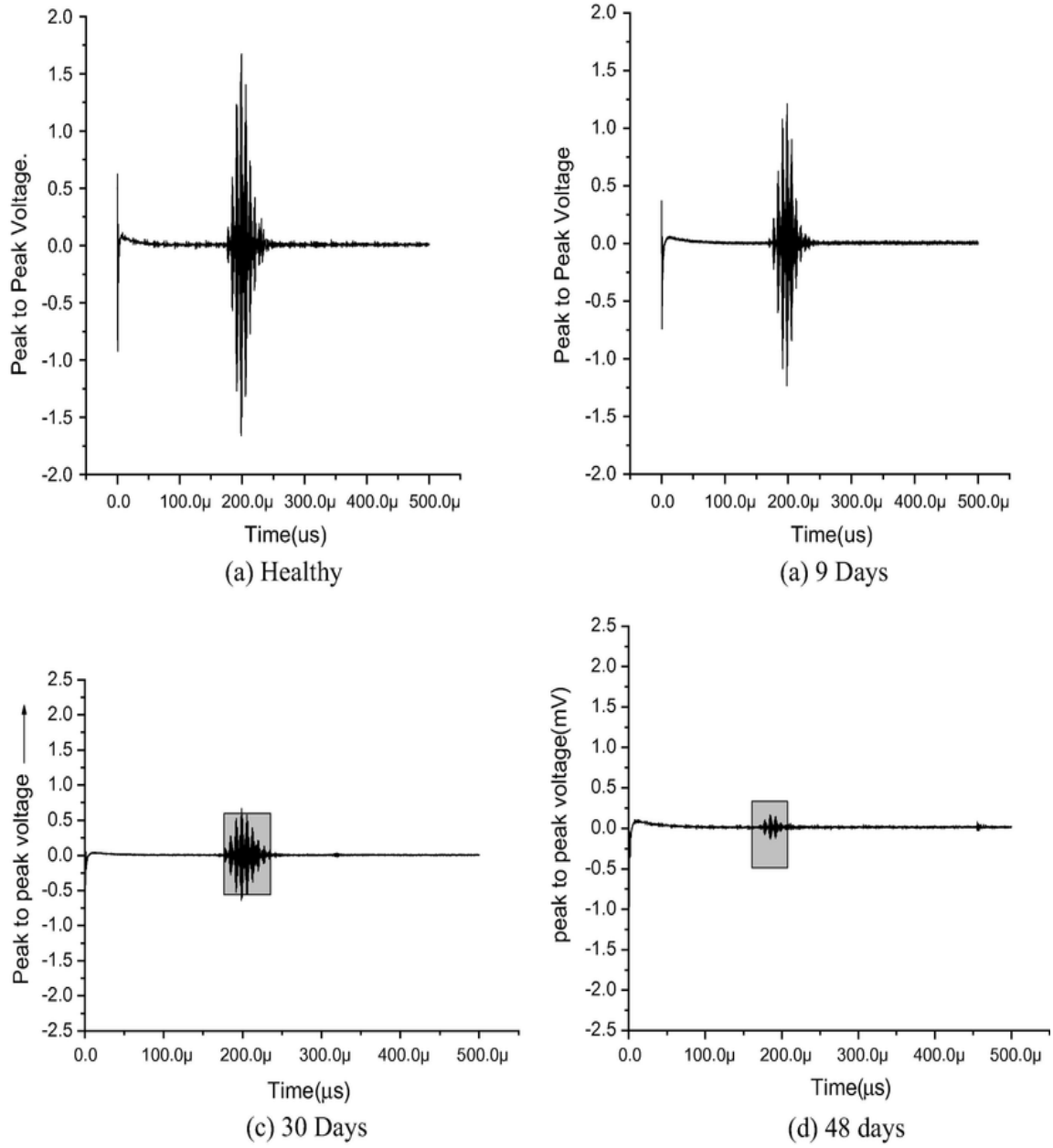

Fig. 4.5 PT signatures for S48 specimens undergoing progressive corrosion with L(0,7) mode at 1 MHz

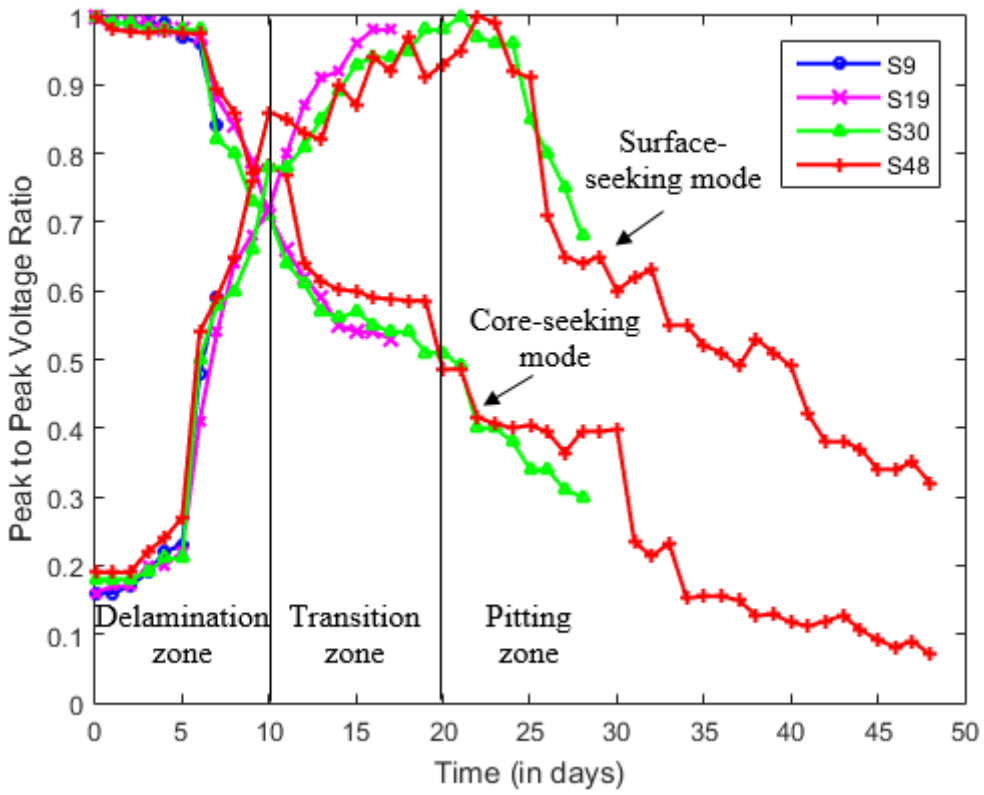

Fig. 4.6 Trends of variation in ultrasonic guided wave signal strengths with core and surface seeking modes

The transmitted signal strengths obtained with core-seeking mode L(0,7) at 1 MHz (**Fig. 4.6)** show no substantial variation for initial 8 days. However, during the remaining exposure duration, fall in transmitted signal strength is observed. The rate of fall in the signal slows down and is marginal between days 35 and 48. The fall in signal strength is primarily because of pitting in rebar due to the action of chlorides. The pits disturb the waveguide leading to scattering, multiple reflections and mode conversions and hence, loss in signal strength.

From the ultrasonic guided wave monitoring using both core and surface seeking modes in all samples (**Fig. 4.6**), it can be identified that corrosion mechanism in the presence of chlorides result in initial debonding of rebar from the surrounding concrete marked by signal rise during days 0–8. It is discerned well by the surface sensitive L(0,1) mode whereas no change in signal strength is observed in this duration in L(0,7) mode. During this period, the corrosion of rebar is mainly on the surface causing delamination of rebar from concrete (*Delamination Zone*). From days 8 to19, the corrosion starts to penetrate into the rebar causing local area loss marked by signal fall in L(0,7) mode but the signal rises in L(0,1) mode. Both pitting and delamination are predominant in this middle phase (11–24 days) and is termed as *'Transition Zone'* of rebar corrosion [19, 21]. During the remaining duration of exposure from days 20 to 35, both modes

show fall in signal strength pointing towards the pitting of rebar and hence loss in signal strength. It is the '*Pitting Zone'* of rebar corrosion. Between days 35 and 48, the rate of drop in signal strength slows down indicating advanced level of corrosion that no longer affects the signals significantly. The combination of two judiciously selected surface and core sensitive modes respectively can discern the initiation and progression of corrosion in rebar in concrete throughout the duration of exposure.

UGW monitoring indirectly picks up the phenomenon of chloride induced corrosion in RC structures by direct measurements of changes in UGW signal strength of carefully selected modes in embedded rebar in concrete. It does not indicate the effect of corrosion of rebar on the surrounding concrete in terms of micro to macro cracking due to corrosion. Hence, AE sensors mounted directly on concrete were used to study the phenomenon, mechanism and effect of corrosion on the surrounding concrete.

4.3.4 Effect of corrosion on concrete using AE monitoring

AE hits picked up by AE sensors mounted on concrete directly was extracted and used to relate to effect of corrosion on concrete surrounding the rebar. Following AE parameters are studied in detail to understand the mechanism and effect of chloride induced corrosion in concrete.

Cumulative AE hits

Cumulative AE hits are plotted for total duration of exposure of 48 days of accelerated corrosion (**Fig. 4.7**). From the graph, it can be seen that there are four distinct stages of AE activity. It is observed that AE hits were recorded right from the beginning of experiment and continuously increased with increasing corrosion up to 8 days. This is in agreement with the *Phase1* of phenomenological model of corrosion. The initial AE activity illustrates that AE activities commence right at the initiation of exposure. The sharp rise in AE hits in this stage can be related with the depletion of passive layer and initiation of corrosion in rebar. It results in the formation of rust product and delamination of rebar from concrete as detected by UGW monitoring in '*Delamination Zone*' (0–8 days) using L(0,1) mode.

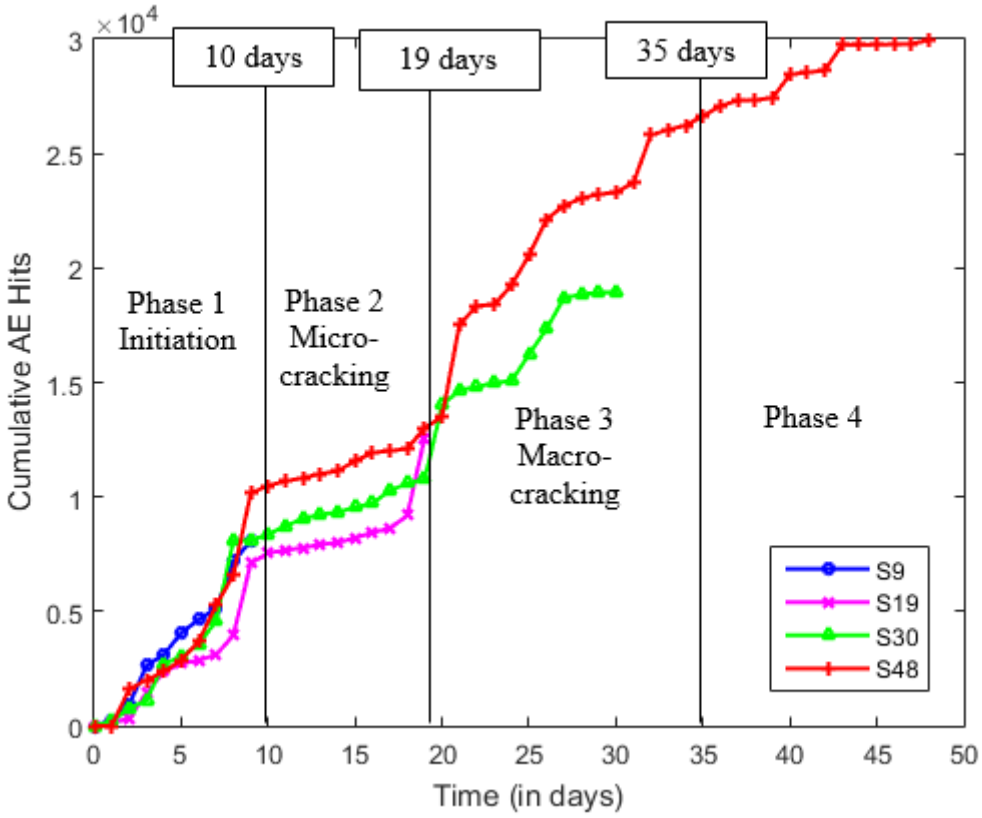

Fig. 4.7 Cumulative AE Hits with corrosion

Between days 9 and 19, there is very slow increase in the number of AE hits. This is analogous to *Phase 2* of the phenomenological model [27]. It is important to note that relationship between corrosion loss and time is non-linear in this phase. This phase corresponds to the '*Transition Zone*' of UGW monitoring wherein both debonding of bar as well as pitting initiates. Possibly, during this period, the corrosion activity shifts towards pitting and therefore, there is lower bursting pressure on concrete.

From days 19 to 35, there is a sharp rise in recorded AE hit data. This could be attributed to the bursting pressure on concrete due to rapid formation of corrosion products, leading to concrete cracking. Large AE activity during this duration is essentially due to the coalescence of micro cracks leading to the formation of continuous cracks. This corresponds with the *Phase 3* of corrosion model. Also, it has been in the *'Pitting Zone'* as recorded by UGW monitoring. Between days 35 and 48, a marginal number of AE hits is observed as the concrete has already cracked profusely and no further cracking is happening. This period is analogous to *Phase 4* of the phenomenological model. Hence, cumulative AE hits correspond well with ultrasonic records to non-destructively estimate corrosion of rebar in concrete.

Cumulative Signal Strength (CSS)

Another AE parameter, Cumulative Signal Strength is a reliable parameter as it is dependent on amplitude and duration of AE signals and is independent of gain. It is a measure of total energy released by the specimen as a result of AE activity [75]. **Fig. 4.8** shows the amplitude of each AE hit with time. It may be recalled that the specimens were exposed to varying lengths of time. As a result, different phases are manifested in different samples. In the first phase, the amplitudes of events were limited within 65 dB with occasional hits crossing that limit. There is a rapid increase in the number and amplitude of hits in the transition zone between *Phases 1 and 2*. Towards the middle of second phase, both the number and amplitude of events went down. The transition between *Phases 2 and 3* once again was marked by an increase in AE activity both in number and amplitude. The same phenomenon was noticed in *Phase 3* with the activities going down in the middle of phase and going up again at the transition between *Phases 3 and 4*. The beginning of *Phase 4* was marked by highest amplitude events in large numbers, which came down gradually as time progressed.

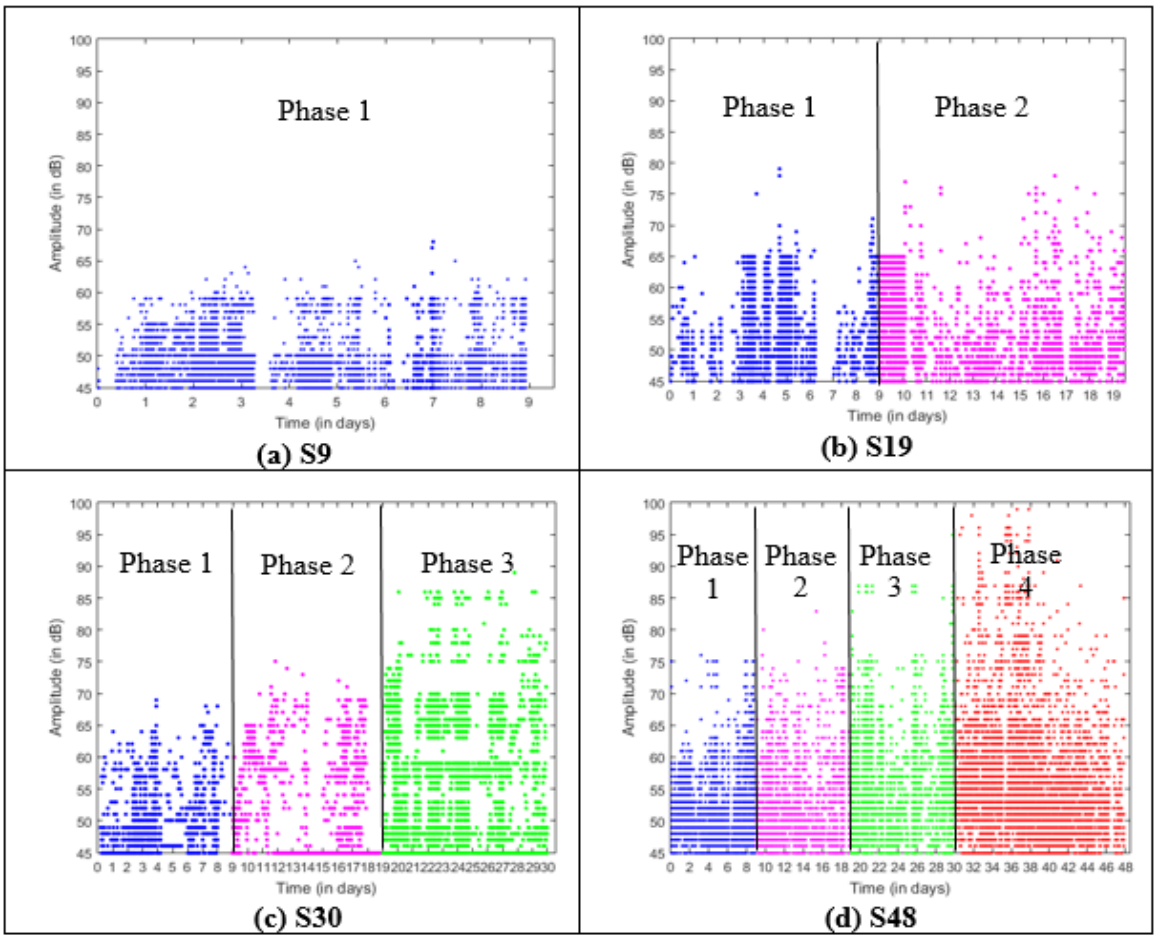

Fig. 4.8 Variation in amplitude of AE signals with increasing corrosion

Fig. 4.9 summarises the phenomenon in the form of CSS of all the specimens. Clearly, there is a great deal of agreement in the behaviour of all the samples. Thus, the present AE experiment is repeatable and reliable. Clearly, there is a sudden burst in signal strength at the transition of Phases 1 and 2 and Phases 3 and 4 known as 1st and 2nd Knees respectively. This phenomenon is not very prominent at the transition of Phases 2 and 3. In Phase 4, the AE activity is moderate. Although the cumulative AE hits and cumulative AE signal strength follow similar patterns, there are subtle differences. The transition between phases 1 and 2 are marked by sharp rise in both hits and strength. In the transition between Phases 2 and 3, AE hits showed a sharp rise but the rise in AE signal strength was moderate. It may be recalled that this transition is postulated as the coalescence of micro-cracks into formation of continuous cracks. At this time, events of smaller strength widespread in the cracking zone is expected. In the transition between Phases 3 and 4, there is a sharp increase in the AE signal strength AE hits is not very significant. At these phases, the cracks open up throughout the length of bar causing large AE amplitude.

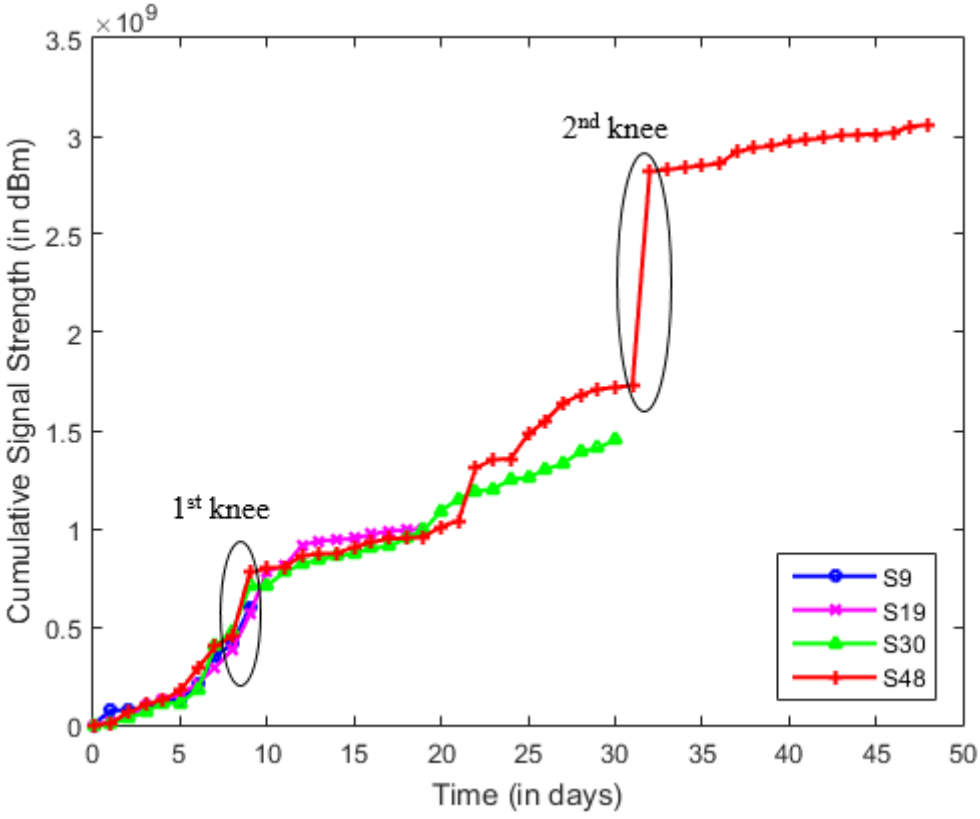

Fig. 4.9 Variation of Cumulative Signal Strength with corrosion progression

AE Event plots

To further understand the sequence of AE events, their locations within the beam have been plotted at different times in the form of event maps. The location of events during the entire process of damage are presented in x-y plots (**Fig. 4.10 (a)–(d)**). It may be recalled that the cracks can be located only in the zones covered by AE sensors. Every crack is labelled as an event recorded by 3 or more sensors.

After 9 days of corrosion exposure, a small transverse crack was observed in the beam out of which brown coloured liquid leaked (**Fig. 4.10(a)**) and this was also well depicted by AE event map with sharp rise in AE events. By day 19, a clear trajectory of longitudinal crack could be observed from the event plot (**Fig. 4.10(b)**). It was visually validated by removing the wire mesh from beam. By day 30, wide spread AE hits were recorded all over the beam (**Fig. 4.10(c)**). However, a clear trend of a longitudinal crack along the length of the bar and a transverse crack across the middle of the beam is clearly discernible. By day 48, AE event map is further crowded with a clear longitudinal and a transverse orientation. **Fig. 4.10(d)** illustrates the agreement between crack geometry and AE event map. Thus, AE event maps provide a real-time plot which is a good indicator of initiation and progression of cracking inside concrete due to corrosion.

4.4 COMPARATIVE ANALYSIS OF NDT FOR PROGRESSIVE CORROSION

All the three corrosion monitoring techniques used in this investigation, HCP, UGW and AE have been able to detect the corrosion. However, they manifest different aspects of it. HCP judges the likelihood of corrosion through the measurement of electro-chemical changes. In our investigation, HCP picked up corrosion but after significant damage had occurred. To get more nuanced information about the state of corrosion, UGW and the AE techniques are useful. Although both have been used in this investigation together, there is a fundamental difference between the two. While UGW monitors the rebar and estimates corrosion in it, AE monitors the events within concrete as a consequence of corrosion in the bar. There are pros and cons of the techniques in terms of convenience of measurement. UGW needs access to rebars whereas the AE sensors can be surface mounted on concrete directly. On the other hand, AE sensors must be mounted at all times during the corrosion process while UGW probes can be mounted as and when measurements are to be taken.

UGW successfully monitors corrosion and distinguishes surface corrosion from pitting. But it is important to note that no significant change in L(0,7) and very nominal change in L(0,1) signal strength is observed during initial days 0–5 days as against 5–15 days.

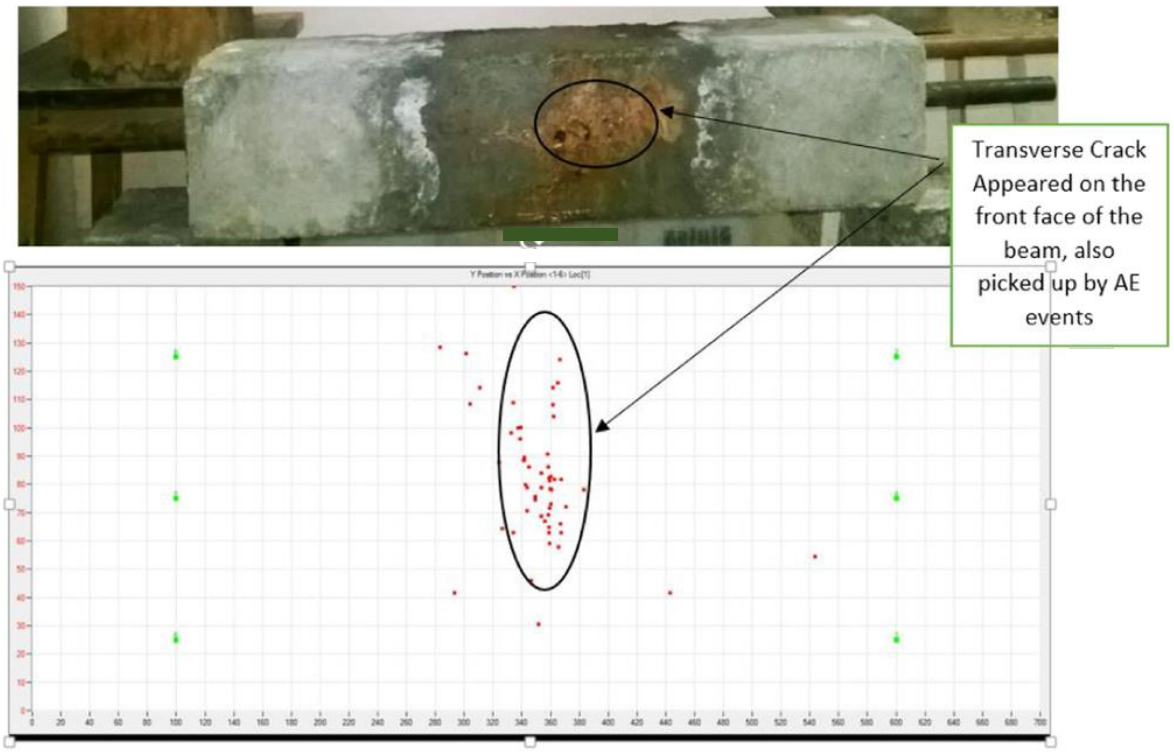
Transverse Crack Appeared on the front face of the beam, also picked up by AE events

(a) S9

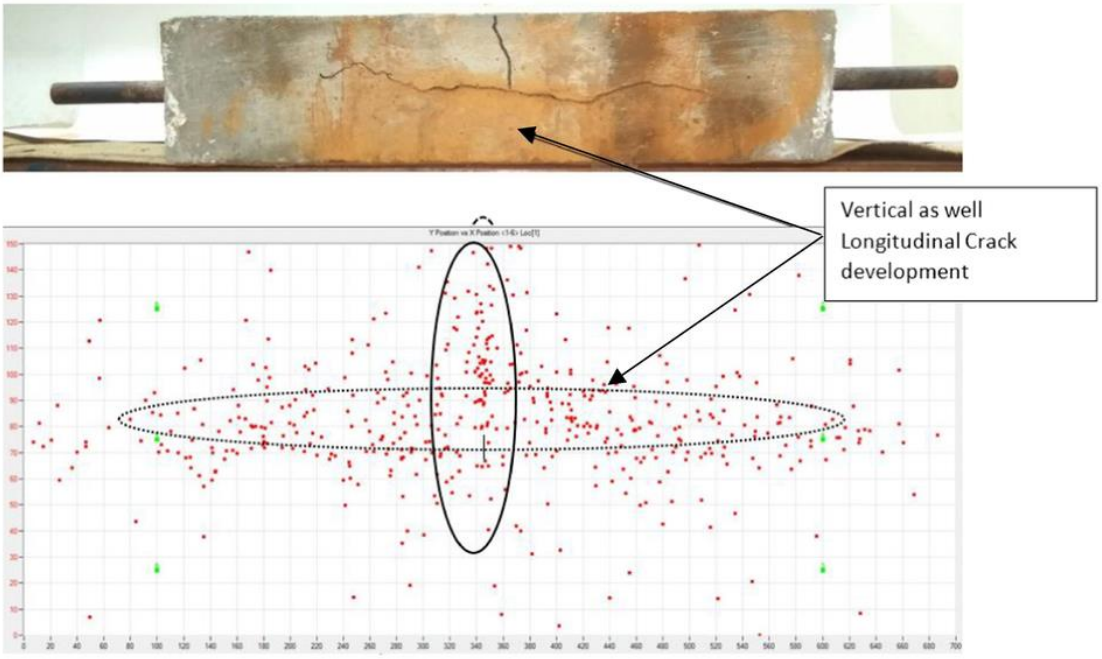
Vertical as well Longitudinal Crack development

(b) S19

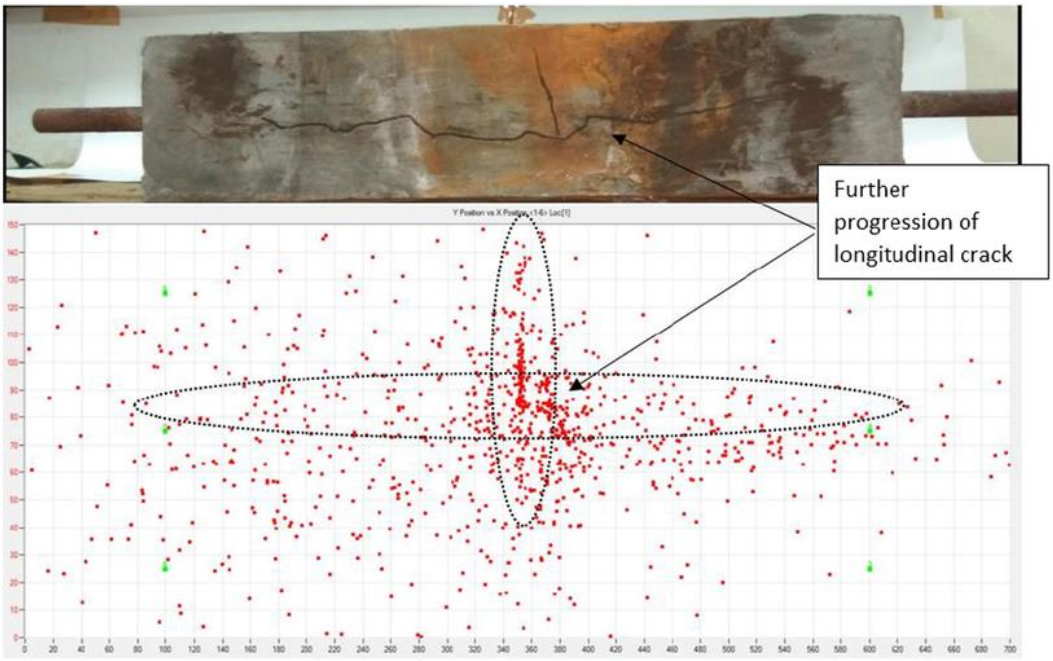

(c) S30

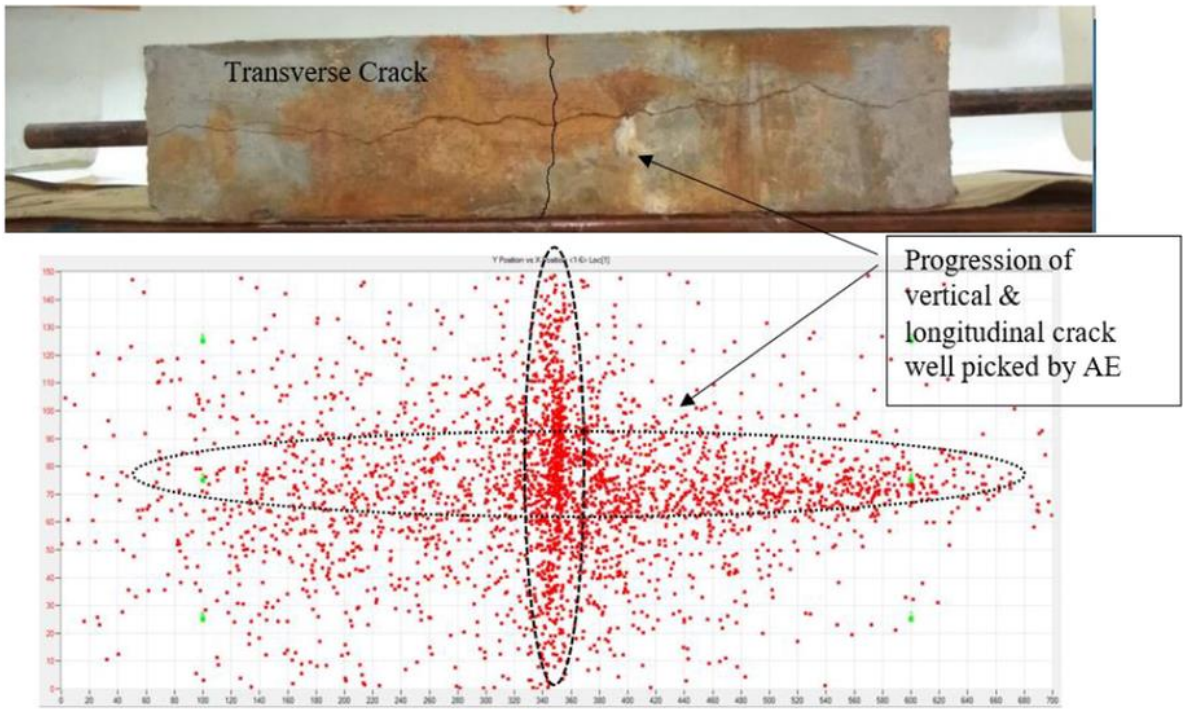

(d) S48

Fig. 4.10 AE Event plots for corroding beams at different levels of corrosion

However, significant AE activity relating to the initiation and onset of cracking inside concrete is observed. Hence, ultrasonic guided waves are more effective when corrosion has advanced. AE has been able to pinpoint the location of events right from the early stages to the end where corrosion was widespread. There is a good agreement among the milestones in the corrosion process observed through UGW and AE. It may also be remembered that while UGW

seeks the change in bar due to corrosion, AE notes the consequence of corrosion as an energy release in concrete. In a field test, AE events may occur due to reasons other than corrosion in the bar, while UGW remains dedicated to measurement of corrosion. Hence, the active UGW in conjunction the passive AE monitoring can be used simultaneously to develop a corrosion monitoring strategy to cover all stages of corrosion.

4.5 DESTRUCTIVE TESTING

After the beam samples had undergone corrosion for the desired periods, the bars were extracted. **Fig. 4.11** shows the condition of bars at different days of exposure. At day 9, surface corrosion is clearly visible. Loss of metal is restricted within the central zone at this stage. It may be recalled that at this time only a small crack in concrete was visible and no clear crack pattern had emerged. At day 19, corrosion had spread over a larger area with some instances of pitting. By this time a longitudinal crack was visible on the surface of concrete. At day 30, pitting corrosion is widespread and a substantial loss of metal is visible. A localised reduction in the cross-section of bar is discernible at this stage. At day 48, large parts of the bar were lost and the bar cross-section is very irregular.

Fig. 4.11 Visual condition of the extracted bars at different ages of corrosion

The bars were cleaned of any loose matter and weighed to estimate the mass loss. The cleaned bars were tested for residual tensile strength test in Universal Testing Machine (Hung Ta make with capacity of 10MN). Stress-strain graphs obtained for all the rebars are presented in **Fig. 4.12**. It can be seen that the bars lost both strength and deformability with advancing corrosion.

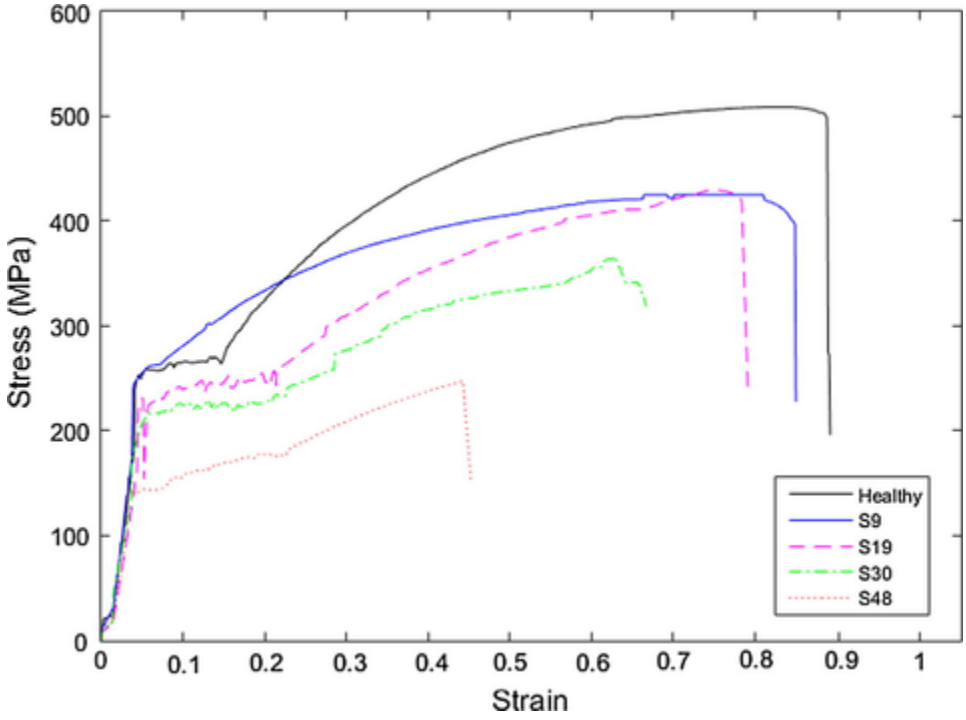

Fig. 4.12 Stress-strain plots for corroded rebar at different stages

Table 4.2 Mass loss and loss in tensile strength

Specimen	Mass loss (%)	Loss in tensile strength (%)	Initial stiffness (N/mm)	Yield stress (MPa)	Yield strain (ε_{y})	Modulus of elasticity (E)	Ultimate stress (MPa)	Ulimate strain (ε_{u})	Ductility ratio ($\varepsilon_u/\varepsilon_y$)
S0	0	0	24.65	257.4	0.0255	208	508	0.356	14
S9	2.1	9.12	24.60	254.4	0.0250	205	425	0.340	13.6
S19	4.6	19.38	24.55	219.2	0.0235	205	429	0.316	13.4
S30	6.63	29.59	24.51	207.4	0.0205	207	367	0.267	13
S48	10.3	44.53	24.15	145.4	0.0300	202	247	0.177	5.9

The key parameters extracted from these graphs have been presented along with the mass loss in **Table 4.2**. It can be noted from **Table 4.2** that the rebars lose their strength at a faster rate than the rate of loss of mass. The significant loss in tensile strength is due to localised pits leading to failure in zones of reduced cross-section. In S48 sample, while loss in mass of only

10.3%, larger reduction in tensile strength (up to 45%) is seen. This suggests that there is a significant drop in load carrying capacity of RC beams even though mass loss is nominal. It was observed that all the rebars failed in the region where huge pits were observed.

The initial stiffness remains largely unaffected regardless of the degree of corrosion. The loss of strength without much loss of initial stiffness indicates that corrosion leads to local pit formation that initiate failure in the bar but the pits have no substantial effect on the overall load-deflection characteristic of the bar. It is also noted that the rate of reduction in the yield stress is slow at the surface corrosion stage (until day 9). But it accelerates as corrosion enters the transition zone and finally drops dramatically in the pitting zone. The yield strain too follows similar behaviour. Thus, at the surface corrosion stage, the post-yield behaviour of the bar is largely affected. At this stage, both ultimate stress and ultimate strain have come down substantially. Large reduction of yield stress happens at a later stage when pitting corrosion sets in. The effect in the post-yield property of bar can be discerned from the ultimate stress and ultimate strain in the bar. The ductility ratio, which is defined as the ratio of ultimate strain and yield strain, depicts the width of post-yield zone relative to the pre-yield zone. It can be seen that the ductility ratio came down drastically at an advanced stage of corrosion.

To summarise, in the surface corrosion zone, the load deflection behaviour of rebar would alter very little on the pre-yield period, but both ultimate stress and ultimate strain would be affected. In the transition zone, the yield stress too would come down drastically, but the initial stiffness would still remain largely unaffected. Thus, load-deflection testing of a structure with loads that do not induce yielding in the bar would be ineffective in detecting corrosion. This observation highlights the importance of identifying the zones of corrosion to non-destructively determine the residual capacity of rebar. This study has delineated a method of identifying the transition zone from a combination of ultrasonic investigation at L(0,1) and L(0,7) modes.

4.6 EFFECT OF VARYING VOLTAGE ON CORROSION PROGRESSION

In order to investigate the efficacy of active UGW and passive AE for monitoring the damage progression at varying rates, RC beams were subjected to accelerated corrosion at varying voltages of 10 V, 20 V & 30 V.

4.6.1 Effect of corrosion on rebar with UGW

Both L(0,1) at 0.1 MHz and L(0,7) at 1 MHz were used for corrosion monitoring in RC beams. **Fig. 4.13** shows the variation of L(0,1) mode for RC beam specimens subjected to accelerated corrosion at voltages 10 V, 20 V, and 30 V. The threshold of plots is similar for all

the acceleration rates. However, a shift in the three phases of delamination, transition and pitting zones are observed in the graphs with varying voltages.

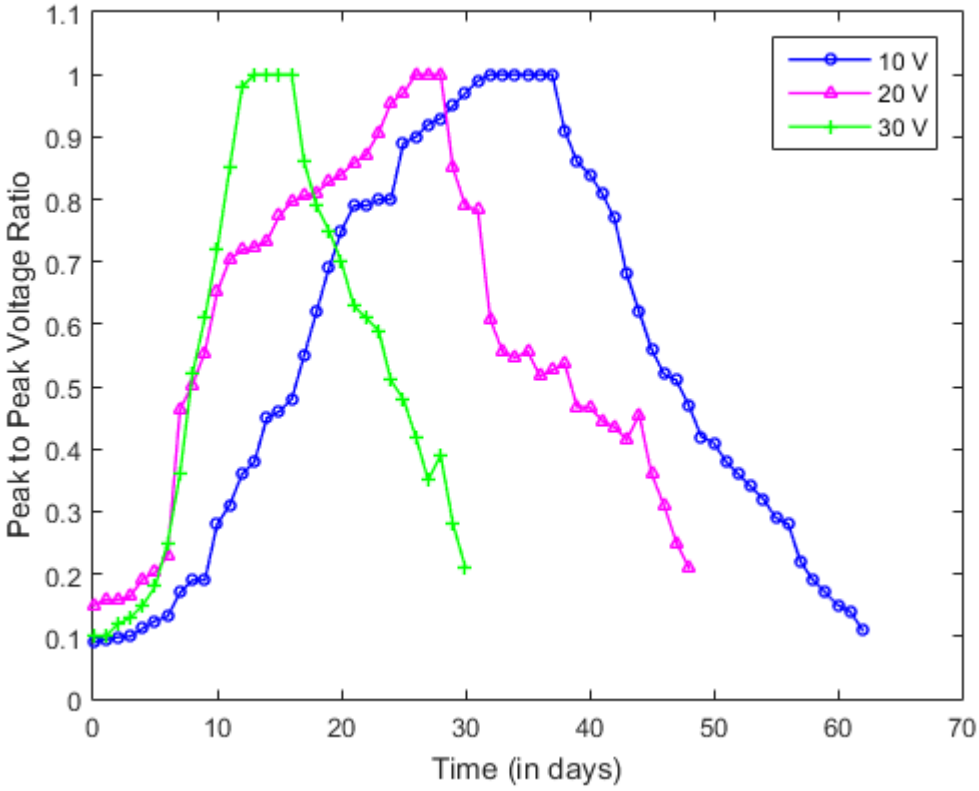

Fig. 4.13 Variation of L(0,1) mode at 0.1 MHz with corrosion accelerated at 10 V, 20 V & 30 V

With L(0,1) mode, rise in signal strength is observed initially owing to debonding of the bar from the surrounding concrete upto 32 days, 26 days and 10 days for RC bam specimens subjected to accelerated corrosion at 10 V, 20 V & 30 V respectively. This shows that mechanism of corrosion remains same and the rate of corrosion does not alter the process of corrosion though a shift in delamination phase is observed indicating slow corrosion at lower voltages. Thereafter, the corrosion ingresses into the rebars causing fall in signal strength upto a period of 62 days, 48 days and 30 days for specimens subjected to accelerated corrosion at 10 V, 20 V and 30 V respectively. The gradual signal drop signifies that the corrosion has reached the inner parts of rebar resulting in pitting and loss of cross-sectional area. Hence, L(0,1) clearly identifies the deterioration of reinforcing bar due to corrosion at varying rates. Both the phenomenon of debonding and pitting are more clearly indicated in specimen subjected to accelerated corrosion at 10 V than the other specimens. The effect of varying rates of corrosion is well picked and differentiated by L(0,1) mode. The UGW works well for picking up all the stages of corrosion at whatever rate corrosion progresses in RC structures.

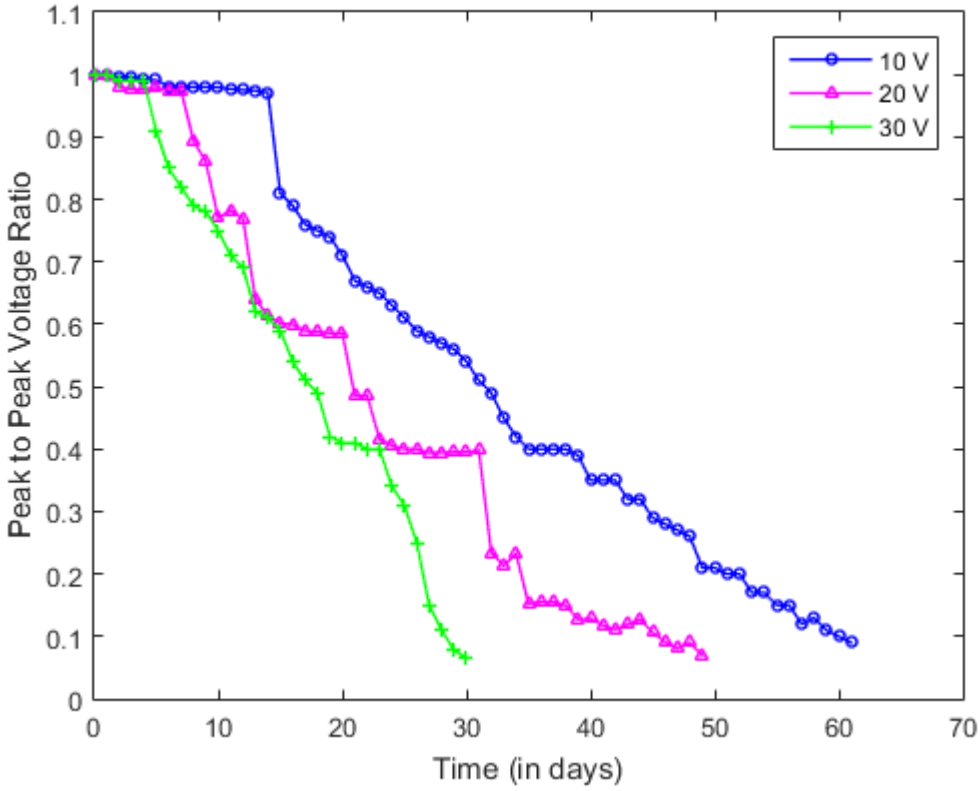

Fig. 4.14 Variation of L(0,7) mode at 1 MHz with corrosion accelerated at 10V, 20 V & 30 V

Similar trends were observed with L(0,7) mode at 1 MHz as shows in **Fig. 4.14**. With L(0,7) mode, initially no change in signal strength is observed until the deterioration marks inroads into the rebar. For samples subjected to increasing voltages, the transmitted signal shows no substantial change initially for all the specimens till 18 days, 8 days and 5 days, for 10 V, 20 V & 30 V respectively, pointing towards the slow corrosion with smaller voltages. The occurrence of pitting in reinforcing bar leads to the fall of signal amplitude as it disturbs the waveguide resulting in scattering and mode conversions. The signals started falling after 5 days, 10 days and 18 days of accelerated corrosion accelerated at 10V, 20 V and 30 V respectively. However, the fall in transmitted signal is more gradual for specimen corroded at 10 V. In case of specimens corroded at 20 V and 30 V, the fall is more abrupt. This further signifies the slower rate of deterioration of reinforcing bar and that it is well picked by the L(0,7) mode at 1 MHz.

4.6.2 Effect of corrosion with AE

AE hits were picked by AE sensors mounted on the surface of concrete in an array as explained in Chapter 3 & 4. The recorded acoustic emissions in terms of cumulative AE hits

are plotted with respect to time for RC beam specimens subjected to different levels and rates of corrosion at 10 V, 20 V & 30 V respectively (**Fig. 4.15)**. It is observed that for all specimens, the stages of corrosion are in coherence with the phenomenological model **(Fig.1.2).** For RC beam sample corroded at 10 V, the four stages of corrosion indicating onset of corrosion, calm phase due to building of layer of rust around the rebar, crack propagation and finally the cracking and spalling are well depicted at 16, 24, 33 days of corrosion. The shift from the initiation phase to the calm phase and from calm phase to macro-cracking phase is very gradual in comparison to the specimens corroded at 20 V and 30 V in which the change of slope. For the samples corroded at 20 V and 30 V, the corrosion mechanism is same, occurring in similar four stages but at a faster rate. A shift in the stages is observed at the accelerated rates of 20 V and 30 V as shown in **Fig.4.15** is abrupt. Hence, the effect of varying rate of corrosion is well picked up by AE technique indicated by shifts in the curve though the nature of the curve and mechanism is similar.

This study points towards the efficacy of UGW and AE techniques to pick up corrosion at whatever rate it cocurs and establishes the practical application of NDT in this work.

4.7 MONITORING CORROSION IN DIFFERENT ENVIRONMENTS

With an objective of simulating the actual corrosion a set of RC beams were also subjected to accelerated impressed current corrosion in the absence of chlorides. Instead of using NaCl solution, plain tap water was used as drip and is referred to as oxide environment (OC). The oxide corrosion was also accelerated at a constant voltage of 20 V. For monitoring corrosion, similar ultrasonic guided wave and acoustic emission set-ups were used. UGW readings were taken after every 24 hours. The results were compared with RC beam specimen corroded in the presence of chlorides (CC environment) at same voltage.

4.7.1 Effect of corrosion on rebar with UGW

In case of RC beam specimens subjected to corrosion in the oxide environment (i.e., in the absence of chlorides), the process of corrosion was very slow and spanned over a period of 120 days as against CC corrosion which lasted for 48 days, subjected to accelerated corrosion at same voltage i.e., 20V. UGW monitoring was carried out with L(0,1) mode at 0.1 MHz and L(0,7) mode at 1 MHz. **Fig. 4.16** shows the variation of L(0,1) mode with time in both CC and OC samples. From the figure, it is clearly seen that the ultrasonic investigations for RC beam specimens subjected to oxide environment and chloride environment, closely match with each other.

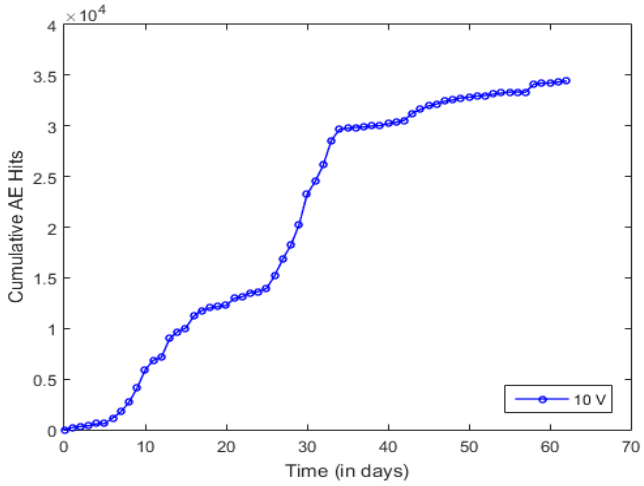

(a) 10 V

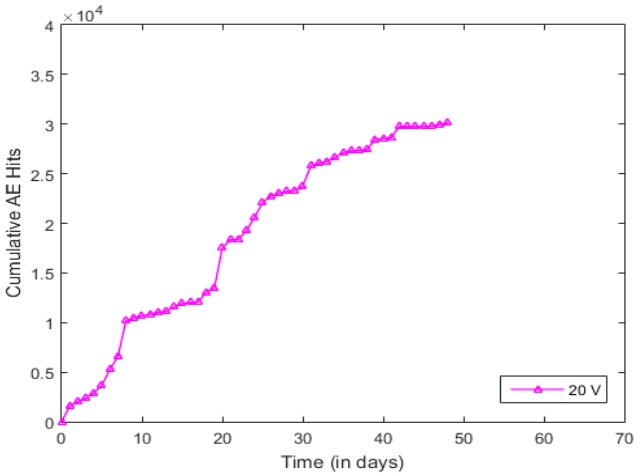

(b) 20V

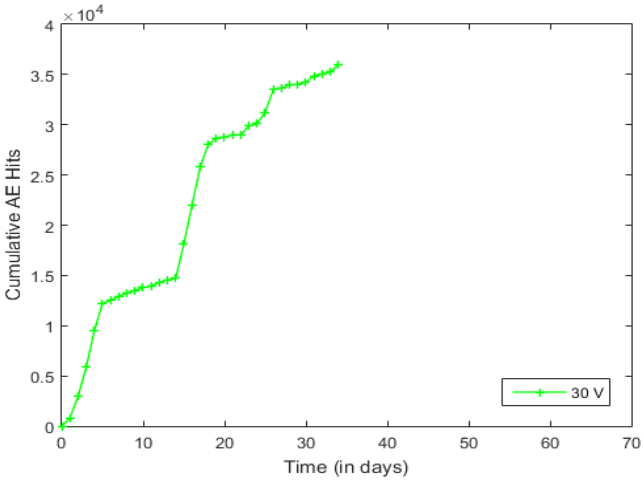

(c) 30 V

Fig. 4.15 Cumulative AE hits with respect to time

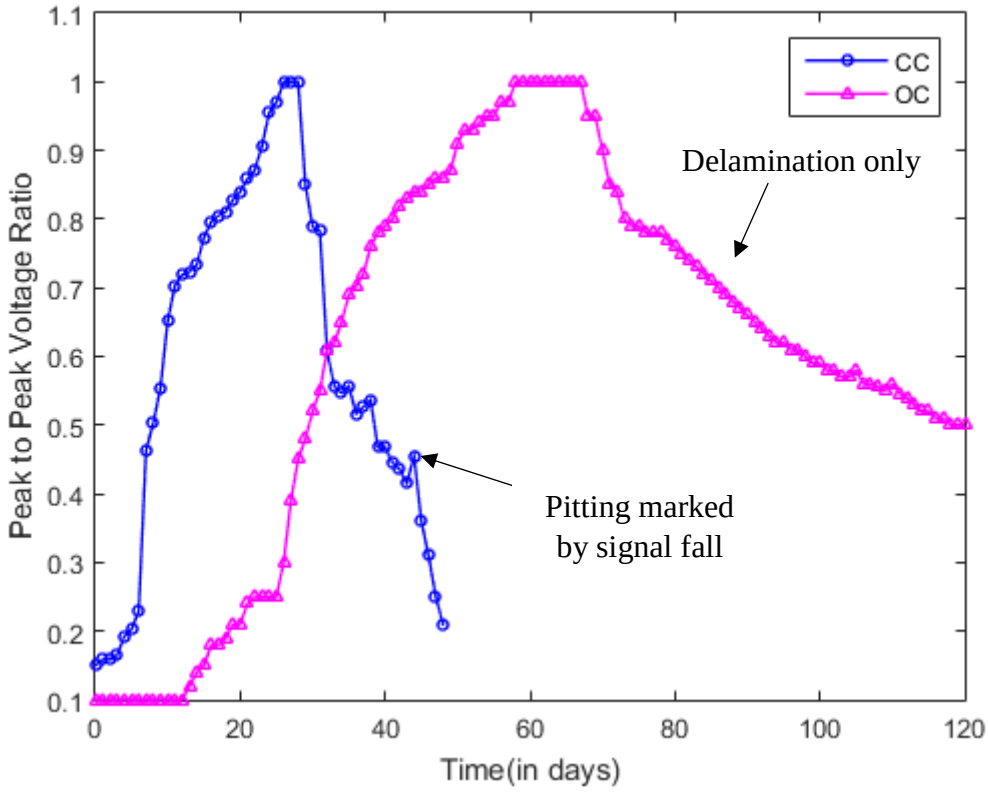

Fig. 4.16 Variation of L(0,1) mode at 0.1 MHz for CC and OC specimens

In CC sample, L(0,1) record delamination upto 22 days indicated by signal rise which further falls pointing towards pitting that lasts till lasts till the end of exposure for 48 days. Further with L(0,7) mode at 1 MHz, pitting is picked up by fall in signal strength after 28 days in CC samples. On the other hand in OC sample, L(0,1) signal shows an increase till 58 days as against 22 days in CC samples implying major changes and delamination during this period. Beyond 58 days, L(0,1) signal became stagnant and further no increase is seen. Thereafter the signal started falling slowly upto 120 days as compared to CC signal which vanished in 48 days. This may be due to the slow corrosion in OC sample wherein the surface modification of the bar takes a very long time as against chloride-induced corrosion.

From **Fig.4.17**, it can be seen that L(0,7) mode did not show any variation until 32 days of accelerated corrosion in OC sample as against 6 days of corrosion in CC sample. This is primarily because L(0,7) is indifferent to the surface modifications and during this period delamination was predominant as predicted by the rise in L(0,1) signal. After 32 days L(0,7) signal in OC started falling gradually upto 120 days as against 48 days in CC specimen. This

further reinforces the fact that the corrosion reached the core of the steel bar very slowly as against chloride-induced damage.

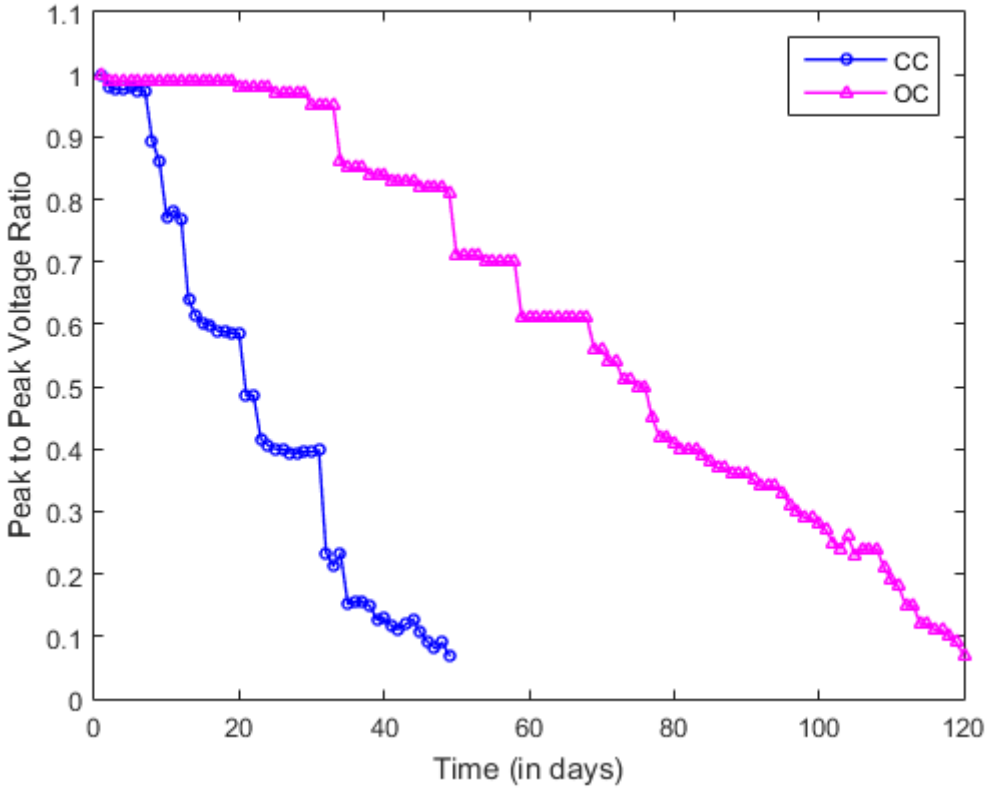

Fig. 4.17 Variation of L(0,7) mode at 1 MHz for CC and OC specimens

From the UGW plots in OC samples with both L(0,1) and L(0,7), corrosion progression though slow, takes place in three stages as in CC.

i) Delamination phase lasted from 0 to 32 days

ii) Transition phase lasted from 32 to 50 days.

iii) Pitting phase lasted from 51 to 120 days

The comparison of visual observation of the CC and OC bars support this fact. In the OC bars, the pits were localised in the middle region of the rebar when it was extracted as against the widespread pitting observed throughout the bar in CC bar (**Fig. 4.18**). It shows that chloride-induced corrosion leads to severe deterioration in the form of area reduction and pits throughout 700 mm embedded length of rebar whereas corrosion in the absence of chlorides (OC) is very nominal with few pits in the middle portion of the bar. Hence, UGW is able to discern corrosion in both environments (CC as well as OC) using a combination of core and surface seeking modes.

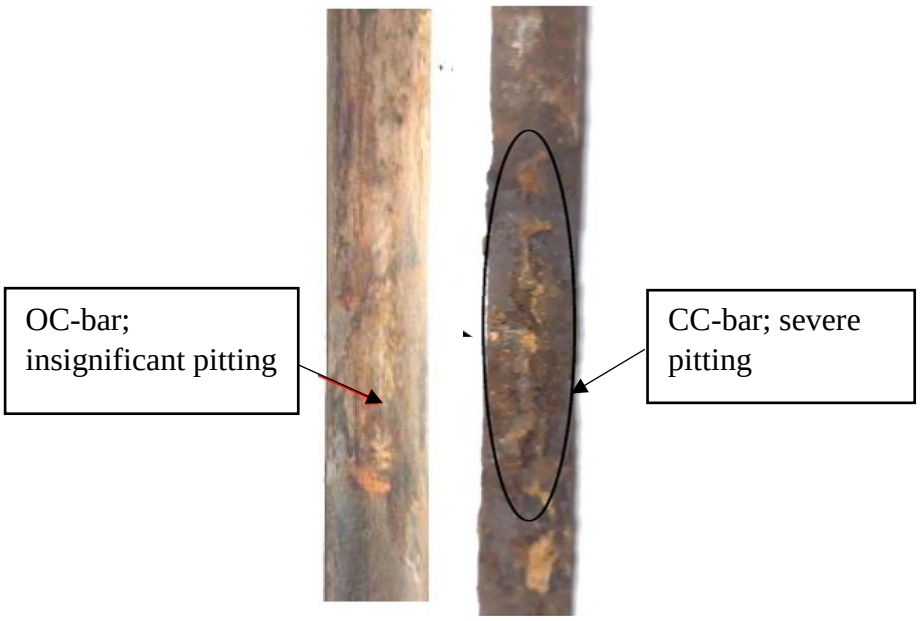

Fig. 4.18 Comparison of extracted OC & CC bars

4.7.2 Effect of corrosion with AE

AE monitoring was also done to study the corrosion-induced damage in RC beam specimens subjected to oxide environments. The similar AE set-up was used for corrosion monitoring with six sensors (three mounted on the front side and the other three mounted on the back side the beam) as was used for monitoring corrosion in chloride environment. **Fig. 4.19** shows the variation of cumulative AE hits with time for corrosion accelerated in oxide environment.

The four stages of corrosion as defined by the phenomenological model can be clearly observed from the plot as in case of CC specimen (z). It can be clearly observed that AE hits are recorded from the day zero which further increased upto a period of around 52 days for OC specimen (Initiation phase, Phase 1). It should be noted that no change in the ultrasonic signal was recorded using both the modes until 15 days of accelerated corrosion in these OC specimens. Hence, it can be clearly concluded that AE has great potential to be able to detect the corrosion-induced damage in the initial stages even when the damage is minor. After 52 days till 79 days, calm phase in CC beams is observed when there is no sharp rise in AE hits. It is certainly because of the developed rust products preventing the progression of corrosion. It is important to note that the initiation and calm phase lasts till 9 and 19 days respectively in CC specimen. It points towards slow corrosion in the absence of chlorides as also pointed by UGW investigation.

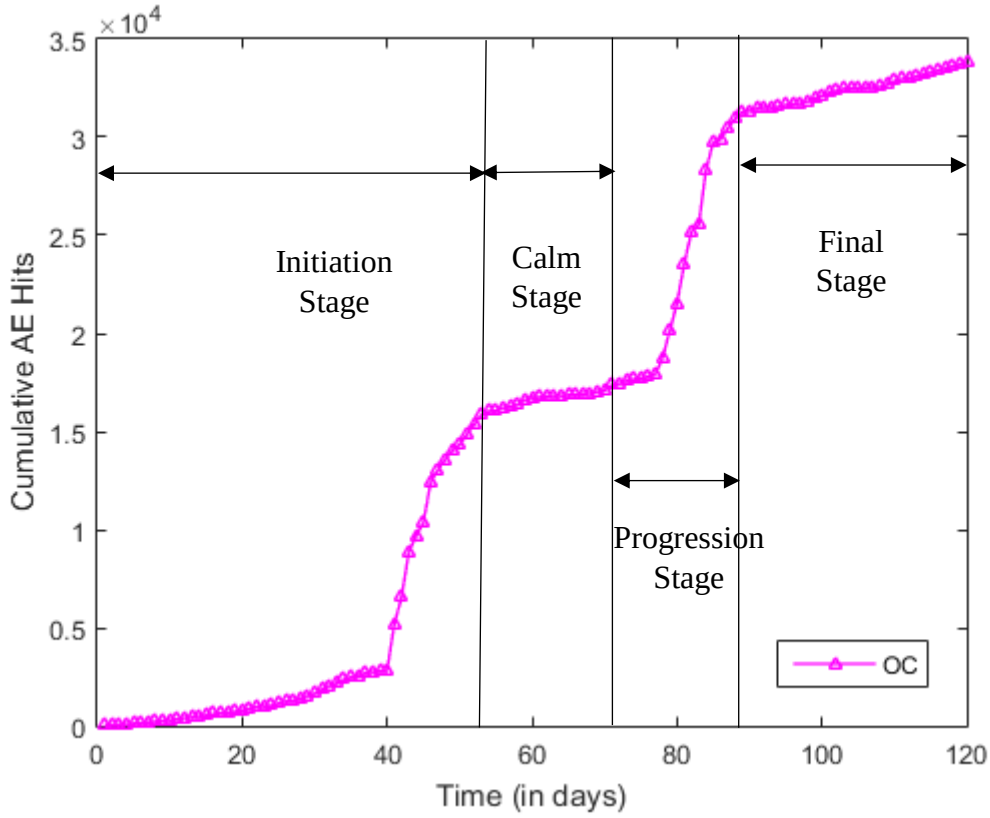

Fig. 4.19 Variation of Cumulative AE hits for OC specimens

Furthermore, from 78 to 94 days of accelerated corrosion in oxide environment, maximum damage is observed as number of recorded AE signals increased significantly during to this period. This indicates that the macro-damage in concrete took place during this period. This is further reinforced from the ultrasonic signals recorded using L(0,1) mode which started falling during this period only, indicating pitting and hence, increase in the tensile stresses(crack progression stage, Phase 3). In the later stages, no significant variation in the gradient of AE curve is observed indicating that most of the damage in concrete has already taken place in first 3 phases in the form of micro-macro cracking. Hence, AE is not able to provide much information in the last phase of corrosion since concrete has already cracked. On the other hand, UGW utilizing both the modes could provide significant and measurable changes in the signal strength pointing towards damage in rebar in the advanced stages of corrosion when AE gives up. **Fig. 4.20** provides a comparison of OC and CC using AE wherein a significant shifts in the phases and rate of corrosion are observed in the two environments.

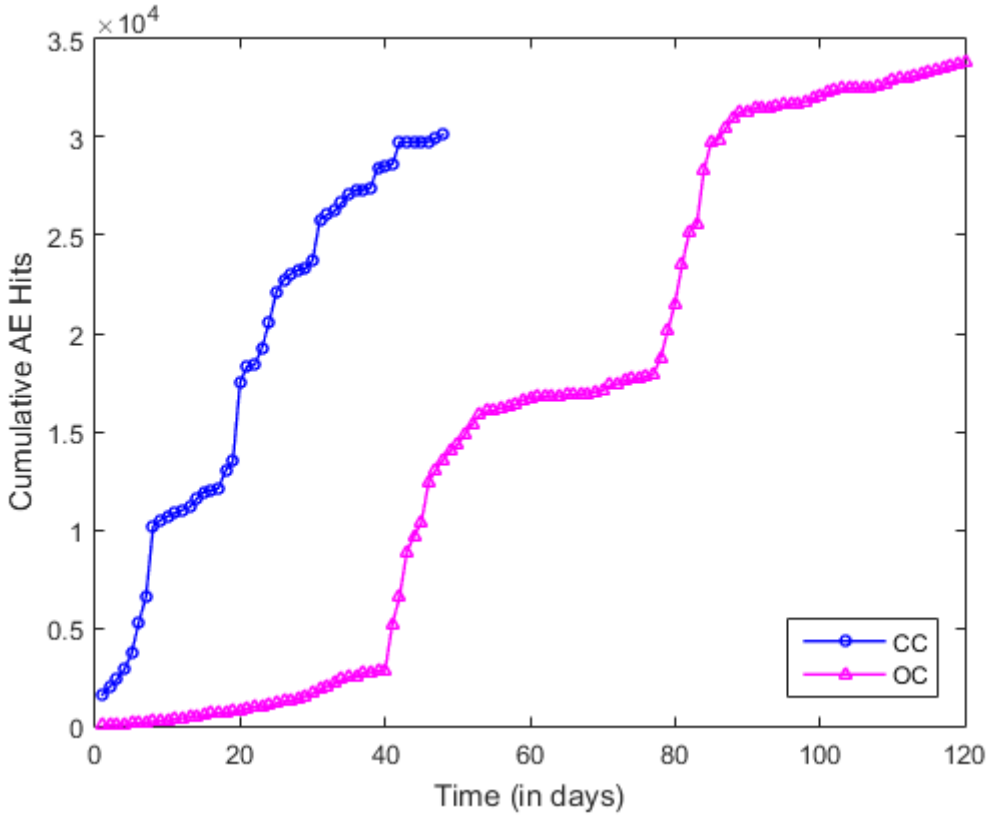

Fig.4.20 Comparison of cumulative AE hits with time

The study of corrosion in two widely varying environments in the absence and presence of chlorides is well picked up by two proposed wave based NDT techniques of UGW and AE. While AE picks up initiation better than UGW, ultrasonic guided waves prove more beneficial in the later stages of corrosion. Both types of corrosion are easily differentiated by shift in UGW as well as AE hit plots. The techniques have the capability to detect as well as differentiate corrosion occurring in the absence as well as the presence of chlorides.

4.8 CLOSING REMARKS

This chapter explores two non-destructive techniques based on wave propagation for estimating residual strength of corroding reinforcement in concrete. Corrosion monitoring was also done at varying rates of corrosion and in widely varying environments as well. The specimens undergoing corrosion were simultaneously monitored by ultrasonic guided wave (active) and acoustic emission (passive) techniques. The specimens were instrumented with AE sensors to record acoustic activities inside the specimens during corrosion. Simultaneously, the bars are also monitored by propagating ultrasonic waves through the bars. Active and passive monitoring results are correlated with already established electrochemical techniques

to determine the relative efficacies of the NDT technologies. The methods could differentiate between corrosion occurring at variable rates and in widely varying environments as well.

CHAPTER 5

EFFICACY OF FRP WRAPS TO CORROSION IMPEDIMENT

5.1 GENERAL

The commonly used methods to protect RC structures from corrosion are epoxy coatings, corrosion inhibitors and cathodic protection. However, these methods only impede the corrosion process and do not increase the strength of RC that might have been lost during the corrosion process. In this chapter, Fiber reinforced polymer (FRP) is used as one of the methods for repair of RC structures against corrosion by wrapping structures using FRP sheets. FRP sheets bonded externally to the corroded concrete helps in not only impeding the corrosion process but also improving the flexural strength and shear of RC structures [105–110]. The ease of handling, high durability in adverse environments and the improved mechanical properties like high strength to weight ratio makes FRP repair unique and far more superior than the conventional corrosion repair methods as reported by various researchers [16,108,111–115,99,95]. Two important implications of FRP wraps against corrosion were reported, one is that it confines the concrete in RC structures affected by corrosion thereby preventing the displacement of concrete cover. Secondly, it acts as a barrier between the reinforcement and surrounding environment thereby blocking further ingress of moisture and thus, impeding corrosion [16,115]. Out of the two commonly used fiber reinforced polymers namely GFRP and CFRP, CFRP offers higher strength, stiffness, durability and electrical conductivity and therefore can be used for cathodic protection [95]. On the other hand, GFRP sheets are thicker than CFRP sheets and has a high electrical resistance which makes them better for passive protection.

In this chapter, the work has been extended to explore the origin, progression and impediment of damage due to corrosion in FRP wrapped RC structures and investigation of the effectiveness of the two elastic wave based techniques (AE & UGW) for the same. While UGW has the potential to monitor the deterioration of rebar due to corrosion exposure and AE has the potential of relating the effect of corrosion in concrete. Therefore, a combination of both these techniques is proposed for the overall monitoring of deterioration of reinforced concrete.

5.2 EXPERIMENTAL INVESTIGATION AND METHODOLOGY

5.2.1 Specimen Details

RC cylinders of diameter 150 mm and height 300 mm with 25 mm reinforcing bar in the middle of cross-section, were cast using M20 grade concrete (1:1.49:2.43) with a water-cement ratio of 0.45. The rebar used was of Mild Steel (MS) with a total length 600 mm, out of which 300 mm length was kept embedded in RC cylinder and the remaining 300 mm protruded from the concrete cylinder (**Fig. 5.1**).

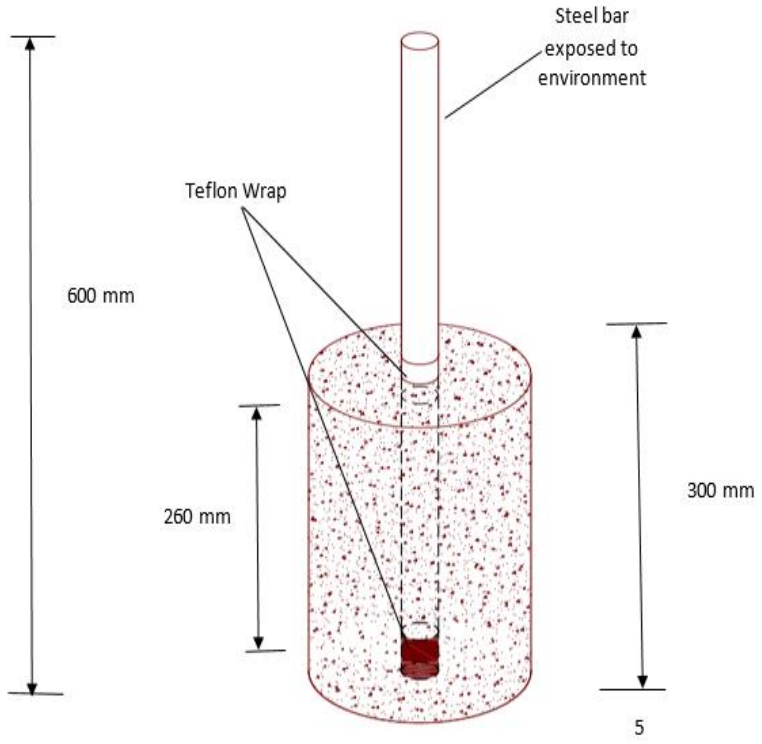

Fig 5.1: Schematic of cylindrical specimen

Before casting, reinforcing bar was sand blasted and dipped in oil immediately to remove impurities that might affect the steel-concrete bond. Teflon tape was wrapped around the bar at two different locations (at steel-concrete interface and the bottom end of rebar embedded in concrete), to serve as bond breakers. A cover of 40 mm to the embedded rebar was maintained from the bottom. Each bar was weighed before casting RC cylinders. The exposed portion of rebar was surfaced with an epoxy to prevent corrosion. The 28 days compressive strength of concrete used for casting concrete cylinders was 36 MPa.

5.2.2 Inducing Corrosion in reinforcing bars in concrete

Impressed current technique was used to induce corrosion in reinforcement embedded inside concrete. RC cylinders were dipped in 3.5% NaCl solution to ensure full saturation and level of solution was kept 30 mm below the surface of cylinder to extenuate corrosion of the

exposed rebar. A constant voltage power source (64 V, 500 mA, APLAB make) was used to regulate voltage and current in the specimens. The reinforcing bar was made anode and the stainless steel wire mesh wrapped around the cylinder was used as cathode. A total of 18 cylinders were cast and a constant voltage of 10 V was impressed for a period of 30 days. However, few samples were wrapped with GFRP and CFRP after accelerated corrosion of 3, 6, 9 and 12 days. Impressed current at constant voltage was monitored after every 24 hours. The number and nomenclature of specimens along with wrapping scheme is presented in **Table 5.1**.

Table 5.1 Nomenclature of Samples

Wrap Material	**Corrosion Exposure in days**		**Nomenclature**
	Before wrapping	**After wrapping**	
Unwrapped samples	30	-	C-1
	30	-	C-2
Wrapped with Glass fiber	3	27	GP3-1
	3	27	GP3-2
	6	24	GP6-1
	6	24	GP6-2
	9	21	GP9-1
	9	21	GP9-2
	12	18	GP12-1
	12	18	GP12-2
Wrapped with carbon fiber	3	27	CP3-1
	3	27	CP3-2
	6	24	CP6-1
	6	24	CP6-2
	9	21	CP9-1
	9	21	CP9-2
	12	18	CP12-1
	12	18	CP12-2

5.2.3 Wrapping of RC cylinders

Two most commonly used FRP wraps of GFRP and CFRP are used in the investigation, in order to offer protection against corrosion. Both types of FRP are quite popular for their remarkable performance in terms of strength, stiffness, durability and fatigue resistance. However, GFRP is a preferred repair and rehabilitation material since it is cheaper than CFRP. The electrical resistance of CFRP is much lower than that of GFRP which makes it better for passive protection against corrosion. For this investigation, commercially available unidirectional CFRP and GFRP sheets were applied on RC cylinders with an epoxy (MBrace saturant) with details as given in **Table 5.2**.

Table 5.2 Properties of CFRP and GFRP sheets

Material	Thickness (mm)	Tensile Strength (MPa)	Tensile modulus (GPa)
CFRP	0.1176	3800	240
GFRP	0.35	2.30	76

The specimens were air dried before wrapping. GFRP and CFRP wraps were applied to four groups of RC cylinders with each group having two RC cylinders, after different days of corrosion exposure viz. 3, 6, 9 and 12 days respectively. During wrapping, an overlap of 25 mm was provided at the ends of sheets. After wrapping, the specimens were again subjected to corrosion keeping the total exposure duration of 30 days (before and after wrapping). The control samples were unwrapped throughout 30 days of corrosion exposure (**Table 5.1**).

5.2.4 Ultrasonic guided wave testing details

For ultrasonic guided wave investigation, a typical ultrasonic testing set-up (**Fig. 5.2**) was used, comprising of pulser/receiver system (DPR 500, Karl Deutsch make), cylindrical piezoelectric transducers of selected frequencies and display devices. Driven by pulser, the transducers generate an ultrasonic pulse that travels through the embedded bar in the form of longitudinal guided waves. The testing was done in Pulse-Echo mode (PE) in which the same transducer serves as a transmitter as well as a receiver. Two kinds of signal were obtained after reflection (**Fig. 5.3(a)-(b)**): the first reflection is obtained from the steel-concrete interface and is named as Interface Echo (IE). The second pulse is reflected from the bar end and is named as Bar End Echo (BE). In this study, only BE is used to relate corrosion in embedded rebar. IE signals are insignificant as they travel in protruded portion of bar that remain exposed to air and hence protected from corrosion.

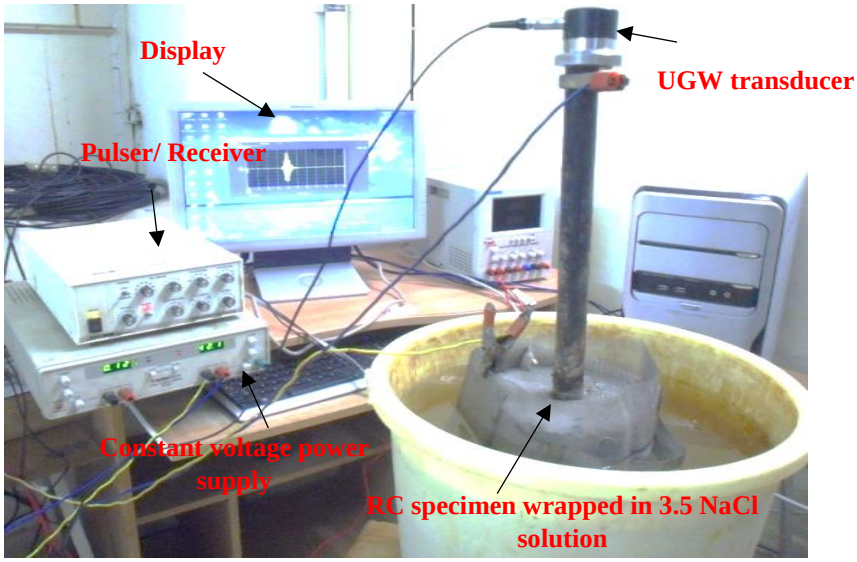

Fig. 5.2 Ultrasonic Guided wave set-up for corrosion monitoring

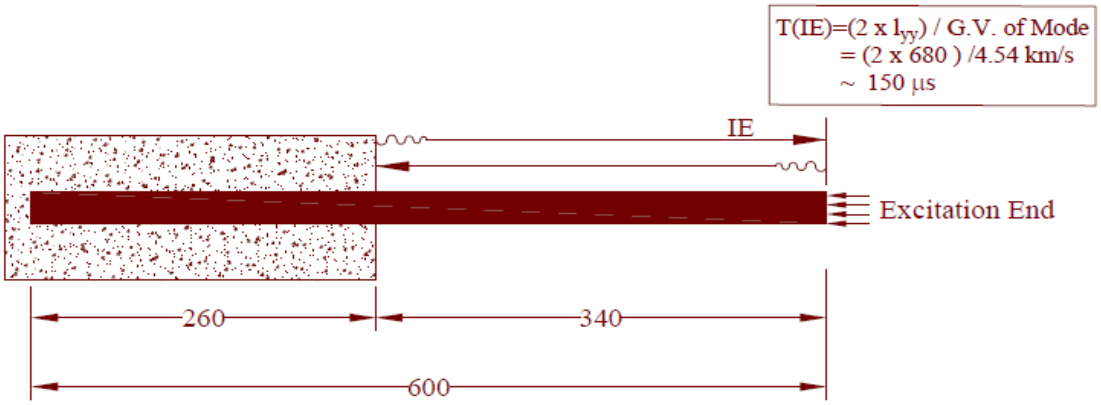

(a) Interface Echo

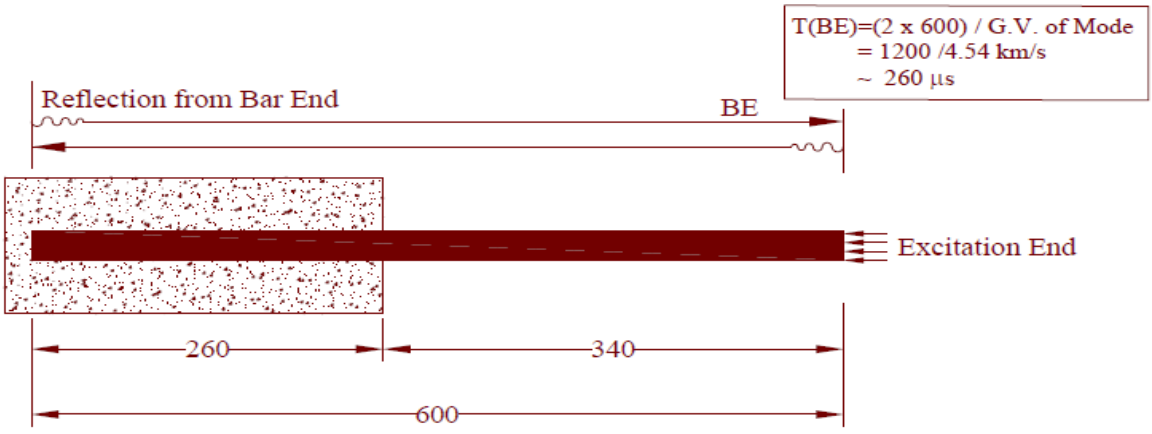

(b) Bar End Echo

Fig. 5.3 Schematic showing IE and BE with corresponding Time of Flight (T)

BE signal is obtained after reflection from back end of rebar twice through the portion embedded inside concrete which is subjected to corrosion, hence, exhibiting greater variations in the signal characteristic with corrosion. It is important to note that arrangement of transducers generate longitudinal wave mode and guided waves investigate the rebar only.

For ultrasonic guided wave investigation, piezoelectric cylindrical transducers having a relatively narrow frequency bandwidth and a longer waveform duration with central frequency of 0.1 MHz (low frequency) and 1 MHz (high frequency) were used. L(0,1) mode at low frequency of 0.1 MHz, is a surface sensitive mode which picks up surface irregularities. L(0,7) mode at high frequency of 1 MHz, is a core seeking mode which picks up corrosion deep inside the core of bar in the form of pitting as explained in chapter 3 & 4.

5.2.5 Acoustic emission set-up details

For acoustic emission monitoring, AE set-up as explained in 3rd chapter was used and a R3α AE sensor with a resonant frequency of 30 kHz was used. The AE sensor was attached to the concrete cylinder using a coupling gel and held in position using a transparent tape till the end of experiment (**Fig. 5.4**). AE hardware threshold was set at 45 dB, since it helps in acquiring AE signals originating due to corrosion of reinforcement [79]. Acoustic emission signals were recorded continuously during the entire duration of exposure to corrosion. AE-win software was used for extracting AE data in order to study the various characteristics of AE signals such as Amplitude of AE hits, AE signal energy, AE duration, AE counts rise time.

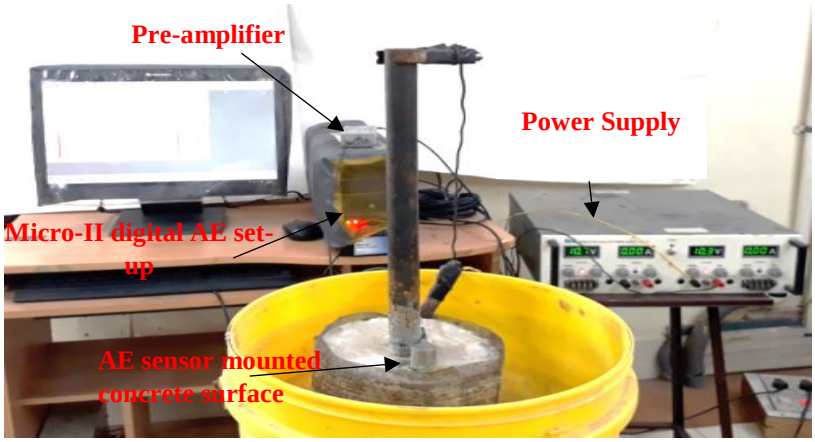

Fig. 5.4 AE set-up for corrosion monitoring

In addition to monitoring corrosion by Ultrasonic guided waves and Acoustic emission technique, fluctuations in current at constant voltage were measured after every 12 hours. It is to be noted that AE data acquisition was stopped whenever UGW measurements were taken. During this period, constant voltage power supply was also turned off, discontinuing the accelerated corrosion to avoid interference of signals.

5.3 INVESTIGATION OF IMPRESSED CURRENT WITH TIME

5.3.1 Control Concrete

The specimens were subjected to accelerated impressed current corrosion at a constant voltage of 10 V till 30 days. The resistance offered to corrosion is measured in the terms of variation of corrosion current with increasing exposure at constant voltage. Cell currents were monitored after every 12 hours for control concrete and FRP wrapped concrete samples. **Fig. 5.5** indicates the variation in corrosion current in control concrete cylinders. A dip in corrosion current is observed in first 4 days of corrosion exposure. This may be due to the passive oxide layer on the rebar surface causing increase in the electrical resistivity and hence, a drop in current. Further, on increased corrosion exposure, the cell current rises till 22 days. It is possibly due to the dissolution of passive layer by the ingress of chloride ions leading to initiation and further progression of corrosion deep inside the bar. In the later stages, the corrosion current finally drops and then becomes constant pointing towards excessive damage in the embedded bar due to corrosion. As indicated from 4-22 days, an increase in the impressed current value indicates likelihood of corrosion but it cannot be used to quantify extent of corrosion and deterioration in RC structures due to corrosion.

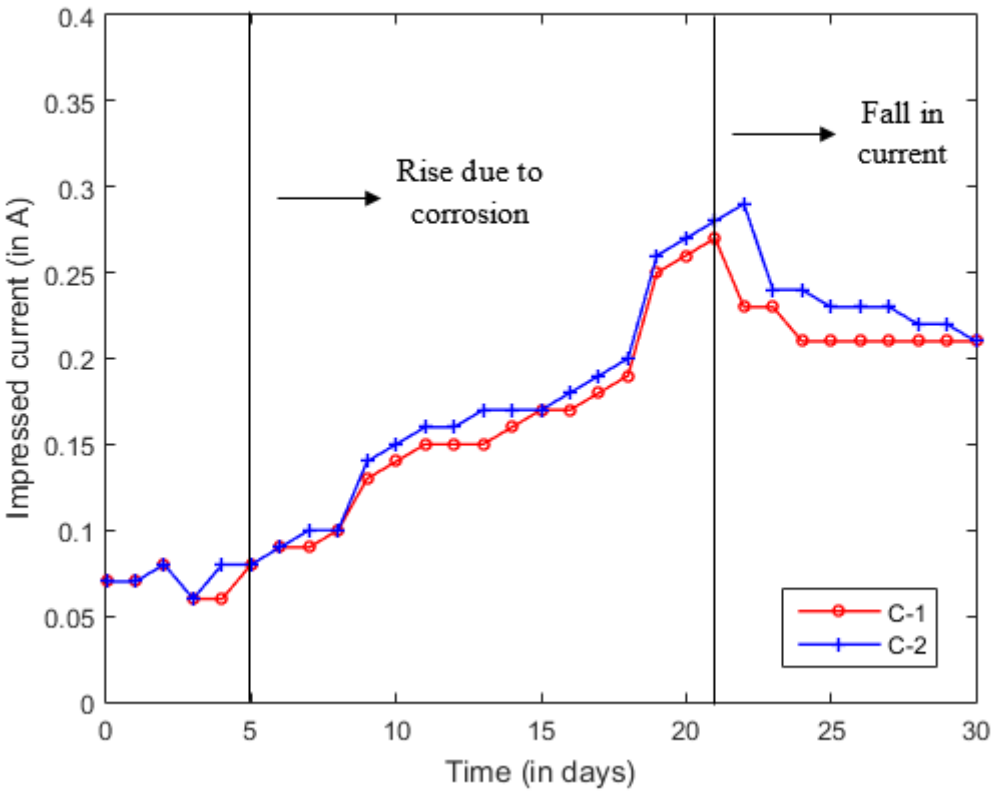

Fig. 5.5 Impressed Current vs accelerated corrosion exposure in control concrete

5.3.2 FRP wrapped concrete

The variation of corrosion current with time for concrete cylinders wrapped with GFRP (GP3, GP6, GP9 & GP12) and CFRP (CP3, CP6, CP9, CP12) after 3, 6, 9 and 12 days of accelerated corrosion, are shown in **Fig. 5.6**. It is observed that there is initial fall in impressed current for all samples in the first 3-4 days, thereafter, the impressed current value rises for control samples till they are wrapped (**Fig. 5.6**). But immediately after wrapping i.e., after 3, 6, 9 and 12 days, the current in all GFRP and CFRP wrapped samples, flowing through the circuit stabilizes and actually falls for the remaining duration of corrosion exposure as against continuous rise in control samples. It points towards the passive protection offered by FRP (both CFRP and GFRP) wraps which is successful in impeding the progression of corrosion indicated by a gradual fall of corrosion current after wrapping. Since the results obtained from corrosion current are only indicative of corrosion, therefore, no comparison between the efficacy of GFRP and CFRP has been made.

5.4 ULTRASONIC GUIDED WAVE INVESTIGATIONS

5.4.1 L(0,1) mode at 0.1 MHz

Ultrasonic guided wave monitoring of control and FRP wrapped cylinders using L(0,1) mode at 0.1 MHz and L(0,7) mode at 1 MHz was done in pulse echo mode as shown by **Fig. 5.7(a)** and **(b)** respectively. The bar acted as a waveguide assisting the propagation of signal. The variations in voltage amplitudes of BE pulses with time is plotted as normalised peak to peak voltages in **Fig. 5.7(a)** and **(b)**. An acclivity is observed in signal amplitude of BE signal amplitude for the first 19 days of accelerated corrosion. This is due to the formation of corrosion products which ultimately gets deposited on the bar itself thereby delaminating the rebar from surrounding concrete. The rust layer prevents the leakage of signal into surrounding concrete, causing the rise in signal amplitude of BE signals with this L(0,1) mode and hence was named as Surface seeking mode. From 0-19 days, the delamination of rebar picked up by this mode is predominant. After 19 days of corrosion exposure, it is observed that the signal amplitude starts dropping rapidly. Since corrosion gets deep into the rebar causing pitting of the bar, it leads to signal scattering and attenuation, causing drop in BE amplitudes with L(0,1) mode. Hence, during the later stages i.e. from 19 to 30 days, pitting dominates.

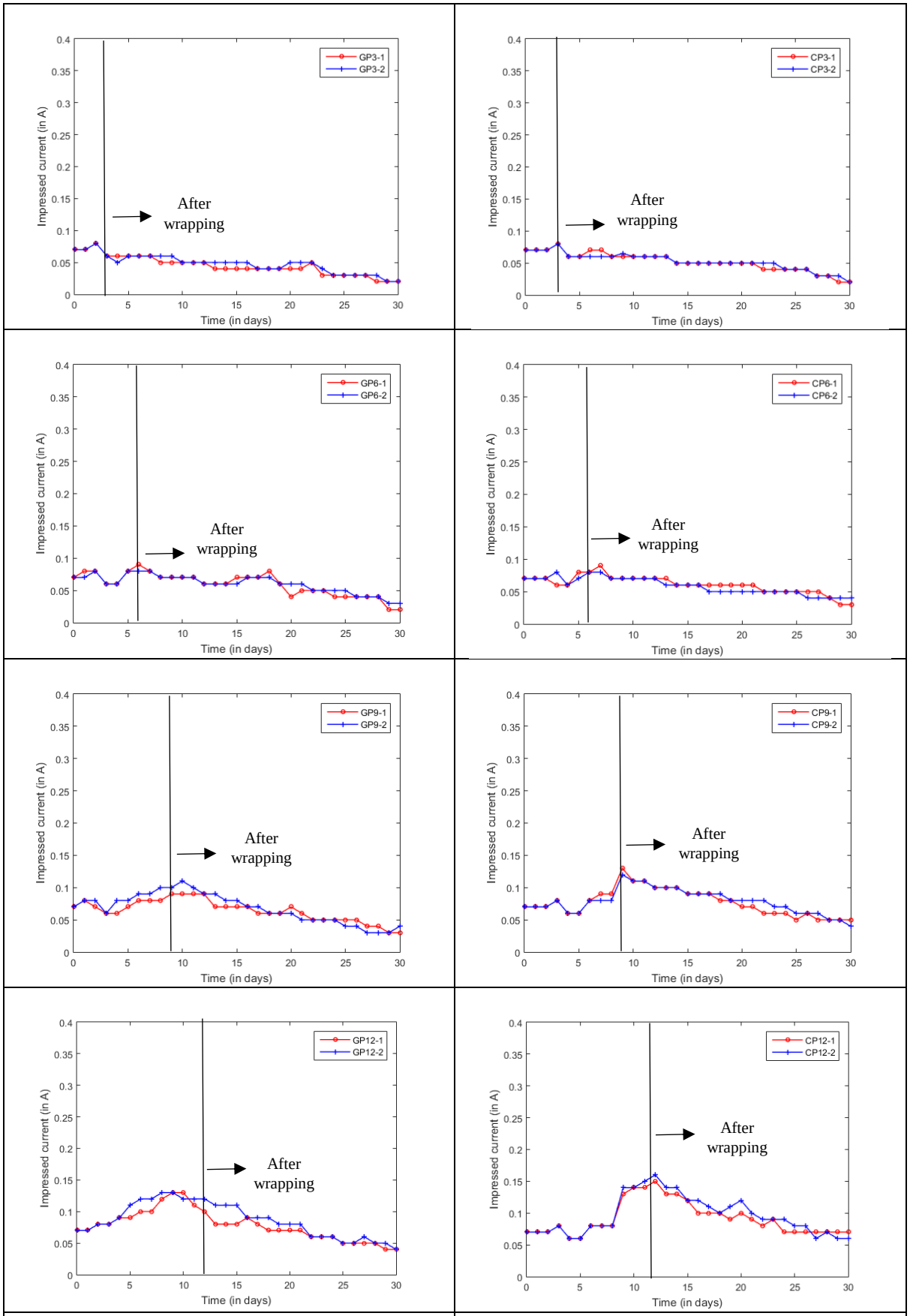

(a) GFRP wrapped samples **(b) CFRP wrapped samples**

Fig. 5.6 Impressed Current vs Time for FRP wrapped concrete

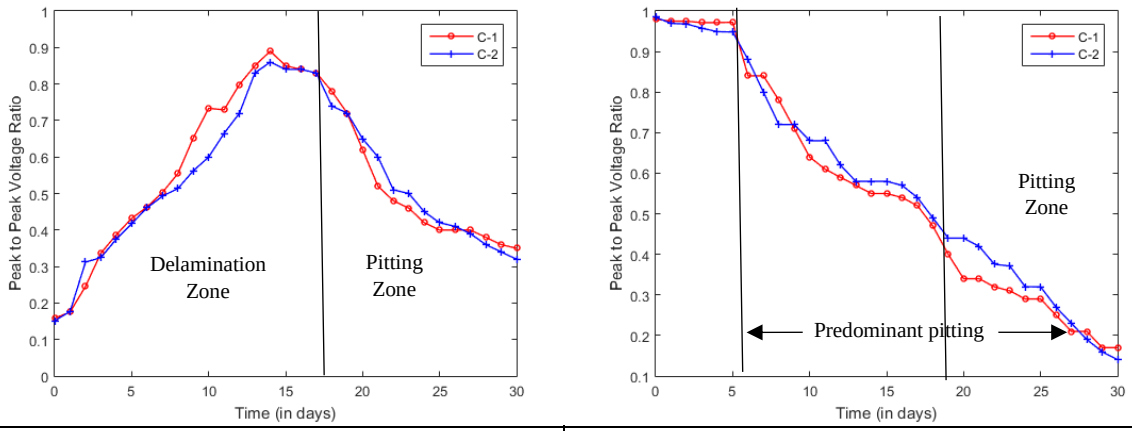

(a) L(0,1) mode at 0.1 MHz | **(b) L(0,7) mode at 1 MHz**

Fig. 5.7 PE trends for Control concrete

For FRP wrapped samples (**Fig. 5.8**), it was observed that GP3 and GP6 along with CP3 and CP6 samples exhibited a small rise in signal before wrapping as in C1 and C2, due to delamination. But, for samples wrapped after 3 and 6 days, the signal actually became constant and then started falling for the remaining duration of experiment. Similar observations were made in GP9 and GP12 along with CP9 and CP12 samples. The fall in signal after wrapping points towards the improvement in the steel-concrete bond thereby increasing signal leakage. Hence, L(0,1) mode not only picks up the signal rise due to delamination because of corrosion initiation in concrete but also successfully monitors the protection indicated by drop in L(0,1) signal as soon as FRP is applied.

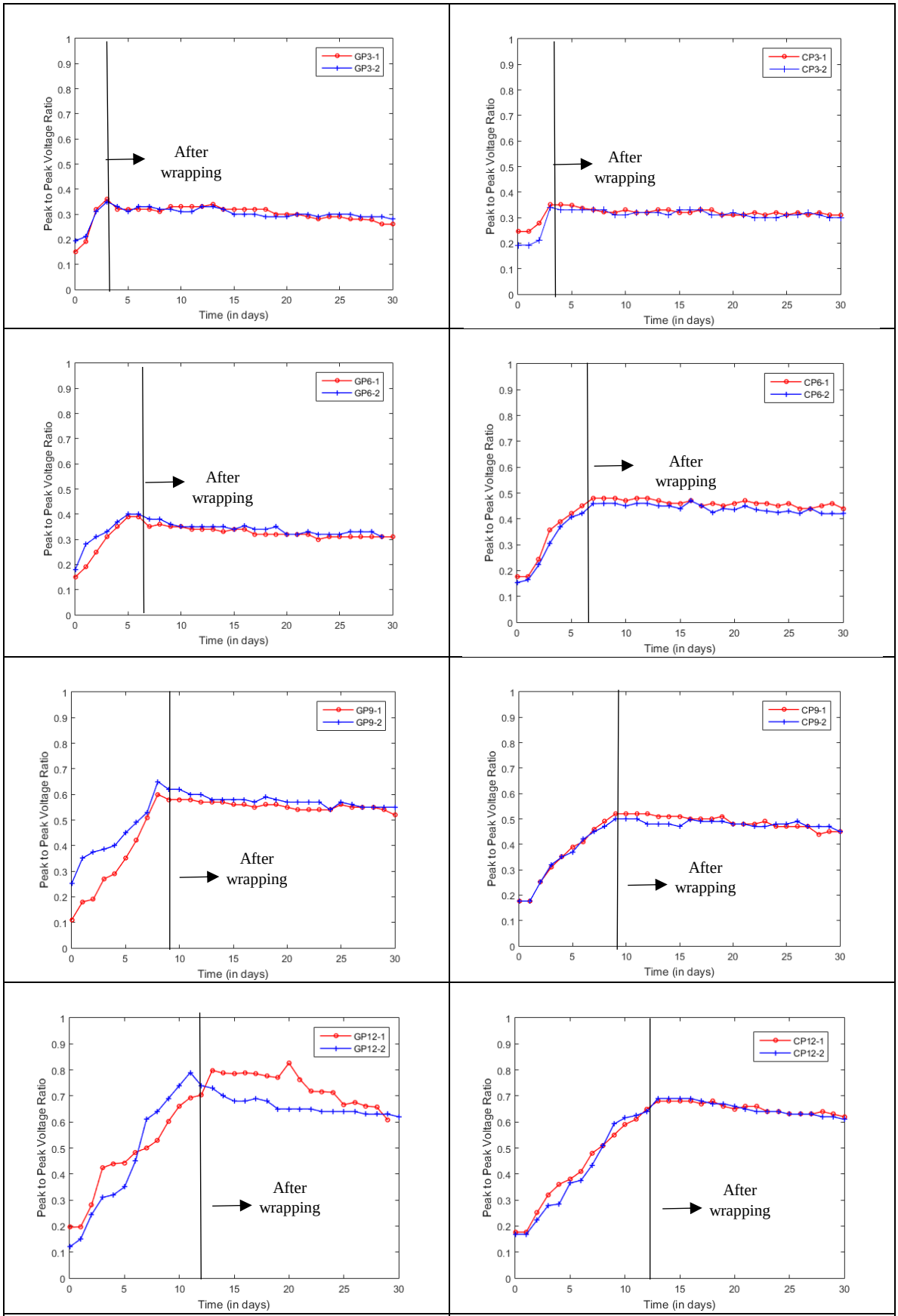

(a) GFRP wrapped samples **(b) CFRP wrapped samples**

Fig. 5.8 PE trends for FRP wrapped concrete using L(0,1) mode at 0.1 MHz

5.4.2 L(0,7) mode at 1 MHz

The reflected signal amplitudes recorded using L(0,7) mode at 1 MHz for control concrete with increasing corrosion exposure are shown in **Fig. 5.7(b)**. It is observed that BE signal amplitude remains almost constant for initial 5-6 days as corrosion begins at the surface of bar, as picked by L(0,1) mode. With further progression, drop in BE signal amplitude is observed from 6-30 days till the end of exposure. Fall in L(0,7) signal points towards corrosion making in-roads to the rebar, leading to pitting. After 21 days, huge pitting is exhibited by the local loss of area in which BE falls using both modes. This was further confirmed by pulling the bars out after different days of exposure. The formation of pits were marked after a period of around 12 days of corrosion. Hence, the corrosion phenomenon in RC cylinders can be represented by three phases: 1) Delamination phase from 0-6 days marked by signal rise in L(0,1) mode; 2) Transition phase from 7-21 days, marked by signal rise in L(0,1) mode and fall in L(0,7) mode signal 3) Pitting phase from 21-30 days where deterioration in the core of bar takes place.

For GFRP and CFRP wrapped cylinders, monitored using L(0,7) mode at 1 MHz (**Fig. 5.9**), it is observed that for GP3 and GP6 along with CP3 and CP6, no marked changes in the signal amplitudes are recorded. This implies that if a specimen is protected before pitting has started, it can be completely prevented by CFRP as well as GFRP wraps. But samples wrapped after 9 and 12 days of corrosion, a significant signal drop was observed in first 9 or 12 days as in case of control concrete. But the signal drop is arrested as soon as the FRP wraps are applied which further suggests that the corrosion progression is successfully arrested by passive protection offered by GFRP and CFRP wraps.

Therefore, it can be concluded that wrapping of RC structures with GFRP and CFRP against corrosion, impedes the rate of both the delamination and the pitting effects due to corrosion. Selective ultrasonic guided waves propagating through rebar have been employed successfully not only to track the onset and progression of corrosion in reinforcing bar but also determining the efficacy of protection provided with FRP against corrosion. Since these ultrasonic guided waves modes travel through rebar, this NDT is corroborated with AE technique in which effects of corrosion and its impediment by wrapping on surrounding concrete, can be studied by mounting AE sensors on concrete directly. Further, the effectiveness of protection against corrosion provided by FRP wraps is studied using AE technique and to compare the vis-à-vis efficacy of two wave based NDT techniques.

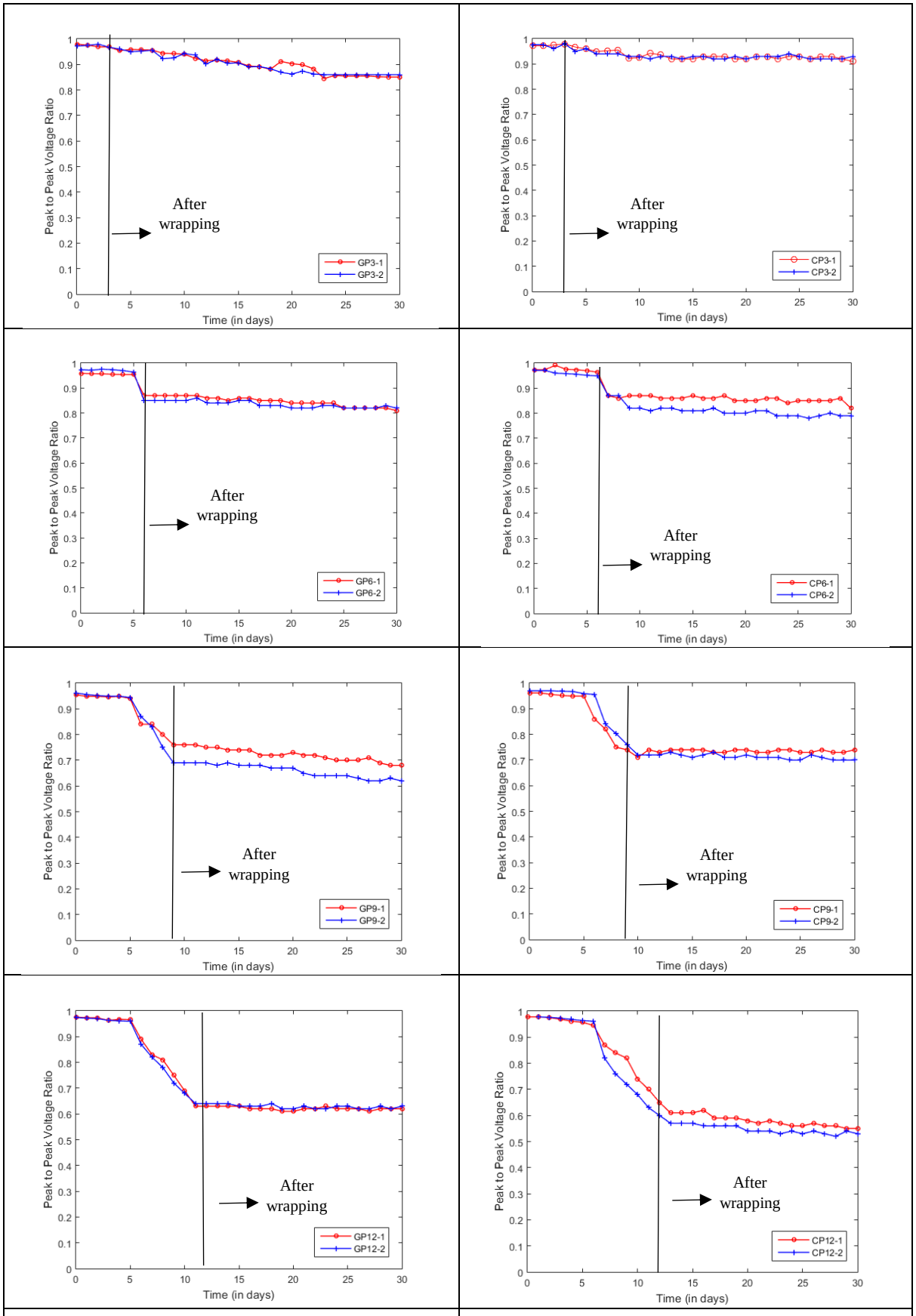

(a) GFRP wrapped samples **(b) CFRP wrapped samples**

Fig. 5.9 PE trends for FRP wrapped concrete using L(0,7) mode at 1 MHz

5.5 ACOUSTIC EMISSION INVESTIGATIONS

AE data picked up by AE sensors mounted on concrete samples (both control and wrapped) was extracted and analysed. As already discussed, Cumulative AE hits, Amplitude of AE hits, Cumulative signal strength and Ib-value analysis are studied to quantify the damage due to corrosion in RC cylinders which are FRP wrapped.

5.5.1 Cumulative AE hits

Control Concrete

Conventional AE hit activity recorded for the entire 30 days of corrosion exposure in control concrete cylinders (**Fig. 5.10**), clearly demonstrates the amount and extent of AE activity due to corrosion.

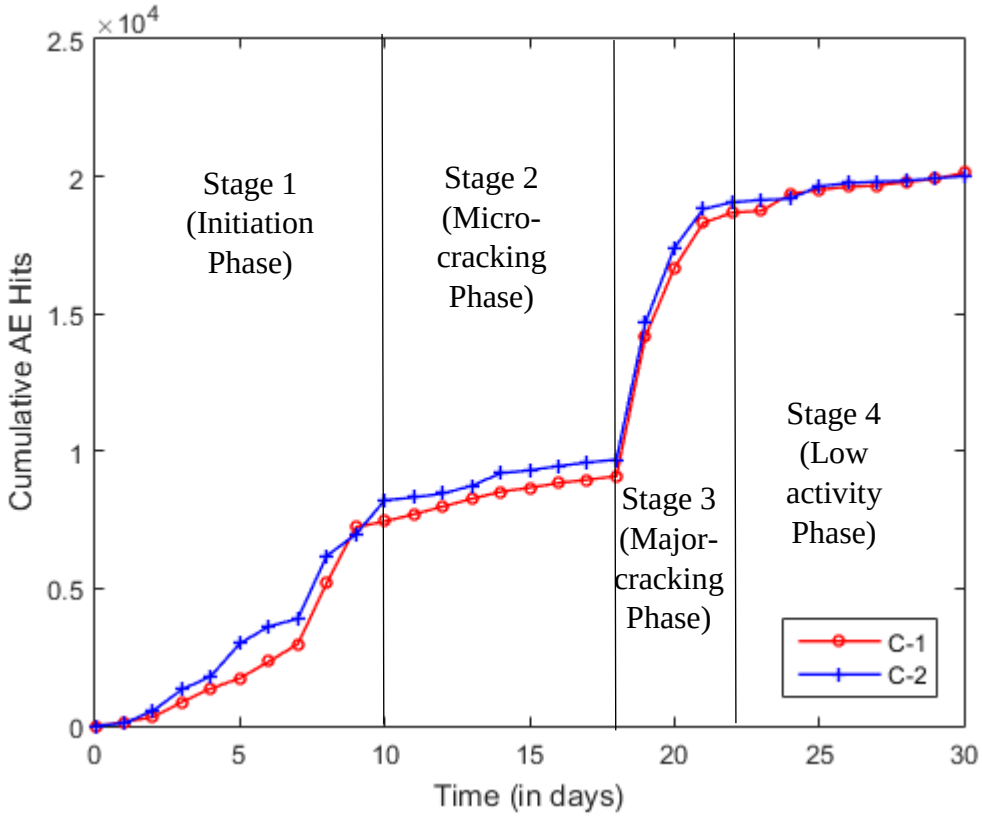

Fig. 5.10 Variation of Cumulative AE hits due to corrosion exposure in control concrete

The regions of higher AE activity where larger number of hits recorded correlate to the regions of high crack growth rate [75] and hence, can be related to corrosion damage. A change in the gradient of cumulative AE hits vs time plot at 9, 17 and 22 days of corrosion exposure, pointing towards significant AE activity at these instants (**Fig. 5.11**). The plot matches closely with the phenomenological model of corrosion. Till 9 days of exposure, a sharp ascent in AE hits is observed pointing towards the initial activity due to corrosion because of depletion of

passive layer and, leading to further ingress of water and oxygen into the rebar, resulting in faster corrosion. This can be referred to as Stage 1 of 'Corrosion Initiation'.

From 9-19 days, AE hits follow a stable profile. This can be the development of initial layer of rust on the surface of reinforcing steel blocking the further flow of oxygen and water. Minor AE activity is due to development of micro cracks and can be named as Stage 2 of corrosion of steel in concrete and very much relates to 'Calm Phase' of Melchers phenomenon logical model of corrosion.

Further from 19 to 22 days, a sharp rise in AE hits is recorded. This is probably because of macro-cracks in concrete due to cracking and spalling of concrete as a result of increased volume of rebar and leading to major acoustic emission activity. This corresponds to Stage 3 of Melchers model in which major degradation due to corrosion in concrete is expected.

In the final stage 4 from 23-30 days, AE hits again stabilizes. The lesser AE activity recorded in the later stages, is essentially because major degradation due to corrosion has already taken place in the Stage 3. This led to increase in signal attenuation and therefore, lesser number of AE hits are recorded in this stage.

Hence, it can be concluded that cumulative AE hits picks up the initiation and progression of corrosion in RC cylinders indicated by various stages of corrosion. The jump in AE activity at various instants points towards the development of micro and macro-cracks in concrete due to corrosion.

FRP wrapped concrete

The plot of cumulative AE hits for CFRP and GFRP wrapped concrete (**Fig. 5.11**) indicate that the number of AE hits recorded after FRP wrapping reduced drastically. In all GFRP and CFRP wrapped concrete, a common observation is the rise in initial AE activity before wrapping till 3, 6, 9 and 12 days, as in case of control samples corresponding to stage 1 and stage 2. But immediately after wrapping, there is a slowdown in AE activity as observed in all samples. After wrapping and no significant change in slope of the cumulative AE hits is observed in all wrapped samples pointing towards protection offered to corroding RC cylinders by FRP wraps. The CFRP as well as GFRP wraps are able to arrest the progression of corrosion significantly, represented by considerable diminution of AE hits with increasing corrosion exposure. No jumps in the AE hits are observed related to advanced stages of corrosion as in case of control samples. Both the micro- and macro cracking phases vanish after wrapping with FRP. Hence, a plot of cumulative AE hits not only pick up the initiation and progress of corrosion in concrete but is also able to track the arrest of corrosion by FRP wrapping (GFRP & CFRP) which passively protects the concrete.

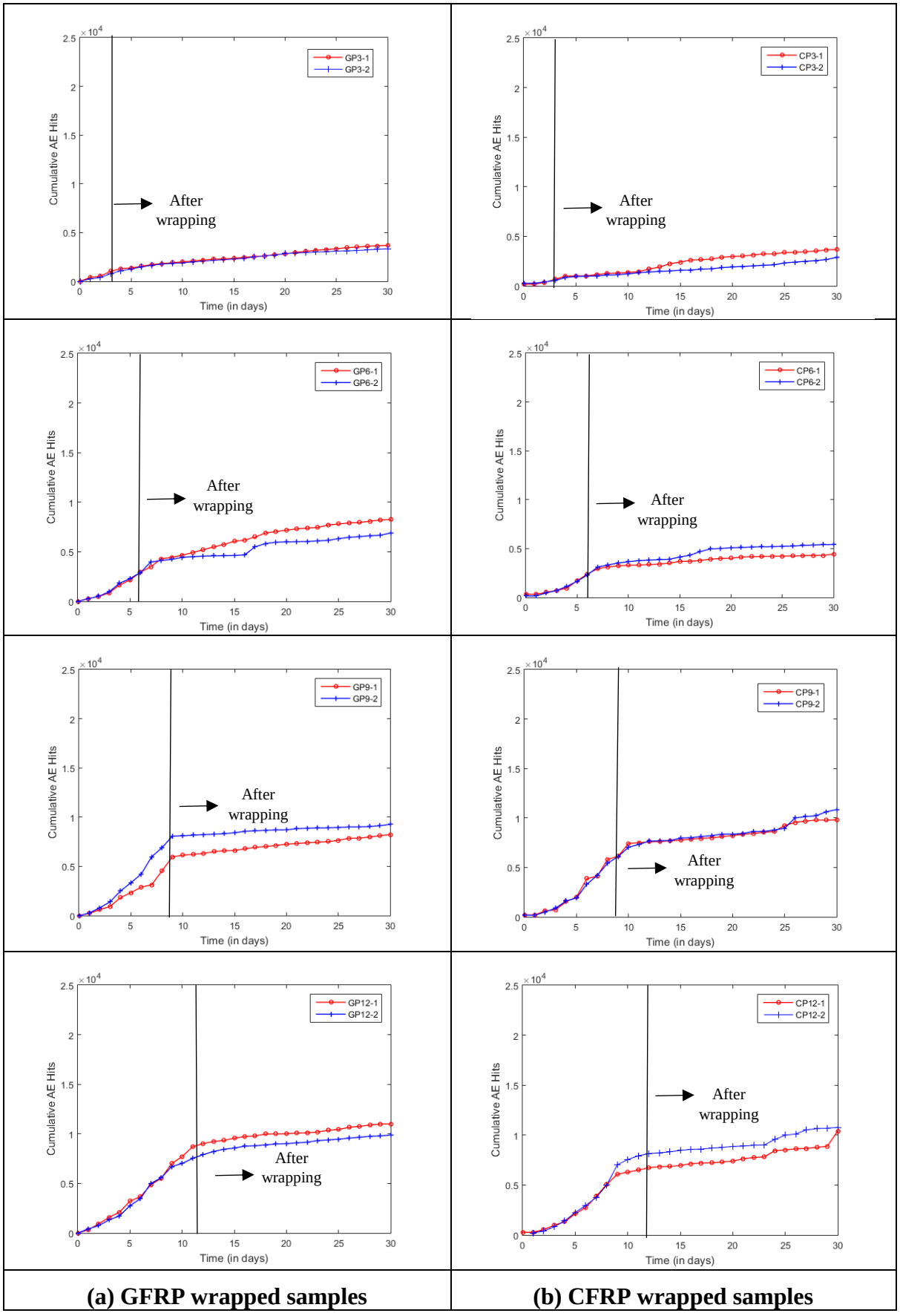

(a) GFRP wrapped samples **(b) CFRP wrapped samples**

Fig. 5.11 Variation of Cumulative AE hits due to corrosion exposure for FRP wrapped concrete

5.5.2 Cumulative Signal Strength

Control concrete

Fig. 5.12 shows the variation of cumulative signal strength for control concrete samples. From the plot, a spike in CSS curve at 5, 9 and 19 days have been observed.

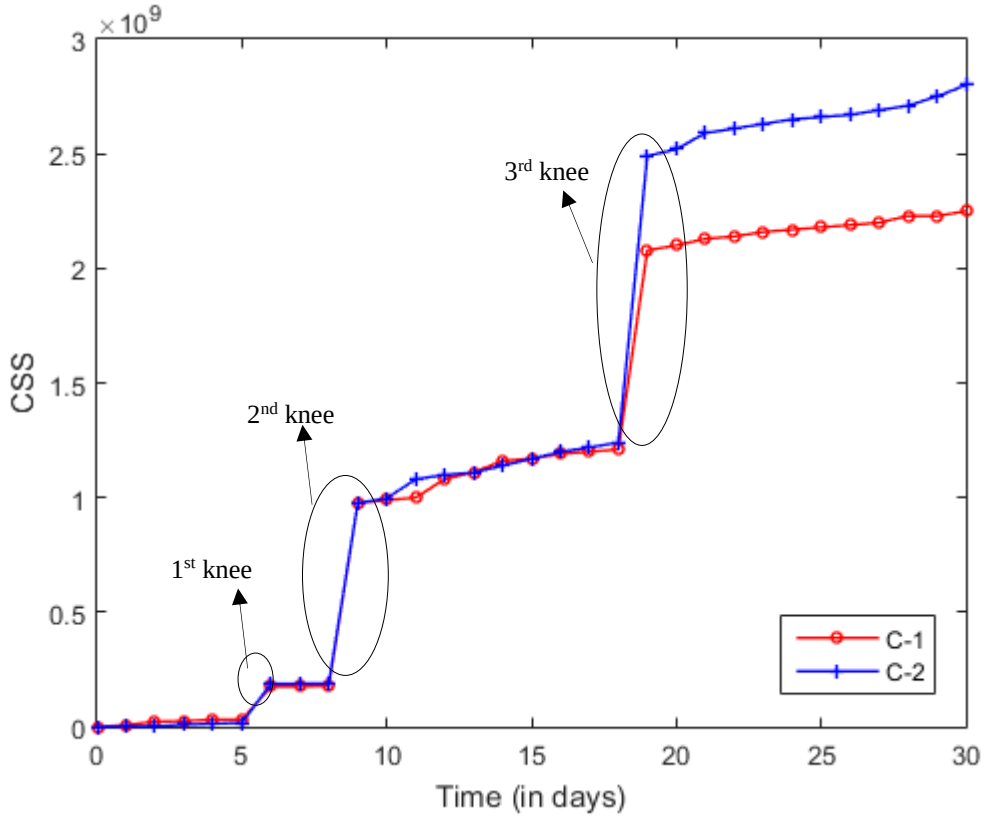

Fig. 5.12 Variation of Cumulative Signal Strength (CSS) vs time in control concrete

These spikes are referred to as 'Knee' in CSS curve and are related to sudden and major damage in concrete due to corrosion. 1st knee at 5th day indicates small stress change taking place in concrete due to initiation of corrosion related to depassivation of rebar. The 2nd major knee observed at 9th day of accelerated corrosion can be related to development of micro-cracks due to the accumulation of corrosion products at steel-concrete interface. This is even reinforced in **Fig. 5.13**, wherein it can be clearly observed that the values of amplitude of recorded acoustic emission are very low during this duration pointing towards micro-small events. This also corresponds with the Stage 1 of Initiation and Stage 2 of micro-cracking. From 9-19 days, no significant knee is observed since it corresponds to 'Calm phase' or 'Stage 2'. At 19th day of corrosion exposure, a significant peak is observed and can be related with evolution of micro-cracks into major cracks. The values of amplitude of AE hits during this duration correspond to higher values ranging between 45-100 dB (**Fig. 5.13**).

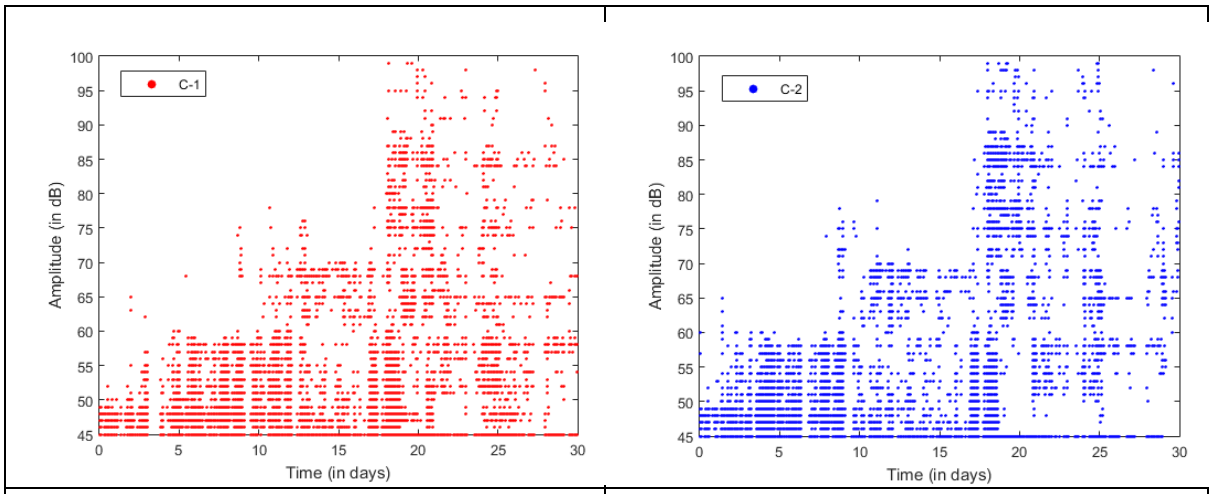

(a) Control sample (C-1) **(b) Control sample (C-2)**

Fig. 5.13 Variation of Amplitude with time for control samples

FRP wrapped concrete

The effect of wrapping to arrest the corrosion progression in concrete is further investigated using CSS parameter (**Fig. 5.14**). It is clearly observed that for GP3 and CP3 samples, no knee/peak is formed as they are wrapped after 3 days of accelerated corrosion and 1st knee appears at 5th day of corrosion exposure in control concrete. Since corrosion was done for first three days and therefore, wrap was applied, no hike/ knee is observed (**Fig. 5.14**) (also picked up by the AE hits graph). Flat CSS curve points towards the arrest of corrosion after initiation (0-3 days) by FRP wraps. Therefore, it can be entailed that FRP protection can be an efficient option for preventing the initiation of corrosion.

From GP6 and CP6 samples, a very small spike is observed at 5th day suggestive of some changes inside concrete similar to control concrete. However, no changes/knees are observed in CSS plots after the application of wrap after 6 days of corrosion exposure. From **Fig. 5.15**, it is confirmed that no prominent damage has occurred due to corrosion after wrapping since amplitude of AE hits recorded also, remain well below 60 dB.

The GP9 and CP9 exhibited a sharp change in gradients of CSS curve at 5th and 9th day of corrosion exposure as in control concrete samples. Amplitude of recorded AE hits exhibit values ranging between 45 dB to 90 dB before the wrapping was applied (**Fig. 5.15**). After wrapping, no significant variations in amplitude of AE hits were observed for the remaining period of corrosion exposure. Therefore, it can be noted that FRP has been able to significantly impede the corrosion progression even after some corrosion has occurred as pointed by CSS and amplitude of AE hits. Similar observations are made for GP12 and CP12 samples. Rise in the amplitude of AE hits (**Fig. 5.11**), has also been observed till 12 days but after protection by

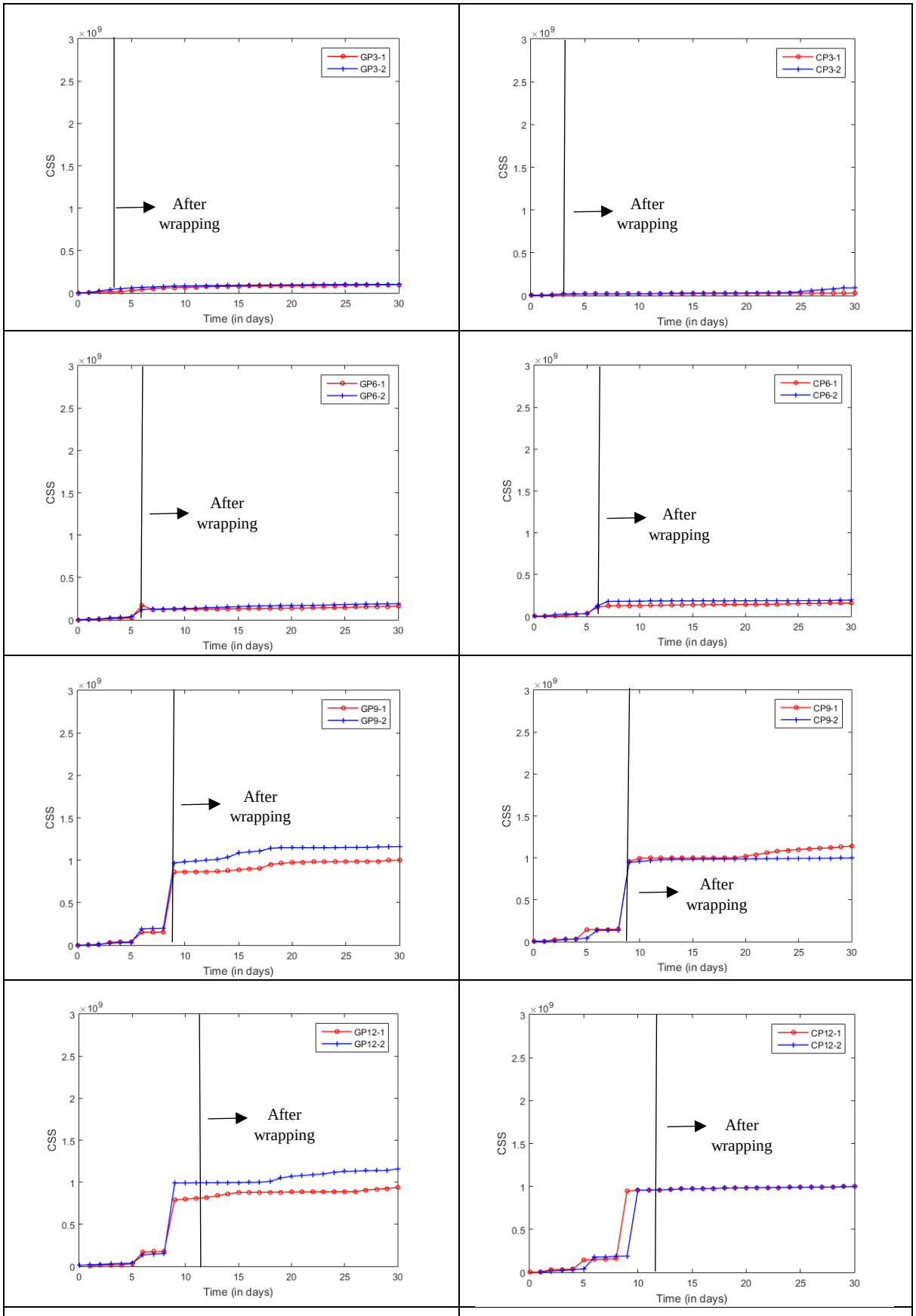

(a) GFRP wrapped samples **(b) CFRP wrapped samples**

Fig. 5.14 Variation of Cumulative Signal Strength (CSS) for FRP wrapped concrete

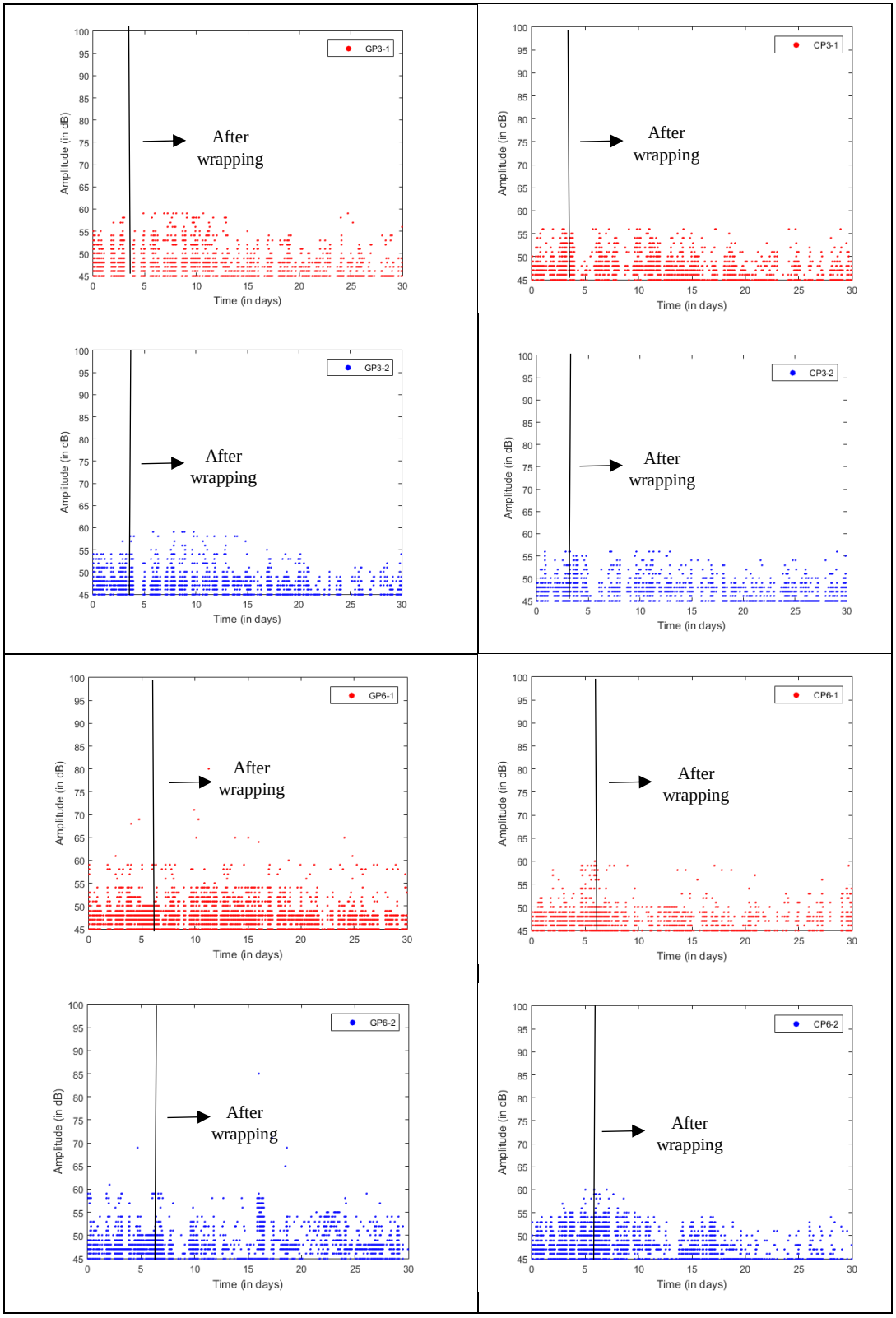
GP3-1
After wrapping
Amplitude (in dB)
Time (in days)
CP3-1
After wrapping
Amplitude (in dB)
Time (in days)
GP3-2
After wrapping
Amplitude (in dB)
Time (in days)
CP3-2
After wrapping
Amplitude (in dB)
Time (in days)
GP6-1
After wrapping
Amplitude (in dB)
Time (in days)
CP6-1
After wrapping
Amplitude (in dB)
Time (in days)
GP6-2
After wrapping
Amplitude (in dB)
Time (in days)
CP6-2
After wrapping
Amplitude (in dB)
Time (in days)

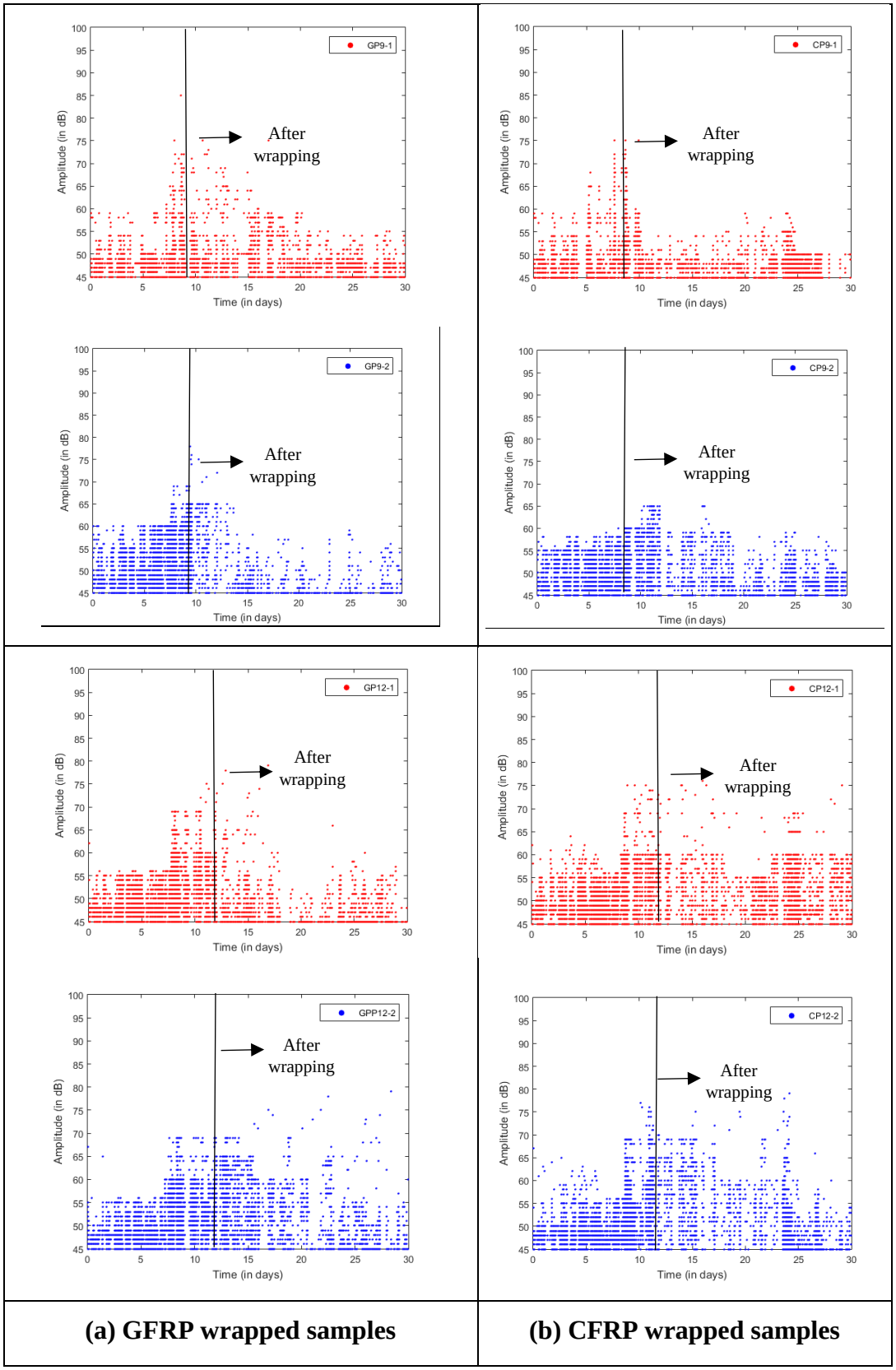

Fig. 5.15 Variation of Amplitude of AE hits vs time for FRP wrapped concrete

FRP, no spike is observed and the values of amplitude of AE hits fall below 60 dB. Hence, it can be concluded that protection with FRP is very effective in curbing the progression of

corrosion RC structures well picked by AE hits and CSS curves. Also, modifications in the amplitude of AE hits and CSS plots point towards not only the progression of corrosion but also the protection offered to corrosion by passive FRP wraps.

5.5.3 Ib-Value Analysis

Ib-value Analysis involves the amplitude distribution of AE signals for damage quantification. The Ib-value is one such AE indicator that bridges the weak AE hits (hits with lower amplitude values as a result of micro-cracks) and strong AE hits (hits with higher amplitude values as a result of macro-cracks). Therefore, micro-cracking leads to higher Ib-values indicating the stress accumulation due to crack propagation, and macro-cracking results in lower Ib-values indicating the release of stress by opening of cracks**.** The method to determine the Ib-value is already discussed in the Chapter 2.

Control Concrete

Fig. 5.16 shows the variation of Ib-value with increasing corrosion for both control samples C1 and C2. The calculated Ib-value for both samples range from 0 to 0.2, suggesting the degree of corrosion induced damage in concrete from intermediate to severe. During the first 9 days, several drops (minima) in the absolute gradient of amplitude distribution is observed suggesting the accumulating stress and commencement of micro-cracking in concrete. The drops further increases progressively with increasing corrosion (**Fig. 5.17)**. During this period, the number of AE hits also increase drastically confirming the development of micro-cracks in RC cylinder.

The slope remains constant for some time until 17 days of accelerated corrosion. From 17 days onwards till the duration of complete exposure, multiple drops with of lesser Ib-values were observed in a very short duration pointing towards the release of accumulated stress in form of macro-cracks with stronger hits and represents the zone of severe damage due to accelerated corrosion in RC cylinder (Ib- values between 0 - 0.1). Afterwards, the Ib-values remain constant but still remain in the zone of severe damage suggesting the extremely deteriorated condition of RC cylinder.

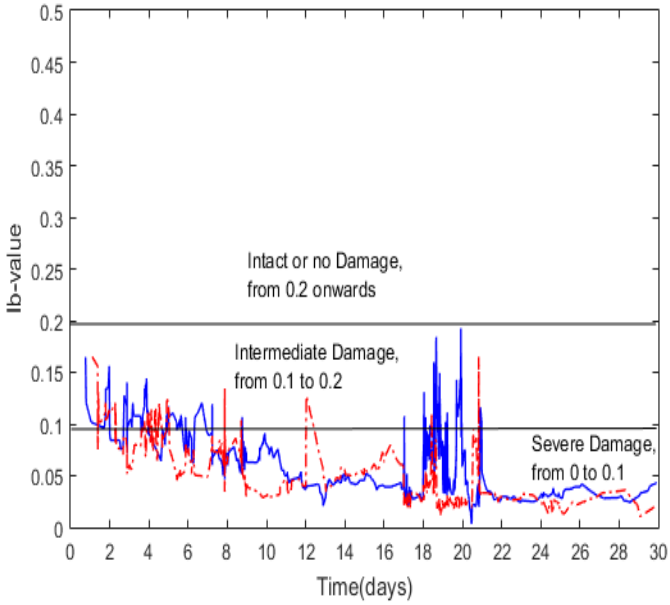

Fig. 5.16 Variation of Ib-value with increasing corrosion in control concrete

FRP wrapped concrete

Fig. 5.17(a)-(h) depict the variation of Ib-value with corrosion for GFRP and CFRP wrapped RC cylindrical specimens. From **Fig. 5.17(a)-(b)**, it can be clearly observed that after the first drop (lying between 0.1 to 0.2) observed during the first 3 days of accelerated corrosion, all other calculated drops have values greater then 0.2, indicating no serious damage in the structure. This further explains that both GFRP as well as CFRP wraps are highly effective in preventing the progression of corrosion if applied during the initial stages (after 3 days of accelerated corrosion).

Fig. 5.17(c)-(d) shows the Ib-values for samples GP6 and CP6 wrapped after 6 days of accelerated corrosion. It can be clearly seen that upto 7 days, few drops in Ib-values (from 0 to 0.1) are observed indicating severe damage. After wrapping, no significant drops from 0 to 0.1 is observed and typically Ib-value lies above 0.2, indicating no further damage due to corrosion and hence successful impediment to corrosion offered by wrapping after 6 days.

Similar observations were made for GP9 and CP9 samples (**Fig. 5.17(e)-(f)**) wherein drops in the Ib-values were observed before wrapping due to corrosion, pointing towards severe damage. After wrapping, the Ib-values shifted to intermediate damage zone and around 13th day, it exceeded to 0.2, indicating no damage zone till the rest of the duration of corrosion exposure. It can therefore, be asserted that both GFRP and CFRP wraps arrests the crack growth thereby impeding the corrosion progression even after some damage has been taken place. **Fig. 5.17(g)-(h)** shows the Ib-values for samples protected after 12 days of accelerated corrosion. Before the wrapping of RC cylinders, several drops indicating lower Ib-values and the

development of micro-cracks has been observed. In this case, however, more drops were seen after the wrapping which could be due to already absorbed moisture and the progressive ongoing damage. After a period of 15 days of accelerated corrosion, the Ib-values increase greatly (to the intermediate zone of damage) and remains constant for the remaining corrosion exposure. This further suggests the efficacy of both GFRP and CFRP wraps for blocking the damage process and impeding the corrosion phenomenon as early as possible.

Mean Ib-value plots of control samples and FRP wrapped samples are plotted (**Fig. 5.18 and 5.19**) GFRP wrapped and CFRP wrapped samples respectively. In GFRP wrapped samples (**Fig. 5.19**), it is clearly visible that corroding control concrete samples experience severe damage whereas the samples wrapped with GFRP after 3 days and 6 days of corrosion lie in the zero damage zone. But these samples wrapped after 9 and 12 days are fall in the Intermediate damage zone and border line of severe- to intermediate damage zones respectively.

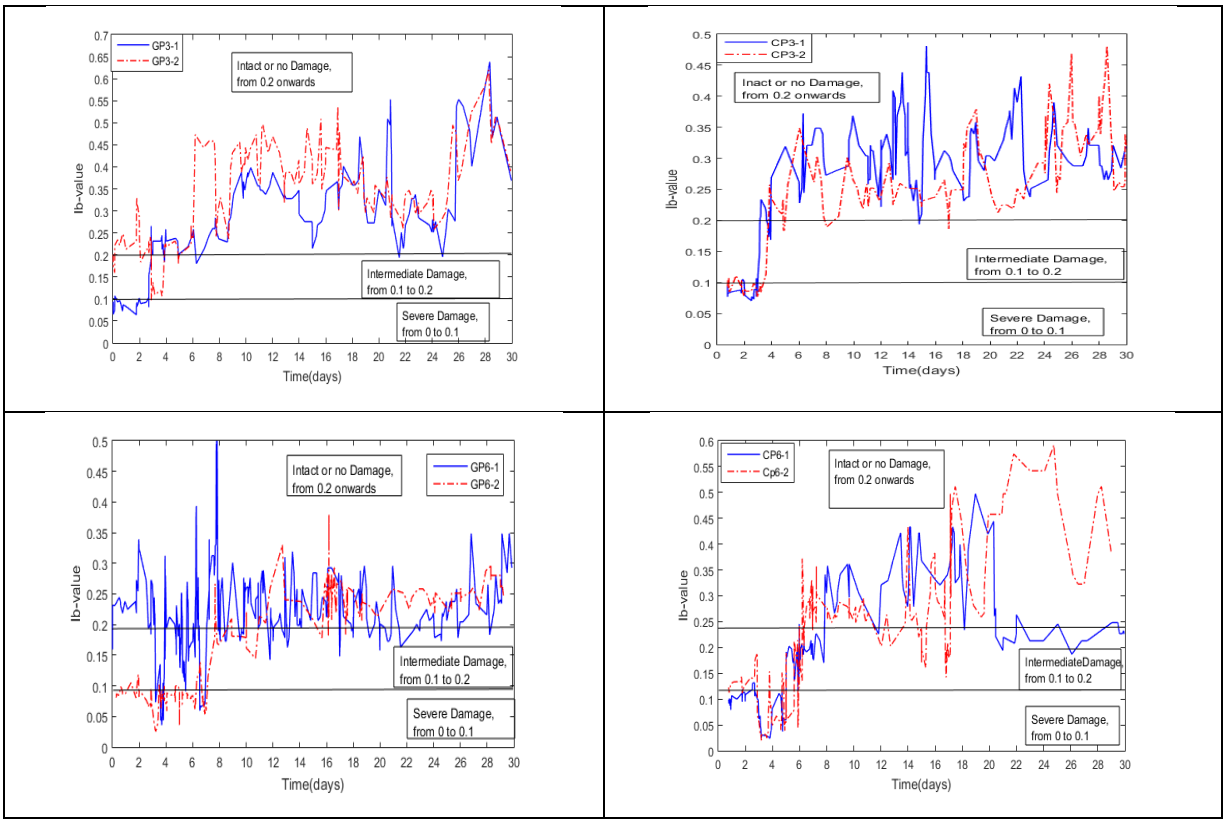

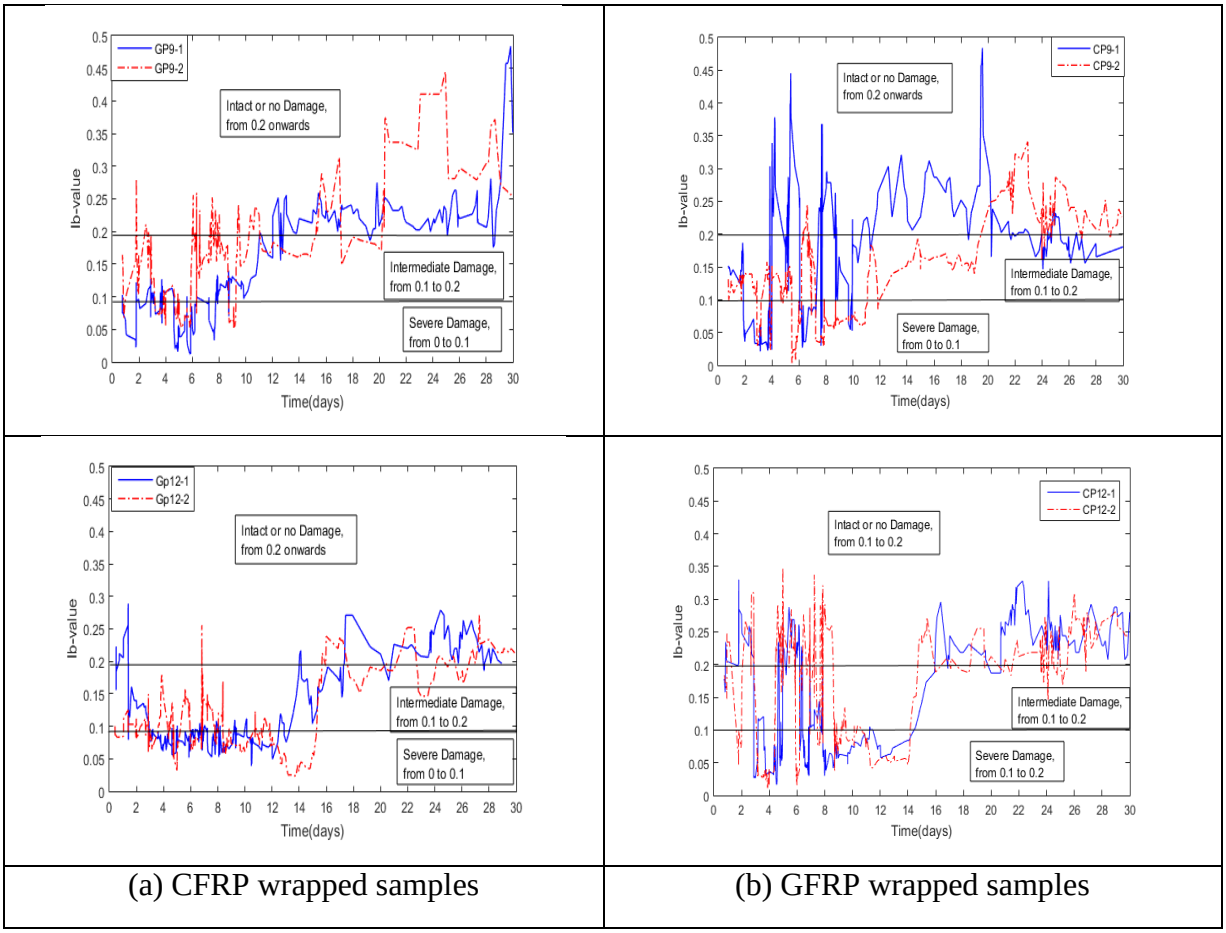

(a) CFRP wrapped samples (b) GFRP wrapped samples

Fig. 5.17 Variation of Ib-value vs time for FRP wrapped concrete

Mean Ib- values indicates the effectiveness of GFRP wrapping for passive protection of RC specimens undergoing corrosion, especially after initiation of corrosion is observed (3-6 days of corrosion).

Similar results are obtained for corrosion impediment in CFRP wrapped samples after 3, 6, 9, and 12 days (**Fig. 5.19**). But, CFRP wrapped samples exhibit lesser Ib-values than GFRP wrapped samples which proves that GFRP wraps are more suitable and efficient for passive protection.

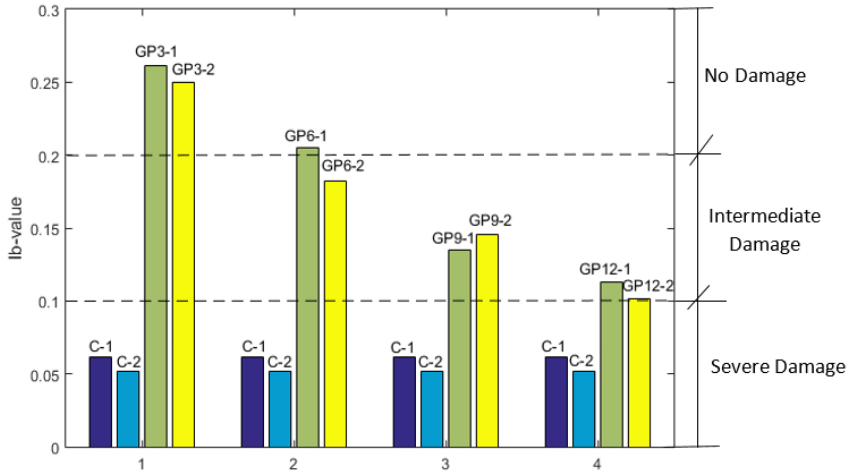

Fig. 5.18 Variation of mean Ib-values for Control and GFRP wrapped concrete

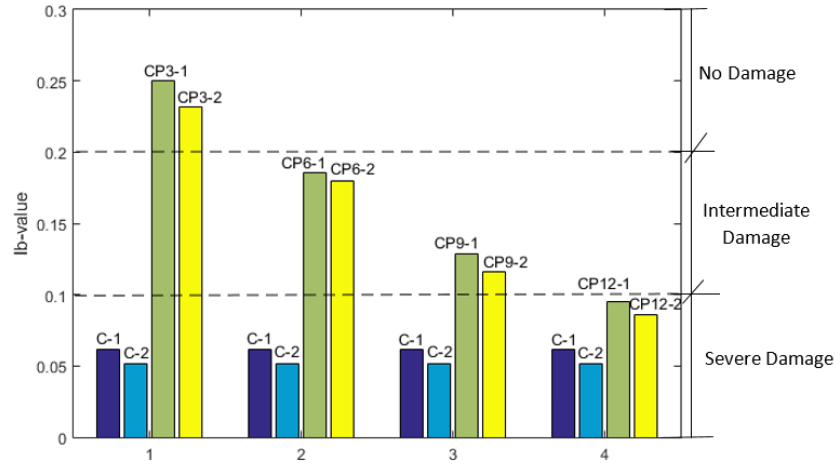

Fig. 5.19 Variation of mean Ib-values for Control and CFRP wrapped concrete

5.6 DESTRUCTIVE TESTS

The extracted reinforcing bars of corroded RC cylindrical samples, were then subjected to pull out test. This was done by fixing the cylindrical RC specimen in a Universal Testing Machine (Hung TA make, capacity of 1000 KN) and then pulling out the rebar from the protruding portion of the reinforcing bar. The amount of force required to pull out bar and the splitting failure of cylinders was observed after the bar was pulled out**. Table 5.3** shows the values of pull-out strength for all the samples (control as well as wrapped).

Table 5.3 Destructive Testing Results

Material	Pull-out Strength (MPa)	Average pull out strength (MPa)	Mass loss (%)
C-1	7.97	8.105	7.7
C-2	8.24		7.2
GP3-1	9.76	9.49	1.92
GP3-2	9.22		1.77
GP6-1	9.68	9.545	1.98
GP6-2	9.41		1.84
GP9-1	8.1	8.155	2.6
GP9-2	8.21		2.3
GP12-1	6.4	6.2	3.6
GP12-2	7.2		3.1
CP3-1	10.3	10.2	2.4
CP3-2	9.8		2.2
CP6-1	9.7	9.675	2.9
CP6-2	9.65		3.1
CP9-1	8.8	8.95	4.1
CP9-2	9.1		4.3
CP12-1	7.7	7.55	4.8
CP12-2	7.4		4.5

From pull-out tests, it is clearly indicated that pull out strength decreases with increasing corrosion exposure. This is primarily a result of debonding of bar from surrounding concrete due to the formation of corrosion products with increasing corrosion. But for FRP wrapped samples, the pull-out strength was much higher than the control concrete samples. This is because FRP wraps prevented the splitting of concrete due to confinement offered by the wraps and therefore, pull-out strength increased. Also, as supported by UGW and AE results, FRP greatly impairs the corrosion progression and deterioration due to corrosion leading to higher pull-out strength.

The extracted bars were cleaned of the corrosion products as per ASTM G1-90 guidelines. The bars were then weighed to determine the loss of mass undergone by the samples with increasing corrosion exposure (**Table 5.3**).

From the mass-loss measurement, it was observed that control samples exhibited greater mass loss (with an average value of 7%). But the average mass loss reduced for FRP wrapped samples. It was recorded as 3% in GFRP wrapped cylinders as against 4% in CFRP wrapped samples. The lesser mass-loss in GFRP wrapped samples may be due to greater thickness of GFRP sheet and higher electrical resistivity than the CFRP sheets and also better confinement offered by GFRP. Hence, mass-loss measurements points towards that impediment of corrosion progression with the help of FRP wrapping in RC structures.

5.7 CLOSING REMARKS

This chapter presents an insight into the effectiveness of two elastic wave based NDT of UGW and AE as health monitoring strategies of repaired RC structures. Steel reinforced concrete cylindrical specimens corroded to different levels, are repaired by wrapping GFRP and CFRP sheets. Before and after wrapping, they are monitored using UGW and AE techniques throughout the corrosion exposure period. While UGW are propagated through rebars in cylinders using a pulse-echo testing mode, AE signals are recorded by AE sensors mounted on concrete. Both the modes L(0,1) at 0.1 MHz and L(0,7) at 1 MHz clearly discerned the delamination and pitting phenomenon of corrosion-induced damage in RC structures. UGW results clearly indicated that FRP wraps offer promising alternative for corrosion impediment in RC structures. On the other hand, AE parameters such as Cumulative AE hits and Cumulative Signal Strength (CSS) not only tracked the initiation and progression of corrosion in RC cylinders but also the impediment offered to corrosion by FRP wraps. Furthermore, the intensity of damage undergone by concrete and the shift of damage mode from severe to intermediate and minor damage, was successfully reported from Ib-value analysis.

CHAPTER 6

CONCLUSIONS

This study suggests that corrosion-induced damage in RC structures can be effectively monitored by an integrated active and passive non-destructive monitoring system utilizing ultrasonic guided waves and acoustic emission monitoring. These measurements would yield more precise information than what is presently available through electrochemical measurements.

6.1 CONCLUDING REMARKS

6.1.1 Monitoring initiation of corrosion

1) HCP measurements only indicated the likelihood of corrosion without any information about the nature and the location of damage.
2) Active monitoring using ultrasonic guided wave is capable of differentiating surface and pitting corrosion using specific surface and core sensitive modes when the corrosion has advanced, but they are of limited significance for tracking the initiation of corrosion where only the outer interface of the bar is affected. However, as the corrosion progresses with time, change in the signal amplitudes from both the modes i.e., L(0,1) and L(0,7) increases and offers greater insight of corrosion inside concrete. In the accelerated corrosion experiment, L(0,1) mode indicated the initiation of surface modifications in the rebar after 5 days whereas L(0,7) mode picked up pitting at 7 days.
3) Passive monitoring using AE has been successful in monitoring the corrosion phenomenon and its consequences in concrete. The various steps of onset, initiation and progression of corrosion during the early stages are very well tracked by AE. It gives a clear picture of the nature of damage in terms of the origin and location of cracks and their rates of growth. Using the numbers and amplitudes of AE hits, different stages of corrosion can be distinguished.
4) AE can locate the acoustic events inside the specimen. It has noted that acoustic events due to corrosion start at a very early stage due to the formation of micro cracks. As corrosion progresses the micro cracks coalesce to form continuous cracks. When the cracks reach the surface of concrete, corrosion becomes visible.

5) While AE gave information on damage in concrete due to corrosion. Extent and nature of deteriorations of the steel bar was discerned through UGW. Thus, a combination of the two techniques is able to reveal the condition of corroded reinforced concrete.
6) It is also important to note that AE sensors need to be installed on the RC structure at all times whereas UGW devices can be attached to the specimens only at the time of monitoring.
7) Though AE is most effective for tracking initial phases of corrosion it may not be reliable in case of a profusely cracked structure whereas ultrasonic guided wave techniques may be more suitable to monitor the manner of corrosion (surface or pitting). Thus a combination of UGW and AE may be optimal for diagnosis and prognosis of corrosion

6.1.2 Monitoring progression of corrosion

1) HCP measurements well indicated the probability of corrosion when the significant damage has already occurred, by relating to steel depassivation but does not quantify the extent and magnitude of corrosion damage. But HCP measurements are critical to make sure that corrosion is in fact taking place. Thus, HCP validates that AE signals are indeed originating from corrosion. It does not quantify the extent and magnitude of corrosion damage.
2) Active monitoring using UGW differentiates surface corrosion from pitting corrosion by direct measurements through the rebar. But it is not very effective in picking up initiation of corrosion whereas AE exactly locates the regions of initiation of steel depassivation and progression of corrosion in the form of micro-and macro-cracking in surrounding concrete well depicted by AE event map. AE technique successfully located the regions of initiation of steel depassivation and progression of corrosion in the form of micro—and macro-cracking in surrounding concrete well picked by the AE hit map.
3) AE parameters like cumulative AE hits and their characteristic amplitudes, clearly distinguished between the various stages of mechanism of chloride-induced corrosion in RC structures.
4) Destructive testing of the corroded bars highlighted the importance of non-destructive monitoring of corrosion in discerning the different zones of corrosion. Specific properties of the rebar is expected to be affected in the specific zones

6.1.3 Monitoring corrosion at varying rates and different environments

1) Both UGW and AE successfully picked up the corrosion mechanism and the consequent damage at varying rates of corrosion at different voltages. With changing rate of corrosion, a shift in the peaks were observed in both UGW and AE results.
2) UGW clearly discerned delamination zone, transition zone and pitting zone of the deterioration of the rebar but with shifts in periods.
3) AE clearly tracked the four phases of corrosion-induced damage in concrete and also the delay in the onset of damage and its progression.
4) Corrosion in the absence of the chlorides was also investigated using UGW and AE techniques. With UGW, oxide corrosion took 120 days as against 48 days of chloride corrosion and was well picked up by both the modes. Slow corrosion in the form of delamination and insignificant pitting was clearly observed.
5) The initiation as well as the progression of corrosion in the absence of chlorides was well tracked by cumulative AE hits and all four stages of corrosion were identified.

6.1.4 Monitoring the efficacy of FRP wraps for corrosion impediment

1) Impressed current values gives the likelihood of corrosion activity without any details of extent and rate of corrosion. It does indicate that with the application of FRP, corrosion phenomenon is impeded but it fails to provide the extent and the efficacy of corrosion impediment.
2) UGW monitoring with surface and core-seeking modes established that pulse echo method is suitable to assess corrosion in FRP wrapped samples. It was marked by the fall in the surface seeking signal as against the rise of the signals due to delamination of the bar from the surrounding concrete. Core seeking mode which measures the deterioration of the bar due to pitting and areas loss after wrapping at later stages, indicated a very slow and marginal fall after wrapping as against a huge and drastic fall in signal with control samples.
3) AE technique successfully been able to evaluate the efficacy of protective wraps for corrosion impediment. The recorded AE hits exhibited insignificant increase after the wrapping was done indicating the success in corrosion impediment. This was confirmed by drop in amplitude of AE hits from 100 dB to 65 dB after wrapping. No peak/knee was observed in CSS curve, indicating that FRP wraps effectively delayed the corrosion progression.

4) In order to quantify the damage control, Ib-value analysis was also performed. Ib-value analysis clearly indicated that GFRP wraps perform much better than CFRP wraps for corrosion monitoring of RC structures.
5) The protected samples exhibited a lower mass-loss and higher pull-out strength than the control samples.

Hence, a combination of electrochemical, ultrasonic guided wave and acoustic emission technique is proposed for corrosion monitoring of reinforced concrete structures.

6.2 RECOMMENDATIONS FOR FUTURE RESEARCH

The proposed research work using Ultrasonic Guided Waves (UGW) and Acoustic Emission (AE) monitoring in RC structures can be further extended as:

1) Fracture monitoring studies of cracking in concrete subjected to corrosion using acoustic emission in combination with other advanced non-destructive techniques.
2) Damage monitoring in concrete structures using UGW and AE considering loading combined with corrosion.
3) Investigation of the efficacy of UGW and AE techniques for damage monitoring in other civil engineering structures of bigger and complex dimensions and sizes.

LIST OF PUBLICATIONS

[1] A. Sharma, S. Sharma, S. Sharma, A. Mukherjee, Ultrasonic guided waves for monitoring corrosion of FRP wrapped concrete structures, Constr. Build. Mater. 96 (2015) 690–702.

[2] A. Sharma, S. Sharma, S. Sharma, A. Mukherjee, Investigation of deterioration in corroding reinforced concrete beams using active and passive techniques, Constr. Build. Mater. 161 (2018) 555–569.

[3] A. Sharma, S. Sharma, S. Sharma, A. Mukherjee, Monitoring Invisible corrosion in concrete using a combination of wave propagation technique, Cem. Concr. Compos. 90(2018) 89-99.

[4] A. Sharma, S. Sharma, S. Sharma, A. Mukherjee, Efficacy of FRP wraps for corrosion impediment in RC structures using wave propagation techniques, Constr. Build. Mater. (Under Review)

REFERENCES

[1] M. Raupach, P. Schießl, Macrocell sensor systems for monitoring of the corrosion risk of the reinforcement in concrete structures, NDT E Int. 34 (2001) 435–442.

[2] L. Bertolini, B. Elsener, P. Pedeferri, E. Redaelli, R.B. Polder, Corrosion of steel in concrete: prevention, diagnosis, repair, John Wiley & Sons, 2013.

[3] C.M. Hansson, Concrete: The advanced industrial material of the 21st century, Metall. Mater. Trans. B. 26 (1995) 417–437.

[4] B. Pradhan, B. Bhattacharjee, Half-cell potential as an indicator of chloride-induced rebar corrosion initiation in RC, J. Mater. Civ. Eng. 21 (2009) 543–552.

[5] M. Raupach, Chloride-induced macrocell corrosion of steel in concrete—theoretical background and practical consequences, Constr. Build. Mater. 10 (1996) 329–338.

[6] G.S. Duffó, W. Morris, I. Raspini, C. Saragovi, A study of steel rebars embedded in concrete during 65 years, Corros. Sci. 46 (2004) 2143–2157.

[7] R.E. Melchers, C.Q. Li, Phenomenological modeling of reinforcement corrosion in marine environments, ACI Mater. J. 103 (2006) 25–32.

[8] K.Y. Ann, H.-W. Song, Chloride threshold level for corrosion of steel in concrete, Corros. Sci. 49 (2007) 4113–4133.

[9] G. Baronio, M. Berra, L. Bertolini, T. Pastore, Steel corrosion monitoring in normal and total-lightweight concretes exposed to chloride and sulphate solutions Part I: Potential measurements, Cem. Concr. Res. 26 (1996) 683–689.

[10] R. Zhang, A. Castel, R. François, Concrete cover cracking with reinforcement corrosion of RC beam during chloride-induced corrosion process, Cem. Concr. Res. 40 (2010) 415–425.

[11] R. Zhang, A. Castel, R. François, The corrosion pattern of reinforcement and its influence on serviceability of reinforced concrete members in chloride environment, Cem. Concr. Res. 39 (2009) 1077–1086.

[12] S. Ahmad, Reinforcement corrosion in concrete structures, its monitoring and service life prediction—a review, Cem. Concr. Compos. 25 (2003) 459–471.

[13] A.A. Almusallam, A.S. Al-Gahtani, A.R. Aziz, Rasheeduzzafar, Effect of reinforcement corrosion on bond strength, Constr. Build. Mater. 10 (1996) 123–129.

[14] J.G. Cabrera, Deterioration of concrete due to reinforcement steel corrosion, Cem. Concr. Compos. 18 (1996) 47–59.

[15] J.P. Broomfield, Corrosion of Steel in Concrete: Understanding, investigation and repair, CRC Press, 2002.

[16] S. Gadve, A. Mukherjee, S.N. Malhotra, Corrosion of steel reinforcements embedded in FRP wrapped concrete, Constr. Build. Mater. 23 (2009) 153–161.

[17] R. Arndt, F. Jalinoos, NDE for corrosion detection in reinforced concrete structures–a benchmark approach, Proc. Non-Destr. Test. Civ. Eng. (2009).

[18] A. Zaki, H.K. Chai, D.G. Aggelis, N. Alver, Non-Destructive Evaluation for Corrosion Monitoring in Concrete: A Review and Capability of Acoustic Emission Technique, Sensors. 15 (2015) 19069–19101.

[19] F. Wu, F.-K. Chang, Debond Detection using Embedded Piezoelectric Elements in Reinforced Concrete Structures - Part I: Experiment, Struct. Health Monit. 5 (2006) 5–15.

[20] S. Sharma, A. Mukherjee, Monitoring corrosion in oxide and chloride environments using ultrasonic guided waves, J. Mater. Civ. Eng. 23 (2011) 207–211.

[21] M. Ormellese, M. Berra, F. Bolzoni, T. Pastore, Corrosion inhibitors for chlorides induced corrosion in reinforced concrete structures, Cem. Concr. Res. 36 (2006) 536–547.

[22] G. Batis, E. Rakanta, Corrosion of steel reinforcement due to atmospheric pollution, Cem. Concr. Compos. 27 (2005) 269–275.

[23] P.R. Vassie, The half-cell potential method of locating corroding reinforcement in concrete structures, TRRL Appl. Guide. (1991).

[24] C. Andrade, C. Alonso, Corrosion rate monitoring in the laboratory and on-site, Constr. Build. Mater. 10 (1996) 315–328.

[25] B. Elsener, Corrosion rate of steel in concrete—Measurements beyond the Tafel law, Corros. Sci. 47 (2005) 3019–3033.

[26] A. Legat, V. Dolecek, Corrosion monitoring system based on measurement and analysis of electrochemical noise, Corrosion. 51 (1995) 295–300.

[27] G.F. Pla-Rucki, M.O. Eberhard, Imaging of reinforced concrete: State-of-the-art review, J. Infrastruct. Syst. 1 (1995) 134–141.

[28] K. Kobayashi, N. Banthia, Corrosion detection in reinforced concrete using induction heating and infrared thermography, J. Civ. Struct. Health Monit. 1 (2011) 25–35.

[29] M.R.A. Hassan, M.H.A. Bakar, K. Dambul, F.R.M. Adikan, Optical-based sensors for monitoring corrosion of reinforcement rebar via an etched cladding Bragg grating, Sensors. 12 (2012) 15820–15826.

[30] V. Talakokula, S. Bhalla, Reinforcement corrosion assessment capability of surface bonded and embedded piezo sensors for reinforced concrete structures, J. Intell. Mater. Syst. Struct. 26 (2015) 2304–2313.

[31] T. Visalakshi, S. Bhalla, Reinforcement corrosion assessment capability of surface bonded and embedded piezo sensors for reinforced concrete structures, 2014.

[32] M. Sansalone, Impact-echo: The complete story, Struct. J. 94 (1997) 777–786.

[33] B.N. Pavlakovic, M.J.S. Lowe, P. Cawley, High-frequency low-loss ultrasonic modes in imbedded bars, Trans.-Am. Soc. Mech. Eng. J. Appl. Mech. 68 (2001) 67–75.

[34] W.B. Na, T. Kundu, M.R. Ehsani, Ultrasonic guided waves for steel bar concrete interface testing, ARIEL. 129 (2002) 31–248.

[35] M.D. Beard, Guided wave inspection of embedded cylindrical structures, Department of Mechanical Engineering, Imperial College, 2002.

[36] W.-B. Na, T. Kundu, M.R. Ehsani, A comparison of steel/concrete and glass fiber reinforced polymers/concrete interface testing by guided waves, Mater. Eval. 61 (2003) 155–161.

[37] G. Miller, P. Gaydecki, S. Quek, B.T. Fernandes, M.A. Zaid, Detection and imaging of surface corrosion on steel reinforcing bars using a phase-sensitive inductive sensor intended for use with concrete, NDT E Int. 36 (2003) 19–26.

[38] T. Kundu. Ultrasonic non-destructive evaluation: engineering and biological material characterization. CRC press; 2003.

[39] M.D. Beard, M.J.S. Lowe, P. Cawley, Ultrasonic guided waves for inspection of grouted tendons and bolts, J. Mater. Civ. Eng. 15 (2003) 212–218.

[40] H. Reis, B.L. Ervin, D.A. Kuchma, J.T. Bernhard, Estimation of Corrosion Damage in Steel Reinforced Mortar Using Guided Waves, J. Press. Vessel Technol. 127 (2005) 255–261.

[41] C. He, J.K. Van Velsor, C.M. Lee, J.L. Rose, Health monitoring of rock bolts using ultrasonic guided waves, in: AIP Conf. Proc., AIP, 2006: pp. 195–201.

[42] P. Cawley, Practical guided wave inspection and applications to structural health monitoring, in: 5th Australas. Congr. Appl. Mech. ACAM 2007, Engineers Australia, 2007.

[43] B.L. Ervin, H. Reis, Longitudinal guided waves for monitoring corrosion in reinforced mortar, Meas. Sci. Technol. 19 (2008) 055702.

[44] B.L. Ervin, D.A. Kuchma, J.T. Bernhard, H. Reis, Monitoring corrosion of rebar embedded in mortar using high-frequency guided ultrasonic waves, J. Eng. Mech. 135 (2009) 9–19.

[45] S. Sharma, A. Mukherjee, Longitudinal Guided Waves for Monitoring Chloride Corrosion in Reinforcing Bars in Concrete, Struct. Health Monit. 9 (2010) 555–567.

[46] T.H. Miller, T. Kundu, J. Huang, J.Y. Grill, A new guided wave–based technique for corrosion monitoring in reinforced concrete, Struct. Health Monit. 12 (2013) 35–47.

[47] S. Sharma, A. Mukherjee, Nondestructive Evaluation of Corrosion in Varying Environments Using Guided Waves, Res. Nondestruct. Eval. 24 (2013) 63–88.

[48] S. Sharma, A. Mukherjee, Ultrasonic guided waves for monitoring the setting process of concretes with varying workabilities, Constr. Build. Mater. 72 (2014) 358–366.

[49] A. Moustafa, E.D. Niri, A. Farhidzadeh, S. Salamone, Corrosion monitoring of post-tensioned concrete structures using fractal analysis of guided ultrasonic waves, Struct. Control Health Monit. 21 (2014) 438–448.

[50] A. Farhidzadeh, S. Salamone, Reference-free corrosion damage diagnosis in steel strands using guided ultrasonic waves, Ultrasonics. 57 (2015) 198–208.

[51] K. Beena, S. Shruti, S. Sandeep, K. Naveen, Monitoring degradation in concrete filled steel tubular sections using guided waves, SMART Struct. Syst. 19 (2017) 371–382.

[52] M.S. Weng, S.E. Dunn, W.H. Hartt, R.P. Brown, Application of Acoustic Emission to Detection of Reinforcing Steel Corrosion in Concrete, CORROSION. 38 (1982) 9–14.

[53] S.E. Dunn, J.D. Young, W.H. Hartt, R.P. Brown, Acoustic emission characterization of corrosion induced damage in reinforced concrete, Corrosion. 40 (1984) 339–343.

[54] R.K. Miller, P. McIntire, Nondestructive Testing Handbook. Vol. 5: Acoustic Emission Testing, Am. Soc. Nondestruct. Test. 4153 Arlingate Plaza Caller 28518 Columb. Ohio 43228 USA 1987 603. (1987).

[55] A. Maji, S.P. Shah, Process zone and acoustic-emission measurements in concrete, Exp. Mech. 28 (1988) 27–33.

[56] Ouyang Chengsheng, Landis Eric, Shah Surendra P., Damage Assessment in Concrete Using Quantitative Acoustic Emission, J. Eng. Mech. 117 (1991) 2681–2698.

[57] A.D. Zdunek, D.W. Prine, Z. Li, E. Landis, S. Shah, Early detection of steel rebar corrosion by acoustic emission monitoring, Northwestern University Infrastructure Technology Institute Evanston, IL, 1995.

[58] S.W. Hearn, C.K. Shield, Acoustic emission monitoring as a nondestructive testing technique in reinforced concrete, Mater. J. 94 (1997) 510–519.

[59] O. Minemura, N. Sakata, S. Yuyama, T. Okamoto, K. Maruyama, Acoustic emission evaluation of an arch dam during construction cooling and grouting, Constr. Build. Mater. 12 (1998) 385–392.

[60] D.-J. Yoon, W.J. Weiss, S.P. Shah, Assessing damage in corroded reinforced concrete using acoustic emission, J. Eng. Mech. 126 (2000) 273–283.

[61] L. Golaski, P. Gebski, K. Ono, Diagnostics of reinforced concrete bridges by acoustic emission, J. Acoust. Emiss. 20 (2002) 83–89.

[62] I.S. Colombo, I.G. Main, M.C. Forde, Assessing damage of reinforced concrete beam using "b-value" analysis of acoustic emission signals, J. Mater. Civ. Eng. 15 (2003) 280–286.

[63] P. Beck, Quantitative damage assessment of concrete structures using Acoustic Emission, Ph.D., Cardiff University, 2004.

[64] S.A. Austin, R. Lyons, M.J. Ing, Electrochemical Behavior of Steel-Reinforced Concrete During Accelerated Corrosion Testing, CORROSION. 60 (2004) 203–212.

[65] A.F. Uddin, K. Numata, J. Shimasaki, M. Shigeishi, M. Ohtsu, Mechanisms of crack propagation due to corrosion of reinforcement in concrete by AE-SiGMA and BEM, Constr. Build. Mater. 18 (2004) 181–188.

[66] B. Assouli, F. Simescu, G. Debicki, H. Idrissi, Detection and identification of concrete cracking during corrosion of reinforced concrete by acoustic emission coupled to the electrochemical techniques, NDT E Int. 38 (2005) 682–689.

[67] V. Leelalerkiet, T. Shimizu, Y. Tomoda, M. Ohtsu, Estimation of Corrosion in Reinforced Concrete by Electrochemical Techniques and Acoustic Emission, J. Adv. Concr. Technol. 3 (2005) 137–147.

[68] T. Shiotani, Y. Nakanishi, K. Iwaki, X. Luo, H. Haya, Evaluation of reinforcement in damaged railway concrete piers by means of acoustic emission, J. Acoust. Emiss. 23 (2005) 260–271.

[69] M. Ing, S. Austin, R. Lyons, Cover zone properties influencing acoustic emission due to corrosion, Cem. Concr. Res. 35 (2005) 284–295.

[70] R. Lyons, M. Ing, S. Austin, Influence of diurnal and seasonal temperature variations on the detection of corrosion in reinforced concrete by acoustic emission, Corros. Sci. 47 (2005) 413–433.

[71] A. Nair, Acoustic emission monitoring and quantitative evaluation of damage in reinforced concrete members and bridges, LSU Masters Theses. (2006).

[72] A. Carpinteri, G. Lacidogna, G. Niccolini, Critical behaviour in concrete structures and damage localization by acoustic emission, in: Key Eng. Mater., Trans Tech Publ, 2006: pp. 305–310.

[73] M. Ohtsu, Y. Tomoda, Corrosion Process in Reinforced Concrete Identified by Acoustic Emission, Mater. Trans. 48 (2007) 1184–1189.

[74] T. Shiotani, D.G. Aggelis, O. Makishima, Global monitoring of concrete bridge using acoustic emission, J. Acoust. Emiss. 25 (2007) 308–315.

[75] C.U. Grosse, M. Ohtsu, Acoustic Emission Testing, Springer Science & Business Media, 2008.

[76] D.G. Aggelis, T. Shiotani, S. Momoki, A. Hirama, Acoustic emission and ultrasound for damage characterization of concrete elements, ACI Mater. J. 106 (2009) 509.

[77] S.G. Shah, J.C. Kishen, Fracture behavior of concrete–concrete interface using acoustic emission technique, Eng. Fract. Mech. 77 (2010) 908–924.

[78] Y. Kawasaki, Y. Tomoda, M. Ohtsu, AE monitoring of corrosion process in cyclic wet–dry test, Constr. Build. Mater. 24 (2010) 2353–2357.

[79] M. Di Benedetti, G. Loreto, F. Matta, A. Nanni, Acoustic emission monitoring of reinforced concrete under accelerated corrosion, J. Mater. Civ. Eng. 25 (2012) 1022–1029.

[80] M.R. Kaphle, Analysis of acoustic emission data for accurate damage assessment for structural health monitoring applications, Thesis, Queensland University of Technology, 2012.

[81] S.G. Shah, J.C. Kishen, Use of acoustic emissions in flexural fatigue crack growth studies on concrete, Eng. Fract. Mech. 87 (2012) 36–47.

[82] H.A. Elfergani, R. Pullin, K.M. Holford, Damage assessment of corrosion in prestressed concrete by acoustic emission, Constr. Build. Mater. 40 (2013) 925–933.

[83] M.K. ElBatanouny, J. Mangual, P.H. Ziehl, F. Matta, Early corrosion detection in prestressed concrete girders using acoustic emission, J. Mater. Civ. Eng. 26 (2013) 504–511.

[84] Y. Kawasaki, T. Wakuda, T. Kobarai, M. Ohtsu, Corrosion mechanisms in reinforced concrete by acoustic emission, Constr. Build. Mater. 48 (2013) 1240–1247.

[85] J. Mangual, M.K. ElBatanouny, P. Ziehl, F. Matta, Acoustic-Emission-Based Characterization of Corrosion Damage in Cracked Concrete with Prestressing Strand., ACI Mater. J. 110 (2013).

[86] M. Di Benedetti, G. Loreto, F. Matta, A. Nanni, Acoustic emission historic index and frequency spectrum of reinforced concrete under accelerated corrosion, J. Mater. Civ. Eng. 26 (2013) 04014059.

[87] Y. Kawasaki, S. Wasada, T. Okamoto, K. Izuno, Evaluation for RC specimen damaged from rebar corrosion by acoustic emission technique, Constr. Build. Mater. 67 (2014) 157–164.

[88] A.A. Abouhussien, A.A. Hassan, Evaluation of damage progression in concrete structures due to reinforcing steel corrosion using acoustic emission monitoring, J. Civ. Struct. Health Monit. 5 (2015) 751–765.

[89] W. Vélez, F. Matta, P. Ziehl, Acoustic emission monitoring of early corrosion in prestressed concrete piles, Struct. Control Health Monit. 22 (2015) 873–887.

[90] A.A. Abouhussien, A.A. Hassan, Application of acoustic emission monitoring for assessment of bond performance of corroded reinforced concrete beams, Struct. Health Monit. (2016) 1475921716681460.

[91] A. Zaki, H.K. Chai, A. Behnia, D.G. Aggelis, J.Y. Tan, Z. Ibrahim, Monitoring fracture of steel corroded reinforced concrete members under flexure by acoustic emission technique, Constr. Build. Mater. 136 (2017) 609–618.

[92] W. Li, C. Xu, S.C.M. Ho, B. Wang, G. Song, Monitoring concrete deterioration due to reinforcement corrosion by integrating acoustic emission and FBG strain measurements, Sensors. 17 (2017) 657.

[93] N.J. Carino, Nondestructive techniques to investigate corrosion status in concrete structures, J. Perform. Constr. Facil. 13 (1999) 96–106.

[94] J.A. González, J.M. Miranda, N. Birbilis, S. Feliu, Electrochemical Techniques for Studying Corrosion of Reinforcing Steel: Limitations and Advantages, CORROSION. 61 (2005) 37–50.

[95] S. Gadve, A. Mukherjee, S. n. Malhotra, Active Protection of Fiber-Reinforced Polymer-Wrapped Reinforced Concrete Structures Against Corrosion, CORROSION. 67 (2011) 025002-1.

[96] P. Dinakar, K.G. Babu, M. Santhanam, Corrosion behaviour of blended cements in low and medium strength concretes, Cem. Concr. Compos. 29 (2007) 136–145.

[97] A.S. Debaiky, M.F. Green, B.B. Hope, Carbon fiber-reinforced polymer wraps for corrosion control and rehabilitation of reinforced concrete columns, Mater. J. 99 (2002) 129–137.

[98] S. Ahmad, Z. Shabir, Effect of Water Cement ratio on Corrosion of Reinforced concrete, in: 30th Conf. OUR WORLD Concr. Struct., 2005.

[99] T. El Maaddawy, A. Chahrour, K. Soudki, Effect of fiber-reinforced polymer wraps on corrosion activity and concrete cracking in chloride-contaminated concrete cylinders, J. Compos. Constr. 10 (2006) 139–147.

[100] National Instruments: Test, Measurement, and Embedded Systems - National Instruments, (n.d.). http://www.ni.com/en-in.html (accessed December 30, 2017).

[101] Nondestructive Testing (NDT) and Services - WavesinSolids, WINS-NDT WavesInSolids LLC. (n.d.). http://wins-ndt.com/ (accessed December 25, 2017).

[102] J.H. Kurz, F. Finck, C.U. Grosse, H.-W. Reinhardt, Stress drop and stress redistribution in concrete quantified over time by the b-value analysis, Struct. Health Monit. 5 (2006) 69–81.

[103] T. Shiotani, K. Fujii, T. Aoki, K. Amou, Evaluation of progressive failure using AE sources and improved b-value on slope model tests, Prog. Acoust. Emiss. 7 (1994) 529–534.

[104] B.B. BuluPradhan, ASTM C 876, Stand. Test Method Half-Cell Potentials Uncoated Reinf. Steel Concr. Annu. Book ASTM Stand. Am. Soc. Test. Mater. (1991).

[105] C.E. Bakis, A. Ganjehlou, D.I. Kachlakev, M. Schupack, P.N. Balaguru, D.J. Gee, V.M. Karbhari, D.W. Scott, C.A. Ballinger, T.R. Gentry, others, Guide for the design and construction of externally bonded FRP systems for strengthening concrete structures, Rep. ACI Comm. 440 (2002).

[106] A. Nanni, J. Giancaspro, FRP Composites for Reinforced and Prestressed Concrete Structures: A Guide to Fundamentals and Design for Repair and Retrofit, Taylor & Francis, 2009.

[107] S. Masoud, K. Soudki, T. Topper, CFRP-strengthened and corroded RC beams under monotonic and fatigue loads, J. Compos. Constr. 5 (2001) 228–236.

[108] J.F. Bonacci, M. Maalej, Externally bonded fiber-reinforced polymer for rehabilitation of corrosion damaged concrete beams, Struct. J. 97 (2000) 703–711.

[109] A. Mukherjee, G.L. Rai, Performance of reinforced concrete beams externally prestressed with fiber composites, Constr. Build. Mater. 23 (2009) 822–828.

[110] A. Mukherjee, T.E. Boothby, C.E. Bakis, M.V. Joshi, S.R. Maitra, Mechanical behavior of fiber-reinforced polymer-wrapped concrete columns-complicating effects, J. Compos. Constr. 8 (2004) 97–103.

[111] K.A. Soudki, T.G. Sherwood, Behaviour of reinforced concrete beams strengthened with carbon fibre reinforced polymer laminates subjected to corrosion damage, Can. J. Civ. Eng. 27 (2000) 1005–1010.

[112] Nur Yazdani, Isaac A. Wootton, Lisa K. Spainhour, Corrosion of Steel Reinforcement in Carbon Fiber-Reinforced Polymer Wrapped Concrete Cylinders, (2003).

[113] Moataz Badawi, Khaled Soudki, Control of Corrosion-Induced Damage in Reinforced Concrete Beams Using Carbon Fiber-Reinforced Polymer Laminates, (2005).

[114] T. El Maaddawy, K. Soudki, Carbon-fiber-reinforced polymer repair to extend service life of corroded reinforced concrete beams, J. Compos. Constr. 9 (2005) 187–194.

[115] S. Masoud, K. Soudki, Evaluation of corrosion activity in FRP repaired RC beams, Cem. Concr. Compos. 28 (2006) 969–977.